Highly Multiplex Imaging Using the Primer Exchange Reaction Method, and the Study of Potential Hydrogels for the Application of Expansion Microscopy

A thesis is submitted by

Millicent Lin

In partial fulfillment for the requirements for the degree of

Master of Science

in

Biomedical Engineering

Tufts University

May 2018

Research Advisor: Yu Wang, PhD, Professor George Church, PhD

Motivation

Fluorescence microscopy has been used as a gold standard tool for characterizing specimens (Kerlopian et al., 2008), however, problems such as diffraction limit (Huang et al., 2009), photobleaching (Gustafsson, 2005) and the limitation of multiple fluorophores (Wang et al., 2017) lead to hindrance in biomedical research that requires further development of super-resolution fluorescence techniques. Understanding how cells in neural circuits are interconnected requires nanoscale resolution that can be hindered by the limitation of traditional microscopes due to diffraction.

We have proposed a method using the primer exchange reaction (PER) in which allows synthesis of single stranded DNA using a catalytic hairpin to achieve highly multiplex resolution imaging. PER cascades are an ideal candidate in amplifying signals with in vitro extended probes in a programmable fashion. PER was first developed to produce single stranded DNA with a prescribed primer in an autonomous fashion, providing an effective platform to construct and expand new DNA materials (Kishi et al., 2017). PER cascades overcome such limitation with a user prescribed sequence and with the help of a strand displacing polymerase. PER mechanism is also responsive to environmental conditions fueled by polymerization via manipulating chemical synthesis. PER reactions can be interfaced with other existing systems, making it more preferable over the conventional methods (HCR, PCR, RCA) that hold limitation in producing exact copies of fixed sequences (Biolabs).

In parallel, we have studied the mechanical properties and contributing factors of different hydrogel composition in the context of expansion microscopy (ExM). ExM enables imaging of cells and tissues with nanoscale precision. Moreover, ExM is compatible with the current conventional microscopy techniques unlike the limitation imposed on the other super-

resolution techniques that heavily rely on complex hardware and specialized instruments. There is a limitation on the imaging speed and the numbers of colors, and volumes of the current super-resolution imaging techniques in which make them a less desired option when handling thick specimens. The current super-resolution imaging methods have drawbacks on providing 3D imaging in which can be overcome by expansion microscopy (Gao et al., 2017).

Expansion microscopy is a newly emerging technology aiming to achieve high resolution via physically expanding the hydrogel to retrieve magnified images of the specimen. Biomolecules or labels can be pulled apart from each other while lipids are fragmented via digestion, providing an extra space for chemical reaction and such extra space can also be used to perform signal amplification. (PER, HCR, and RCA). However, the knowledge regarding the gel properties and composition is limited, and the current expansion methods lack the mechanical supports, making the handling of hydrogels laborious and difficult. The conventional gels used for expansion microscopy are usually fragile and easy to rupture when a strain is applied, resulting in sample damage or distortion (Calvert, 2009) (Lake, 1995). Thus, it is important to better understand the mechanical properties and chemical composition of various hydrogels to develop a robust gel that can also achieve high expansion factor. In the thesis, we have explored the utility of PER signal amplification method and the desired gel properties that can be applied to expansion microscopy in hope of achieving super-resolution imaging. Our goal is to develop a platform that will provide nanoscale precision when visualizing synapses and synaptic proteins in 3D scale to better understand the brain circuits.

Acknowledgements:

Committee Members:

Yu Wang, PhD
Xiaocheng Jiang, PhD
Mark Cronin-Golomb, PhD

Church Laboratory:

Yu Wang, PhD
Richie Kohman, PhD
Kathleen Leeper

Yin Laboratory:

Yu Wang, PhD
Josie Kishi, PhD

Wyss Institute:

Jack Alvarenga
Cathy Zhang
Chris Johnson

I need to thank Yu Wang for being my thesis mentor and for providing all the support, advice and motivations I needed for this project.

Family:

I need to thank my wife, Yilin, for being supportive emotionally, always lifting me up when I fail, and let me see my way through all the difficulties.

Table of Contents

List of Tables

List of Figures

List of Abbreviations

PER (Primer exchange reaction)
DNA (Deoxyribonucleic acid)
ExM (Expansion microscopy)
HCR (Hybridization chain reaction)
PCR (Polymerase chain reaction)
RCA (Rolling circle amplification)
STED (Stimulated emission depletion microscopy)
SIM (Structured illumination microscopy)
PALM (The photoactivated localization microscopy)
STROM (Stochastic optical reconstruction microscopy)
NSOM (Near-field scanning optical microscopy)
FIONA (Fluorescence imaging with one nanometer accuracy)
CycIF (Cyclic immunofluorescence)
SIMPLE (Sequential immunoperozidase labeling and erasing)
ER (Endoplasmic reticulum)
MELC (Multi-epitope-ligand cartography)
MxIF (Multiplexed fluorescence microscopy)
GFP (Green fluorescent protein)
LAMP (Loop-mediated isothermal amplification)
CRH (DNA-based copy-and-release hairpin)
ExFish (Expansion FISH)
MA-NHS (Methacrylic acid *N*-hydroxysuccinimidyl ester)
GA (Glutaraldehyde)
MAP (Magnified analysis of the proteome)
DMAA (*N,N*-dimethylacrylamide)
AFM (Atomic force microscopy)
RT (Room temperature)
Min (minute)
Hr (hour)
PBS (Phosphate-buffered saline)
RCF (Relative centrifugal force)
DTT (Dithiothreitol)
EDTA (Ethylenediaminetetraacetic acid)
DMF (Dimethylformamide)
TEAA (Triethylamine acetate)
HPLC (High-performance lipid chromatography)
NHS (N-hydroxysuccinimide)
DMSO (Dimethyl sulfoxide)
NAHCO3 (Sodium bicarbonate)
NH4Cl (Ammonium chloride)
BSA (Bovine serum albumin)
BS(PEG)9 (PEGylated bis(sulfosuccinimidyl)suberate)
TBS (Tris-buffer saline)
SDS (Sodium dodecyl sulfate)

NaCl (Sodium chloride)
No Amp(No amplification)
2'Ab (Secondary antibody)
APS (Ammonium persulphate)
TEMED (*N,N,N',N'*-tetramethylethylenediamine)
AA (Acrylamide)
SA (Sodium acrylate)
3D (Three-dimensional)

Chapter 1: Background

1.1. Fluorescence Microscopy

Development of imaging methods allows us to better understand the molecular mechanism as well as the molecular networks within a cell (Kerlopian et al., 2008). By directly visualizing the biological specimens, we can gain insight on the biological functions at the cellular level. Among all the available imaging techniques, fluorescent microscopy is considered the most powerful tool in the context of observing the structure of live samples due to the use of fluorophores that exhibit multiple advantages such as high absorption cross-sections and high quantum efficiency.

Through the application of molecular-specific labeling, we can observe the specific component of cells in real time. Such technique is capable of imaging protein expression, activities, and localization in three dimensions as a consequence of the development of fluorescent proteins. The advantages of fluorescence microscopy include inexpensive, noninvasive, and can be used in a variety of biomedical applications. However, the fluorescent microscopy is restrained by low resolutions due to the diffraction limits (200-300 nm) as well as the spectral overlap of multiple fluorophores (Huang et al., 2009).

1.2. Existing Technologies

New developments in super-resolution fluorescent microscopy have emerged to solve the problem associated to diffraction barrier. Imaging methods such as STED (Hell et al., 1994), SIM (Schermelleh et al., 2008), PALM (Betzig et al., 2006), STROM (Rust et al., 2006), NSOM

(Betzig et al., 1991) and FIONA (Yildiz et al., 2003) have become commercially available to scientists and researchers to break the diffraction limitations, however, they are not as user friendly as the conventional microscopy. **(i) The basic concept of stimulated emission depletion (STED) microscopy** is to illustrate imaging a specimen through point by point scanning with the application of a laser beam in which suppresses the fluorescence emission from the fluorophores. The fluorophore in the excited state is brought back to the ground state as wavelength of the excitation beam matches with a photon. In principle, the point spread function (PSF) decreases in size when the fluorescence near the zero point is suppressed as a matter of saturated depletion, which holds the key to achieving super-resolution (Hell et al., 1994). **(ii) Structured Illumination Microscopy (SIM)** is an alternative approach to overcoming the limitation caused by diffraction. The nonlinear phenomenon of the SIM enhances the resolution power due to introduction of high-frequency harmonics generated by saturation. However, the number of photons each molecule can emit decreases, leading to accelerated photobleaching rate of some fluorophores. Other problems can occur with the application of SIM such as the phototoxicity in which cause damages to the live specimens owing to the saturation conditions. Sedat and his coworkers have proposed three-dimensional structured illumination microscopy (3D-SIM) to solve the low resolution corresponding to the scale of cellular components. The concept of 3D-SIM involves extracting new information from reciprocally encoding the image information to construct super-resolution images. SIM is the only technique that enables detection of multiple wavelengths to study the structure and localization of nuclear components (Gustafsson, 2005). **(iii) The photoactivated localization microscopy (PALM)** uses serial photo-activation of photoactivatable fluorescent protein molecule (PA-FP) until the unbleached molecules are diminished. Photo-induced modified ions enable PA-FP to be optically converted

due to a break in the peptide bone (Betzig et al., 2006). **(iv) Stochastic optical reconstruction microscopy (STORM):** STORM enables high-accuracy of photo-switchable fluorophores. The position of fluorophores is determined with high accuracy when the molecules emit fluorescence under the red laser pulse until they are switched off. A fraction of the fluorophores is exposed to green laser illumination to become active, resulting in optically resolvable fluorophores. The image can be obtained from the fluorophore positions derived from the multiple imaging cycles. Zhuang and his coworkers have introduced using cyanine dye, Cy5 as a primary fluorophore that can be switched on and off to activate a subset of fluorophores, thus allowing the fluorophore positions to be determined in which holds the key to constructing images. A large number of switches are easily controlled within the diffraction limit, making it a desired candidate to construct live cell imaging with high-resolution (Rust et al., 2006). **(v) The near-field probe (NSOM)** breaks the barrier of diffraction limit by introducing a near-field prove that can yield a resolution of ~12 nm. The probe is produced by a single-mode fiber that enables the radiation to be adhered to the core, making the intensity at the aperture greater. The signals become stronger with less background noise since the probe promotes effective delivery of light to the aperture. (Betzig et al., 1992). However, NSOM is considered difficult to operate in a noninvasive condition and the imaging depth is low compared to other methods (Rust et al., 2006). **(vi) The single molecule fluorescent imaging technique (FIONA)** is created to test the step size of the myosin V that moves on actin. FIONA has been designed to harness the problem of sub-diffraction limit. Such technique is capable of locating molecules with high photostability. Total internal reflection epi-fluorescence microscopy is used to acquire multiple sequential images. FIONA has improved the accuracy in localizing a single molecule by 20 fold. The key to localizing the molecule with high accuracy lies in curve fitting the image to a Gaussian function

with nanometer spatial localization (Yildiz et al., 2003). **(vii)** Other technologies have been developed to overcome sub-diffraction limits and multi-target detection. Zhang and his coworkers have used the magnifying superlens deposited with anisotropic material, allowing the evanescent field to propagate in radical directions once entered the medium. The images are magnified as a result of the waves that travel outward of the hyperlens (Liu et al., 2007). **(viii) Cyclic immunofluorescence (CyclF)** introduced by Sorger and his coworkers, allowing for up to four to six channels at a time to enhance multiple signaling that adds more fine details on the cell morphology. The concept of CycIF involves an extra round of staining after the removal of primary and secondary antibodies by a stripping process (low pH, heat, salt, denaturing agents). The multichannel image is built upon inactivation of fluorophores and rounds of staining with fluorophore-conjugated antibodies. However, improvement can be made on extending the channels for more complex multiplicity of cell measurement (Lin et al., 2015). **(viii) Sequential immunoperoxidase labeling and erasing (SIMPLE)** allows visual expressions of at least five markers within the same section. Protein-protein interactions can be further understood when multiple antigens presented on the cells are observed. This technology is made possible by applying alcohol-soluble red peroxidase substrate 3-amino-9-ethylcarbazole (AEC) to retrieve antigens in the fixed tissue samples (Glass et al., 2009).

1.3. Current Applications

Super-resolution fluorescent microscopy has been widely used to study the molecular structures such as cytoskeleton, microtubules, actin filaments, keratin, neurofilaments of living cells. Hell and his coworkers have used STED microscopy to image GFP-labeled viruses as well as the endoplasmic reticulum (ER) of mammalian cells (Willig et al., 2006).

Hess and his coworkers have used photoactivated localization microscopy to image vinculin at focal adhesion and the distribution of protein Gag inside the plasma membrane (Betzig et al., 2006). Dress and his coworkers have combined fluorescence technique to map proteins in tissue or cell samples to acquire information on cell interactions and networks that are considered essential in aiding the development of new therapies (Schubert et al., 2006).

It becomes feasible to image sufficient numbers of proteins in a sample through multi-epitope-ligand cartography (MELC) by undergoing multiple rounds of fluorescent detection. By repeating steps of bleaching, relabeling and imaging, distribution map can be formed detect hundreds of proteins. Dress and his coworkers have used MELC to identify protein association and protein co-localization in a single sample to study diseases that are impossible to be done using the conventional fluorescence microscopy (Schubert et al., 2006).

Ginty and his coworkers have presented a multiplexed fluorescence microscopy method (MxIF) to characterize cancer in the context of comprehensive genomic analysis. The molecular profiling of cancer promotes the translational cancer research in developing targeted therapies or diagnostics. The procedure consists of antibody staining, inactivation of dye, and re-staining in multiple cycles to deplete the antigens (Gerdes et al., 2013).

1.4. Conclusion

The applications of optical microscopy range from imaging living cells to studying and analyzing cell networks, micro-environments, and dynamic processes in living cells (Leung et al., 2011). However, there are some technical concerns that still need to be addressed such as photobleaching that can usually happen to SSIM and STED, resulting in destruction of fluorophores by exposure to light and subsequently producing a dimmer image (Rust et al.,

2006). Although the resolution is improved by reducing the PSF, the long dwell time will introduce photobleaching to the specimen. The spatial resolution of PALM and STORM can be hindered by the fact that the quality of resolution is mainly based on the number of detected and emitted photons. Super-resolution fluorescence microscopy has greatly contributed to a deeper understanding of biological and cellular mechanisms, although there are weaknesses in those techniques that can be further improved, they open doors and expand the potentials for biological and medical research (Leung et al., 2011).

Chapter 2: Imaging the Architecture of Neural Cells and Tissues

2.1. Introduction

Many researchers have used fluorescence microscopy to study the complex physiology and structure of the brain. Our understanding of the molecular architecture of neurons has also expanded due to the improvement in the ability to observe the fine details of the specimens. Tremendous efforts have been made in developing technology that enable obtaining the fine detailed information from the neural cells or tissues.

Synapses in the neuronal cells play a role in processing signals. Super-resolution fluorescence is required to image the distribution of synaptic proteins (Dani et al., 2010). The Brain Activity MAP Project launched by Church aims at understanding how the brain functions. Neural circuits that involve millions of neuron play a role in understanding the basic brain processes. The project focuses on reconstructing the complete record of neuronal activities by recording the action potential within the circuit of every neuron. The result of the project will benefit the society tremendously such as developing new tools to study brain diseases or understanding and providing more treatment options for diseases like Alzheimer's disease or Schizophrenia (Alivisatos et al., 2012).

2.2. Current Technologies

Electron microscopy is an alternative method for obtaining images of highly complex networks of neurons. However, the method is only limited to a small piece of tissue. Neurologists have turned to fluorescence microscopy to build a connectome, a map that shows

the connections and networks of neurons in the brain (Albanese and Chung, 2016). **Figure 1** illustrates that electron microscopy can be used to map neurons of the brain tissue.

Scientists at the Allen Institute have first demonstrated imaging the brain at the interval of 0.1 mm using two-photon microscopes (Oh et al., 2014). Nevertheless, the ability to track individual neuron is not an option for such technique. Publications have reported employing immunohistochemistry to investigate the distribution of tubulin in the brain specimen, revealing that the synaptic cleft and the presynaptic axon terminal lack tubulin antigen (Matus et al., 1975). Other groups also have introduced green fluorescent protein (GFP) for staining and imaging neuronal cells (Feng et al., 2000).

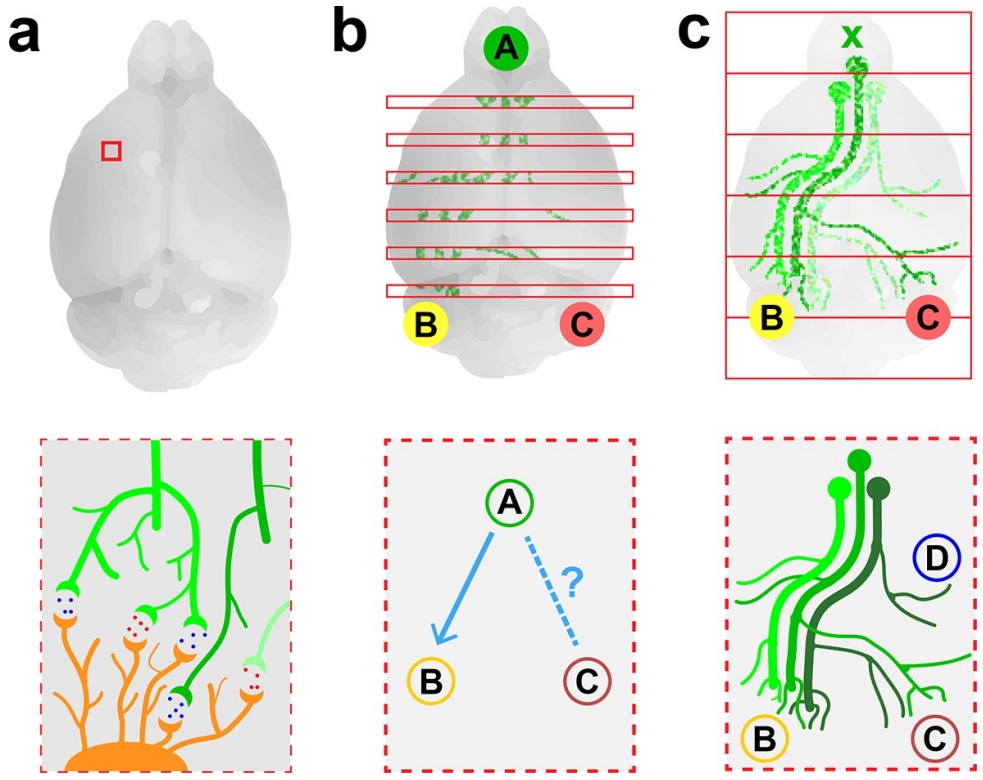

Figure 1. a) Neurons of the brain tissue can be mapped using electron microscopy in a small volume. b) The connections between different regions of the brain can be mapped using

fluorescence microscopy by recording and combining images of multiple slices. c) Tissue clearing is another method introduced by Economo et al. to enable projections of the entire brain (Albanese and Chung, 2016).

2.3. Tissue Clearing

Tissue clearing is a method used to observe detailed information of a sample in three dimensions (Albanese and Chung, 2016). Tissue clearing holds numerous advantages in obtaining a high resolution of a brain section. It also promotes immunohistochemistry and antibody labeling as well as in situ hybridization. This is especially important for studying the complex architecture of nervous systems. However, such method is often prone to distortion, shrinkage or loss of individual sections, making it technically challenging when reconstructing the information. If done correctly, samples no longer need to be sectioned to image. Tissue clearing promotes a uniform density of scattering molecules, allowing all wavelengths of light to be penetrated through the tissue. Most of the clearing techniques focus on avoiding inhomogeneities of scatterers in the sample.

Multiple methods have been explored and developed to solve the problem of inhomogeneities such as solvent-based clearing, simple immersion, hyperhydration and hydrogel embedding (Richardson and Lichtman, 2015). Other groups have tried to solve the problems by reducing the emerged scattering light to allow deep-tissue imaging (Tomer et al., 2014). Chung et al. has demonstrated the possibility of revealing the mapping work of the brain based on using a hydrogel-based meshwork that is built from the tissue. In **Figure 2**, the lipid bilayers can be removed in a non-destructive way by creating a barrier to allow chemical penetration. The polymerization is triggered by infusion of monomer molecules into the brain with the help of

crosslinkers, resulting in removal of lipids that lack the necessary reactive groups. The detergent is applied to the sample for subsequent removal of the additional lipids. The hydrogel-tissue hybrid is compatible with most of the fluorescence techniques and it holds the potential for studying the molecular phenotyping of tissues (Chung et al., 2013).

However, Chung et al. has also observed the expansion of tissue after tissue clearing which also implied the possibility of distortion or loss in structural information, causing damages to the tissue. It has reported that about 8% of the protein is lost during this application (Chung et al., 2013).

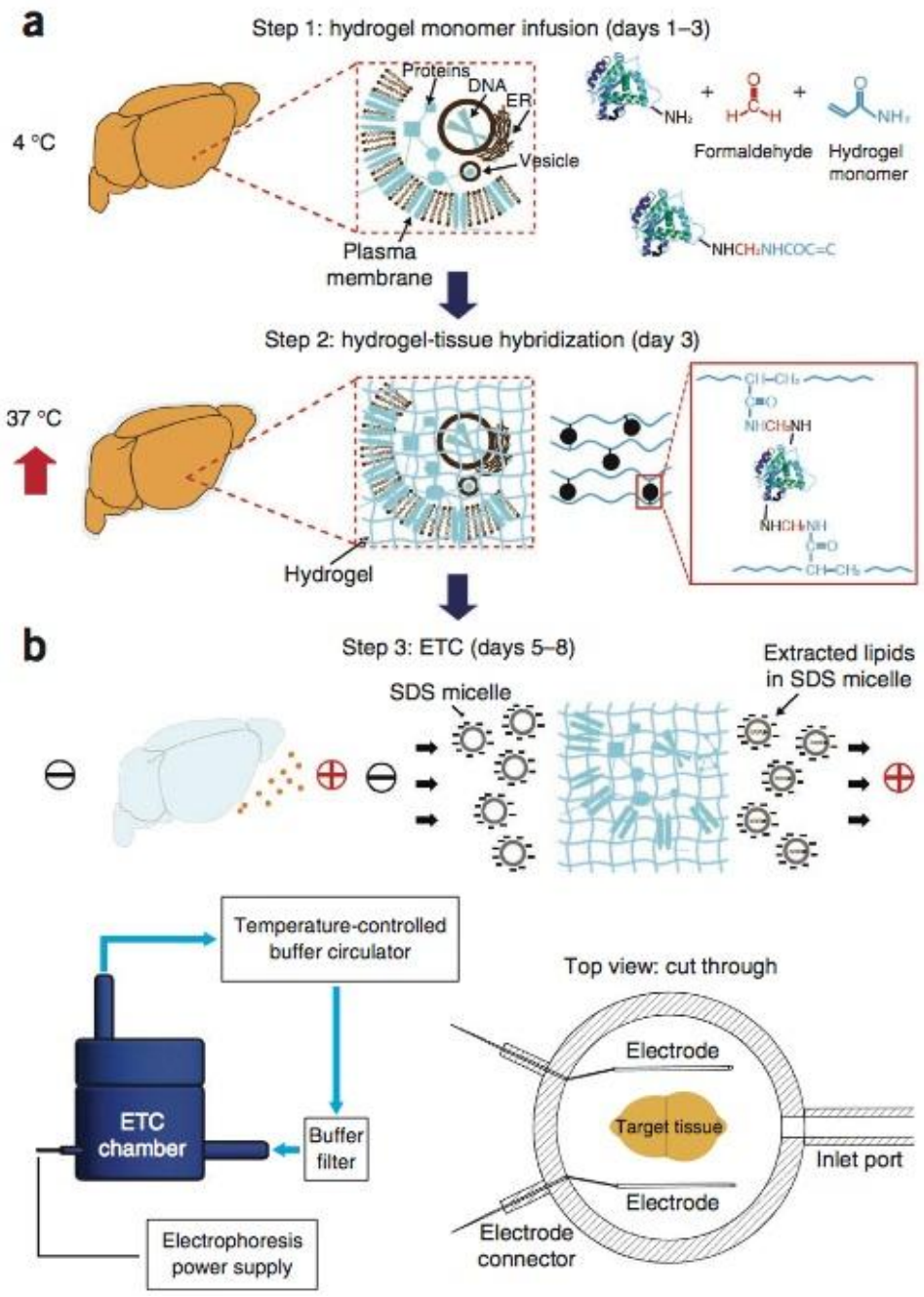

Figure 2. The hydrogel monomer composed of acrylamide and bisacrylamide are infused into the tissue along with formaldehyde at 4 C. In this process, the formaldehyde crosslinks the monomers to proteins. The biomolecule conjugated monomers will initiate the polymerization process when the tissue is incubated at 37 C (Chung et al., 2013).

The process supports the structural integrity of the tissue thus obtaining the important molecular information. Lipids that lack the functional group appear unbound for further removal. Chung and his coworkers have further developed a method using ionic extraction technique (active-transport organ-electrophoresis) in replacement of the hydrophobic organic solubilization because organic solvents tend to alter the imaging time. The ionic micelles allow thorough extraction of lipids due to its highly charged nature while obtaining the molecular information. The set back to this technique is to make a large data sets, because it requires both the electron microscopy and light microscopy to visualize the entire patterns of neurons, postsynaptic cells, axon terminals and synaptic contacts (Chung and Deisseroth, 2013). **Figure 3** illustrates different methods of clearing techniques that can be used to remove the excess lipids.

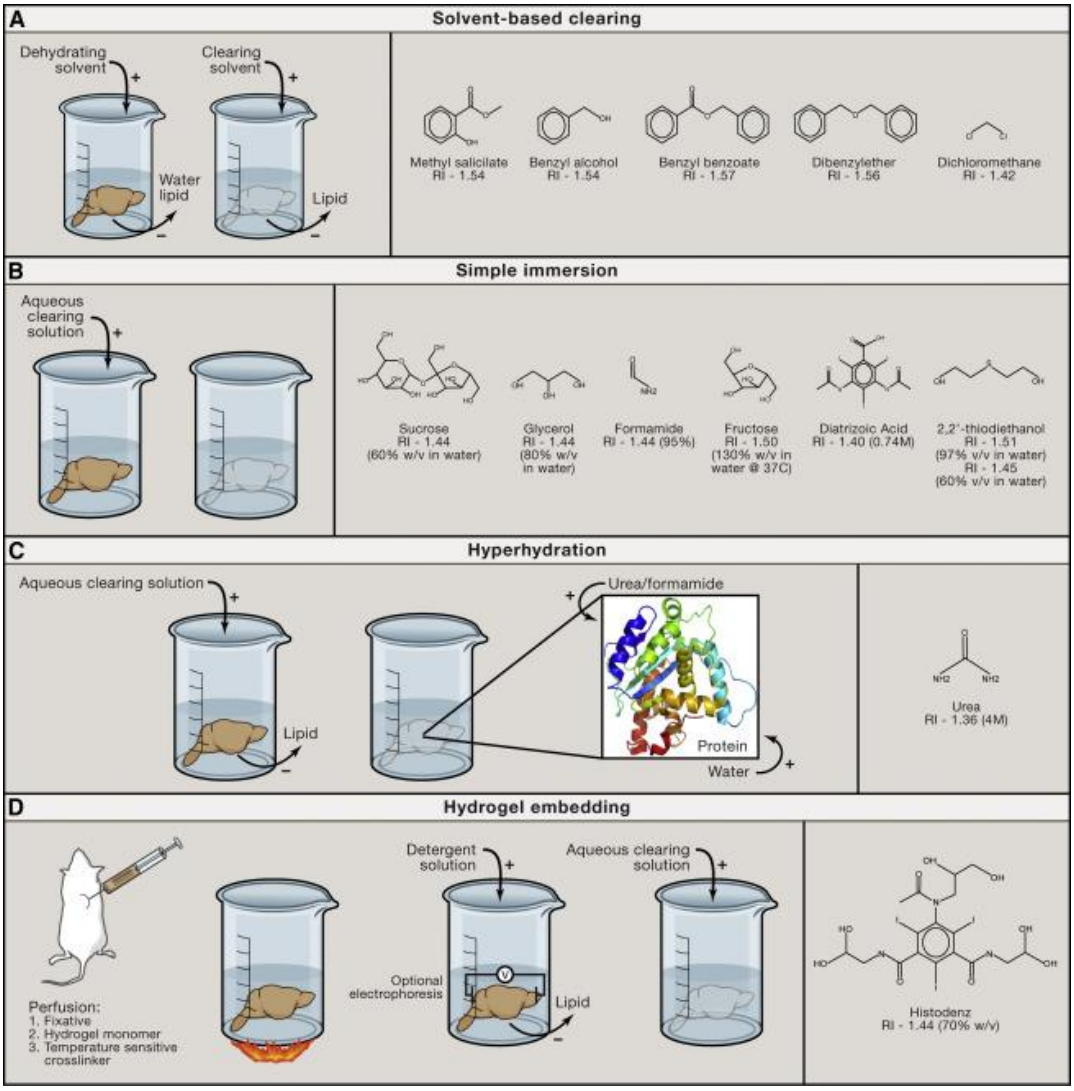

Figure 3. a) Solvent-based clearing: Dehydration of the tissue and removal of lipids. Second, high refractive index solvent is applied to the tissue as lipid solvation and clearing occur. b). Aqueous clearing solution: Simple immersion occurs when the tissue is immersed in the solution that matchs the refractive index. Then the sample undergoes hydration to remove lipid, causing the refractive index to become lower. Lastly, the tissue is immersed in a medium that corresponds to the new refractive index. c). Hyperhydration: This technique involves a clearing step where urea or formamide enters the regions that are composed of highly refractive index proteins, resulting in an osmotic pressure. d). Hydrogel embedding involves a fixative, a

temperature sensitive crosslinker and the monomer. The tissue is immersed in a detergent solution aiming to remove the lipid. The lipid-free tissue then is immersed in a refractive index matched solution (Chung and Deisseroth, 2013).

Chapter 3: Development of an Imaging Technique Using PER as a Method for Signal Amplification

3.1. Background

High selectivity and sensitivity in detecting a region of genomes among a pool of gene sequence can be difficult due to single nucleotide differences. Rolling circle amplification (RCA) and hybridization chain reaction (HCR) are two signal amplification techniques that demonstrate high sequence specificity, enhancing genetic analysis through exploration of point mutations found in human genomic DNA.

RCA occurs when the ligated padlock is formed while the gap of the open circle probe is filled by small oligonucleotides. The padlock then becomes bound to the complementary primers for amplification, followed by catalysis of the DNA polymerase to promote the activity of strand displacement (Lizardi et al., 1998). HCR is a technique that involves hybridization between two sets of DNA hairpin for detecting specific DNA sequences. The scheme of HCR is as follow: A chain reaction of hybridization is triggered by adding an initiator stranded DNA to two hairpins of mixed species (**Figure 4**). The hairpin of one species then opens as the DNA initiator is added to the mixture, making the new single-stranded DNA region exposed to the hairpin of the other species. Nicked double helix forms as the result of chain reaction and grows until the hairpin supply depletes (Dirks and Pierce, 2004).

The multiplex fluorescent in situ hybridization method holds advantages such as deep sample penetration and precise signal localization. It has been reported that in situ amplification method has been considered the method of choice due to its high signal to background ratios (Choi et al., 2010).

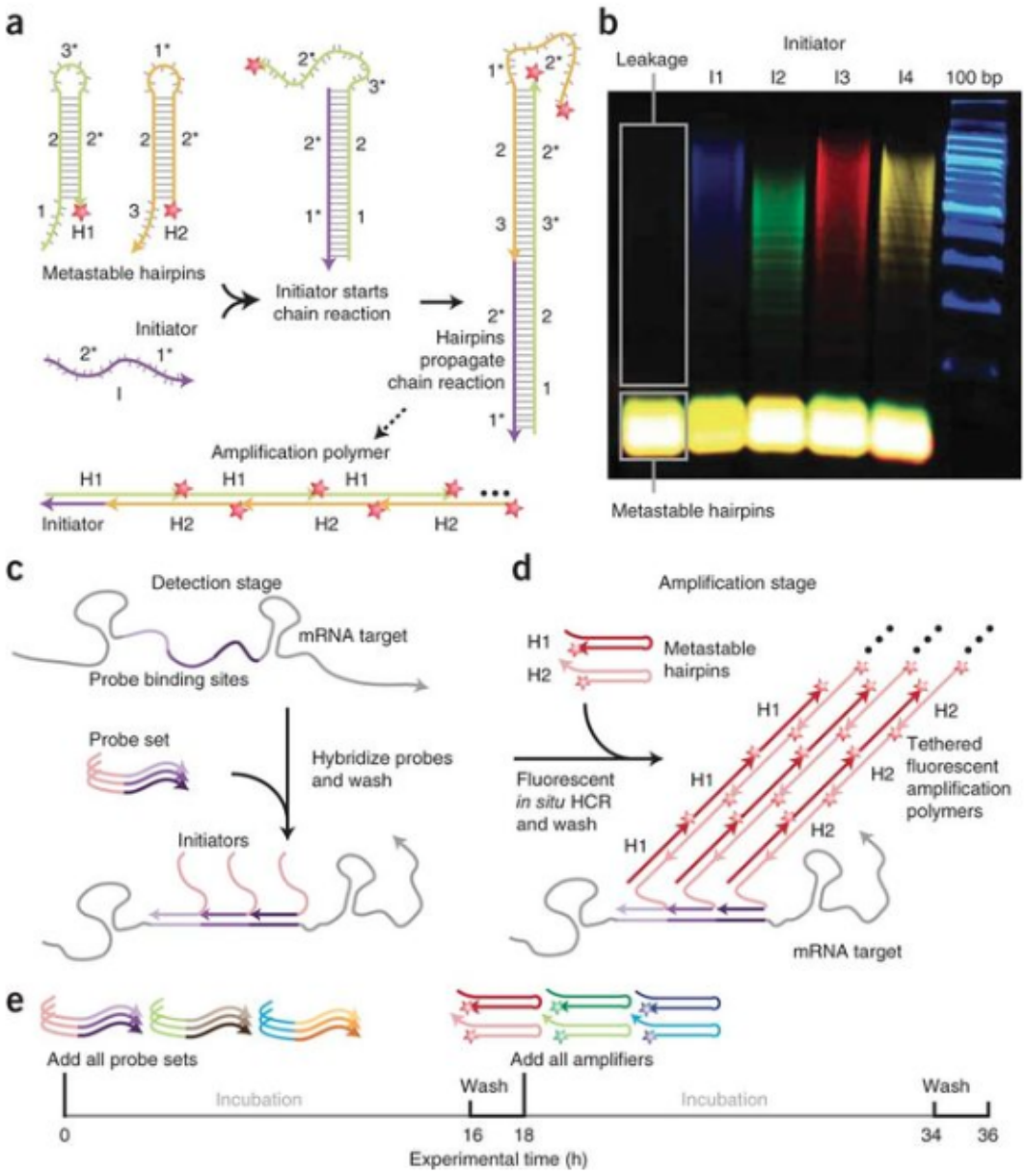

Figure 4. a) The HCR consisted of two hairpin species that are designed without an initiator. Hybridization of the initiator to the hairpins results in breaking the hairpins and forming a nicked double-stranded polymer. b) An orthogonal amplification is demonstrated using an agarose gel. c) All the targets are shown to be detected using complementary RNA probes after in situ hybridization while unused probes are being washed away. d) In the amplification stage, the addition of initiators triggers the self-assembly of the fluorescent amplification polymer. e) The

experimental timeline demonstrates the feasibility to perform orthogonal HCR amplification regardless of the number of target mRNAs as different target mRNAs carry the complementary initiators labeled with specific fluorophores (Choi et al., 2010).

Moreover, staining can be done via polymerization mechanism. The probes that carried orthogonal initiators are used to detect targets, and the HCR amplifiers with distinct fluorophores are used to perform the amplification. The accuracy of the signal localization remains high because each amplification polymer is bound to its initiating probe. However, although in situ hybridization has become the method of choice when studying architecture and biological functions of the circuits, the details on the molecular information about the relationships between each neuron circuits remain unclear due to insufficient knowledge (Choi et al., 2010).

3.2. DNA Synthesis

DNA encodes genetic information of living organisms and it stores information that holds an important key in discovering the foundational elements in the genome that can benefit in biology, biotechnology, and medicine (Douglas et al., 2009). DNA can also be used to construct complex synthetic molecular architectures or devices in 3D shapes such as DNA origami (Dunn et al., 2015), DNA tiles (Wei et al., 2012), DNA nanotubes (Mohammed et al., 2016), DNA bricks (Ke et al., 2012), DNA crystals (Winfree et al., 1998), opening doors for expanding the materials for medical applications.

Constructing new DNA sequences helped scientists unravel genetic sequences to better understand biology (Kosuri and Church, 2014). There are several applications for DNA synthesis that are considered superior to the natural sequence due to easy accessibility and manipulation.

Column-based oligo synthesis reported by Todd includes phosphodiester, H-phosphonate and phosphotriester approaches (Michelson et al., 1995). The phosphoramidite chemistry consisted of a 4-step cycle has been widely used in producing DNA constructs. Array-based oligo synthesis developed by Affymetrix involves the use of light-activated chemistry that also attributes to DNA microarray development (Singh-Gasson et al., 1999). Gene synthesis is another method for oligo synthesis introduced by Gobind Khorana and his coworkers by employing T4 DNA ligase to seal the oligos. Large fragments are produced as a result of joint complementary overlapping strands (Agarwal et al.,1970).

Although array-based gene synthesis is cheap, it is difficult to use for the purpose of gene synthesis due to a large production of oligos, resulting in low concentration of each oligo. Tian et al used PCR amplification to overcome the issue regarding low concentration of the oligos before hybridization. Kosuri et al. tried to solve the problems for pool complexity in which add difficulty in constructing individual genes due to cross-hybridization via a predesigned barcode that allowed categorization of oligos. However, DNA oligos are often synthesized in a non-autonomous way by applying different chemical methods to achieve the outcome (**Figure 6**) (Kosuri and Church, 2014). **Figure 5** illustrates different amplification methods that are limited to producing a fixed copy of existing sequences.

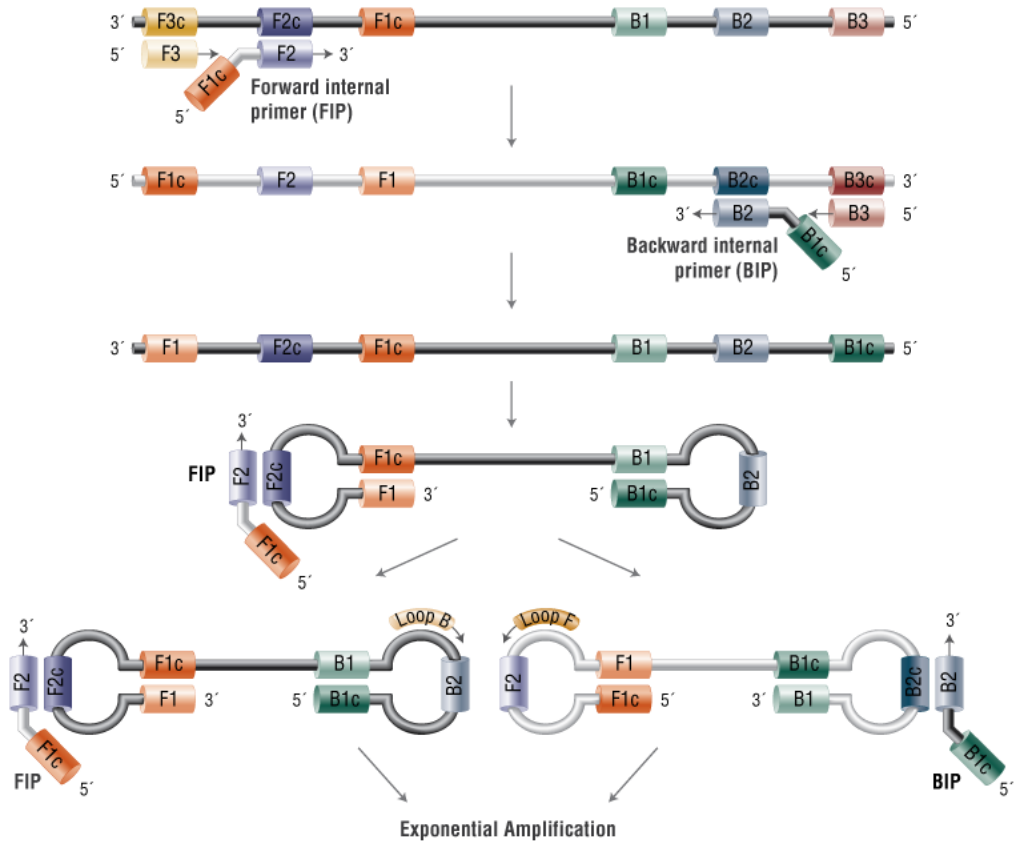

Figure 5. Amplification methods (e.g. PCR, LAMP and RCA) are limited to producing identical copies of existing sequences (Biolabs).

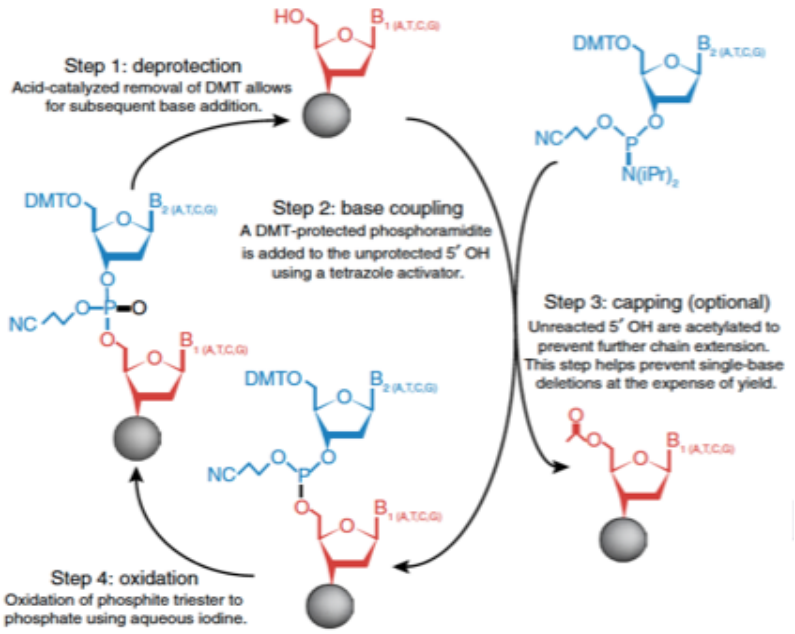

Figure 6. Chemical synthesis is another method that is also non-autonomous, and the method is not compatible with some synthetic systems (Kosuri and Church, 2014).

3.3. Primer Exchange Reaction

Our group has initially developed this method to overcome the problems associated to the limitation on autonomously synthesizing single stranded sequences. Chemical synthesis and other amplification methods (PCR and RCA) are non-autonomous and they are limited to producing identical copies of existing sequences.

PER is a programmable method that enables precise control of the structure and function of a single stranded DNA through a user-specific sequence. PER cascades start off with a prescribed primer. PER adds a new primer with a specific sequence to the existing primer, and the formation of a programmable cascade is triggered by the newly extended primers (**Figure 7**). The cascade enables a nascent DNA strand to grow along a predesigned pathway in an autonomous fashion. A new strand will only be produced in situ when the PER hairpins coexist

with a complementary PER primer. **Figure 8** illustrates PER reaction cycle in which the primer is bound to a user prescribed hairpin, followed by strand displacing elongation via polymerase, a random walk process known as branch migration where the newly synthesis domain competes with the hairpin, and transcript dissociation.

PER provides a way to program the sequence to cope with different environmental conditions. The PER cascades can also be implemented on molecular staining. Primer exchange hairpins utilize the auto-cycling proximity recording mechanism where the APR cycle copies and releases hairpins. The DNA-based copy-and-release hairpin (CRH) solves the challenges in recording in the circumstances of target proximity (Schaus et al., 2017). CRH allows copy and release of a specific sequence onto the primer strand to extend the primer strand on the single stranded template. Polymerization can be terminated when coupling to a stop sequence (G-C pair). PAGE denaturing gel is used to track the primers labeled with dyes on the 5' ends along with the progression of PER (**Figure 9**). Bst large fragment polymerase is considered our choice of reagent due to its strong strand-displacing capability and the lack of exonuclease activity. The number of steps and sequences can be prescribed by adding additional bases in the copy region of PER, resulting in efficient binding of primers as well as effective dissociation of the elongated hairpins. A special hairpin (Clean G) undergoes pre-incubation before the introduction of telomerization primers to clean up extra dGTPs. Adding magnesium helps increase the reaction rate of telomerization. A protector strand is introduced to block the binding sites of a specific primer, leaving an extra region ('clamp' sequence) to solve leakage problem (Kishi et al., 2017).

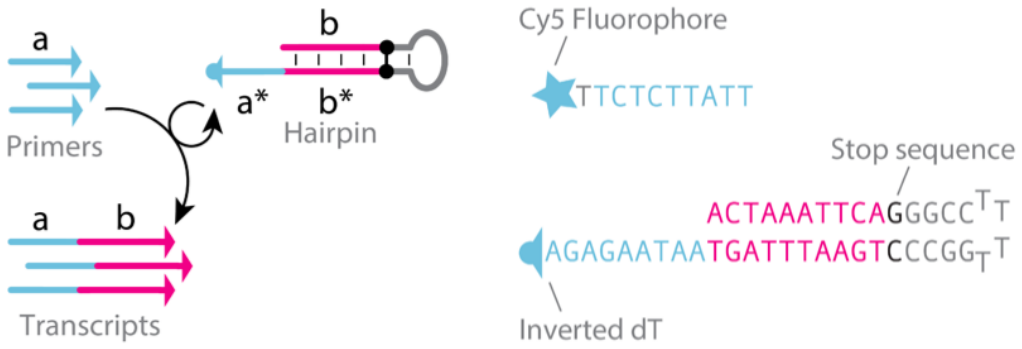

Figure 7. PER mechanism. The PER reaction is triggered by the user-specific catalytic hairpin to produce transcripts. Chemical modifications can also be used as an alternative method to terminating a sequence. The stop sequence in conjunction with methylated RNA bases and iso-dG/iso-dC pairs promote inactivation of the extension of ssDNA oligos by inhibiting the action of polymerase. On the other hand, the inverted dT or a polyT tail can be utilized in blocking the extension of hairpins to prevent further extension (Kishi et al., 2017).

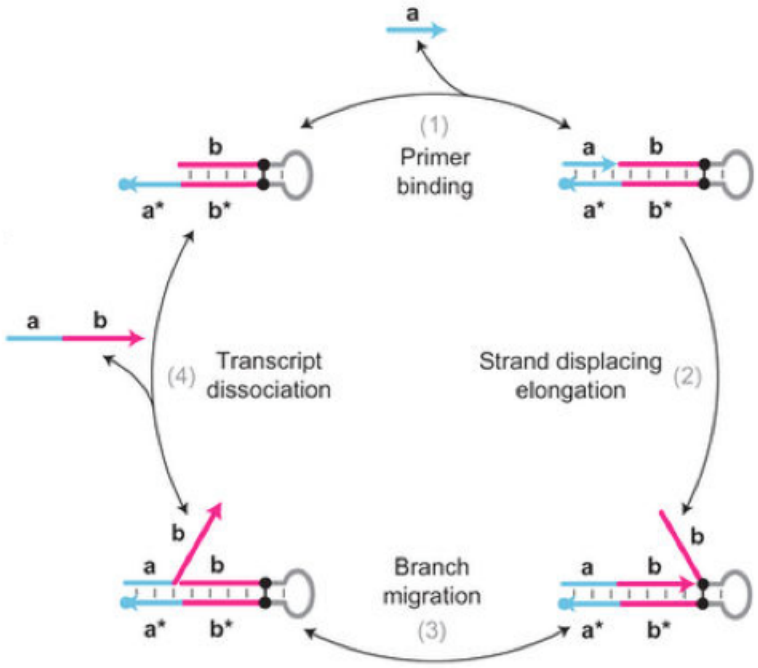

Figure 8. PER reaction cycle. In step 1, the primer with a user-specific sequence is bound to the complementary sequence on the 3' end of the primer. The Bst large fragment polymerase elongates the primer by copying the PER hairpin region. Branch migration demonstrates the copied domain competing with the region on the hairpin through a random walk process (Lee et al., 1970). In step 4, replacing of the copied domain results in detachment of the extended primers from the hairpin. Another cycle can occur as the unoccupied hairpin interacts with other primers. (Kishi et al., 2017).

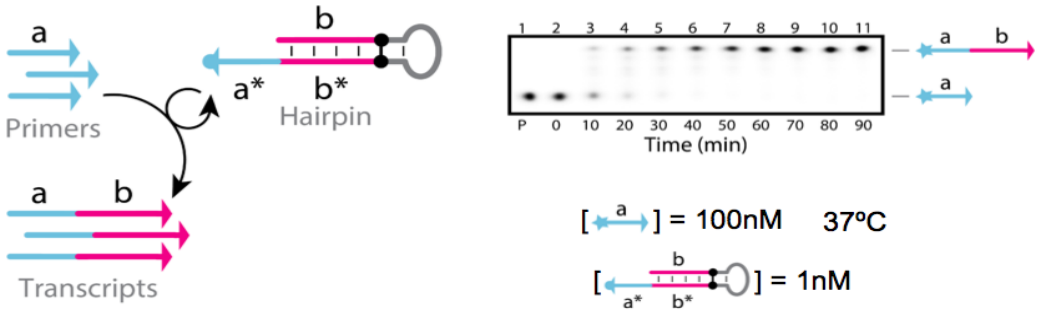

Figure 9. Gel electrophoresis is used to track primers that are labeled with dyes on the 5' ends. Extension products for different concentration of hairpins can be demonstrated by the PAGE denaturing gel with the primer at 100 nM. Formamide and EDTA are used to stop the reaction prior to enzyme inactivation by heat (Kishi et al., 2017).

3.4. The extension reaction resulted from concatemerization can be used to amplify signals

Fluorescent concatemers can be constructed when incubating the primers with specialized hairpins in the presence of the complementary miRNA. Visualization of a specimen is accomplished by fluorescent hybridization.

3.5. AIM

The PER reaction driven by polymerase recognizes specific DNA sequence using a pre-designed hairpin to achieve autonomous DNA synthesis. A growth pathway occurs as a random sequence is engineered into a wanted sequence in a programmable fashion, allowing construction of new DNA materials that can cause responsiveness to the environmental changes. PER cascades can further be implemented on the immunofluorescence to amplify signals with in vitro extended probes to effectively achieve high-resolution imaging.

Chapter 4: Achieving Super-Resolution Imaging by Employing Expansion Microscopy

4.1. Background

Expansion microscopy is a recently emerging technology that uses the swellable properties of the hydrogel to increase the magnification of a specimen. ExM enables 3D resolution imaging of a specimen that is out of the question for the conventional light microscopy. ExM works by anchoring the fluorescent dyes to the absorbent hydrogels that can be formed via polymerization. The biomolecules fixed on the specimen retain the spatial architectures and biological information of the specimen as the monomers and the crosslinkers permeabilize the tissue, resulting in densely crosslinked hydrogels with the aid of an initiator and an accelerator. Homogenization of the embedded hydrogels is accomplished by high temperature denaturation. The swelling behavior of the crosslinked hydrogel could be observed by adding the solvent, subsequent to digestion process to allow the biomolecules to be pulled apart (Gao et al., 2017).

The discovery of the expansion microscopy was first reported by Boyden and his coworkers. Boyden and his coworkers demonstrated utilizing the polyelectrolyte gel to enable physical expansion through dialysis of a solvent. The procedure began with staining the specimen with probes that could be incorporated into the polymer. They developed a fluorescent labeling technique composed of a methacryloyl group linking to the polymer network, a chemical fluorophore and an oligonucleotide to recognize specific sequences on the secondary antibody. They applied the techniques to both the culture cells and brain tissue and retrieved magnified images with ~ 60 nm lateral resolution (Chen et al., 2015).

Boyden and coworkers also developed protein-retention expansion microscopy by replacing the proteins with the labeling biomolecules to overcome the barrier of imaging without antibody labeling. The nanoscale imaging is demonstrated by anchoring the genetically encoded fluorescent proteins along with the conventional secondary antibodies that survive the digestion process (Tillberg et al., 2016). Boyden and coworkers further developed expansion FISH (ExFish) to achieve nanoscale-resolution imaging of RNA which has been remained as a difficult task to be solved. Meanwhile, Boyden and coworkers developed a strategy using a small molecule linker to covalently attaching RNAs to the swellable gel, thus allowing RNA to be identified and visualized throughout the cells and tissues in nanoscale precision (Chen et al., 2016).

Vaughan and coworkers also worked on developing new methods to covalently attach the fluorophores to the polymer. Vaughan employed the conventional fluorophore-tagged secondary antibodies to ExM. Vaughan proposed that the conventional fluorescently labeled antibodies would survive the protease treatment if the number of linkages was sufficient. The fluorescent signal after digestion treatment could still be preserved by fixing the immunostained culture cells with the amine-reactive small molecule methacrylic acid *N*-hydroxysuccinimidyl ester (MA-NHS) or glutaraldehyde (GA) (Chozinski et al., 2016). Others have reported using GA crosslinking to covalently link the proteins or enzymes to the polymer (Weston et al., 1971). The distortions in correlation with pre-expansion and post-expansion were significantly reduced in the presence of GA.

Vaughan reported that although the fluorescent retention after post-expansion was better using the DNA-labeled antibodies, the culture cells that were treated with either MA-NHS or GA

demonstrated 4x brighter in fluorescent signal (Chozinski et al., 2016). **Figure 10** illustrates the comparison between DNA method and MA-NHS/GA methods.

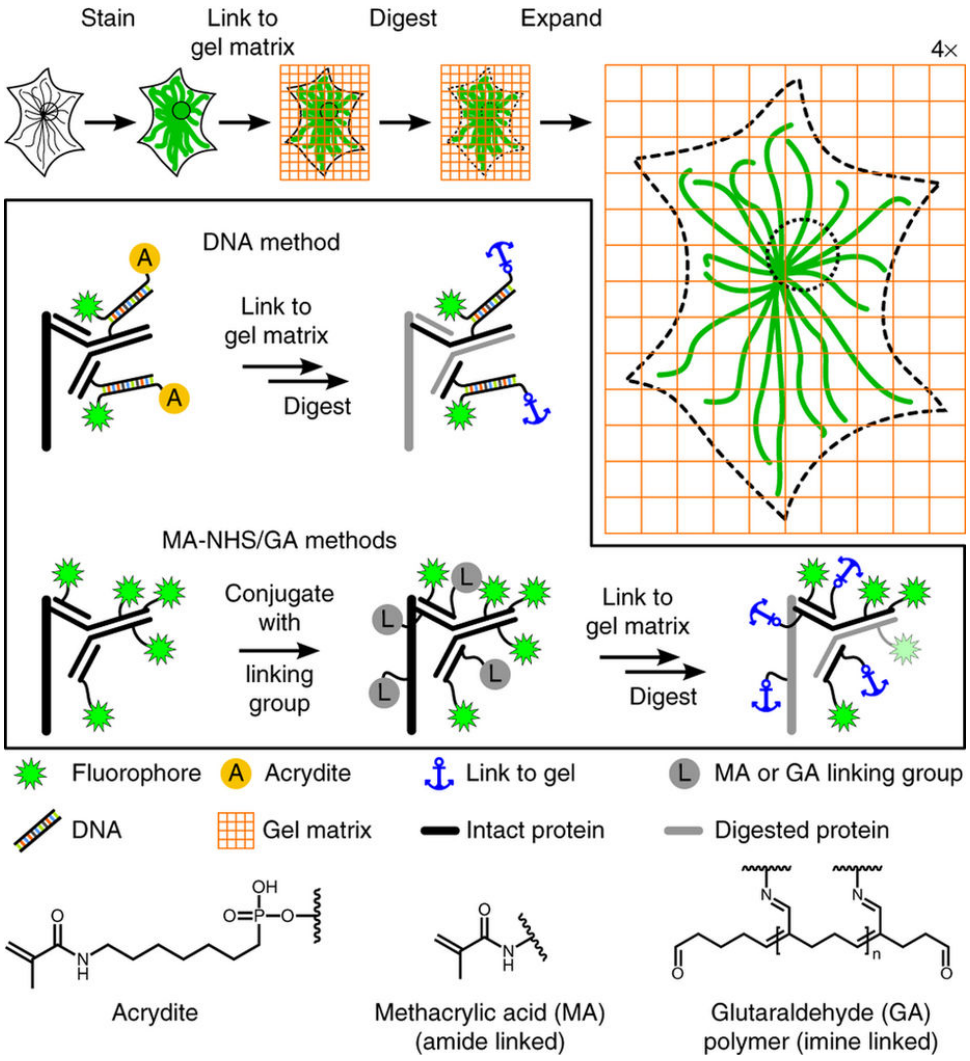

Figure 10. The original DNA method highlighted in the box region uses a DNA oligonucleotide to hybridize to the complementary sequence that is attached to a particular secondary antibody. A chemical fluorophore has been used for direct visualization. On the other hand, the MA-NHS/GA methods demonstrate similar results by employing the samples with polymer-linking groups via MA-NHS/GA treatment (Chozinski et al., 2016).

ExM has become more accessible to the public after introducing the polymer-linking methods to replace the customized fluorescent label initially reported by Boyden. Chung and coworkers introduced a method called magnified analysis of the proteome (MAP) to achieve super-resolution in sample specimens. The method enables a multilevel of imaging of intact biological samples by preserving the 3-D subcellular architecture and molecular information that have been lost by the digestion step during the ExM (Chung et al., 2013). The loss in structural and intercellular connectivity during the hydrogel- tissue hybridization step is reported in CLARITY that can result in limitation on gel permeability and tissue damage.

Chung demonstrated using high concentration of acrylamide monomer to prevent the crosslinking between the intra- and inter-proteins. The reactive methylols result from amine residues can react with excess acrylamide monomers, hence anchoring the proteins to the swellable hydrogel while limiting interprotein crosslinking behavior (Ku et al., 2015).

4.2. Development of Superabsorbent Hydrogels that Are Tough and Highly Stretchable

Superabsorbent polymers have been commonly used as a tool to absorb liquids as well as scaffolds for tissue engineering (Lee et al., 2001). Developing hydrogels that are robust to withstand the resistance while preserving the swelling property can benefit biological studies (Rehfeldt et al., 2007). There are several published works focusing on adding more strengths to the hydrogel such as double network hydrogels that are composed of two intertwined cross-link polymer networks which tend to display a higher mechanical strength (Gong et al., 2003).

Hydrogels that are developed to be ionically crosslinked are shown to be mechanically strong and elastic (Henderson et al., 2003). The key properties in making the hydrogels superabsorbent rely on the capacity to swell and expand. Superabsorbent hydrogels are typically

made by free-radical initiated polymerization with a cross-linker in aqueous solution (Sun et al., 2012). The concentration of monomer contributes a role in affecting the property of the hydrogel. The toughness increases as a result of higher monomer concentration. The polymerization is typically initiated using thermal initiators. The cross-link polymer becomes neutralized once the polymerization process is complete (Peak et al., 2013).

Most hydrogels lack the capability to be stretched, because the short-chain network of the gel exhibits rupture and inhomogeneous deformation when a force is applied (Peak et al., 2013). Vlassak and Zhigang demonstrated synthesizing the hydrogels that were stretchable and tough via combination of ionically and covalently crosslinked networks. The hydrogels made from ionically crosslinked alginate and covalently crosslinked polyacrylamide could be stretched >20 times its original strength without cleavage (Sun et al., 2012). Srinivasa and coworkers found a class of hydrogels that provided high swelling property while preserving the toughness. The gel was made using the monomer *N,N*-dimethylacrylamide (DMAA) which was a derivative of the acrylamide group. DMAA can undergo self-crosslinking without any presence of the crosslinking monomers. The gel can expand significantly in aqueous solution with the help of ionic co-monomer sodium acrylate (SA) while exhibiting high mechanical properties (Cipriano et al., 2014).

4.3. Studying the Mechanical Properties of Hydrogel via Atomic Force Microscopy

The atomic force microscope (AFM) is a scanning probe microscope that has been widely used in diverse biological applications. The AFM uses cantilevers which can be referred to as a type of spring to measure the force between the sample and the tip. The cantilever deflection or bending can be detected by measuring the local attractive or repulsive force

between the sample and the tip (**Figure 11**, **Figure 12**). Electrical signals are collected from the cantilever deflection to produce images (Eaton and West, 2010).

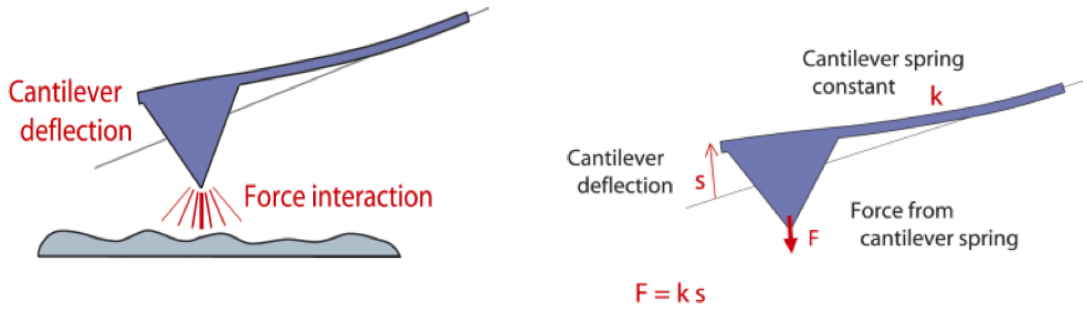

Figure 11. The reflection of the cantilever can be caused by the attractive or repulsive force between the tip and the sample, resulting in the cantilever moves toward or away from the sample (Web).

The photodiode is a four quadrants that are used to calculate the deflection signal as the angle of the reflected laser beam changes due to cantilever deflection, causing laser spots to fall on different locations of the photodetector. The AFM provides high-resolution imaging as well as 3D topography information and mechanical properties relating to samples. Cantilevers can be referred to as springs, and the extension of springs can be explained by Hooke's law.

$$F = - k * s.$$

The force **F** is required to extend the spring depending on the distance **s** that travels in a linear way. Hence, the force is doubled when the deflection of the spring doubles (Cleveland et al., 1993).

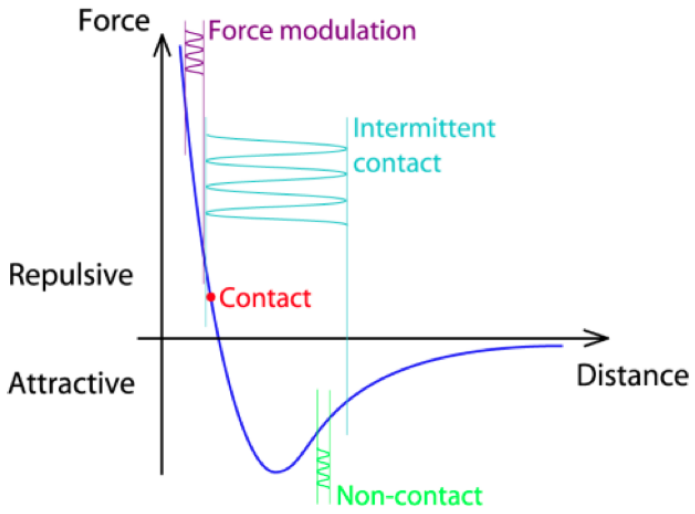

Figure 12. A general curve is drawn showing the general approximation of the tip-sample force against distance. Force modulation happens when the model of two objects interact with each other in a range of distance separating the two. Intermittent contact mode moves between the repulsive and the attractive curves. No contact mode is the only mode that stays in the attractive curve (Web).

4.4. Force Spectroscopy

AFM can be used as a useful tool in measuring the sensitive force. Force spectroscopy is a force measurement provided by AFM that moves the cantilever towards the surface in a vertical direction until the cantilever is retracted. The initial force is too small to provide measurable deflections of the cantilever as the cantilever first approaches the surface of the sample. Van der Waals and capillary forces are known as the attractive force that overcomes the spring constant of the tip at some point when the tip contacts the surface. The repulsive contact forces increase as the space between the sample and the base decrease, resulting in deflection of the cantilever. The tip may remain on the surface due to adhesion when the cantilever is retracted

from the surface (**Figure 15**). The tip can also break free when the force coming from the cantilever is sufficient to overcome the adhesion (Morita et al., 2015). **Figure 13** illustrates that there may not be any obvious snap to contact when the sample is in liquid due to the insignificant compression that can be ignored.

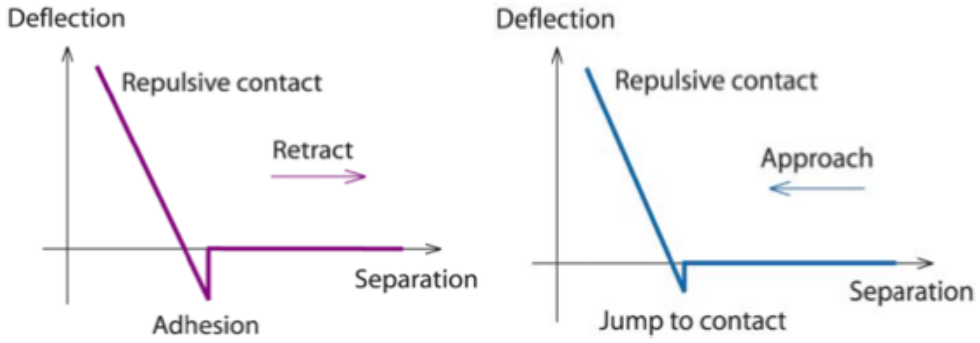

Figure 13. The force increases gradually shown in the force curve without the obvious snap to contact when the sample is in liquid. Hence, it may be difficult to consider the point when the tip and the sample come into contact since the initial compression of the surface may be insignificant enough to show any deflection of the cantilever (Web).

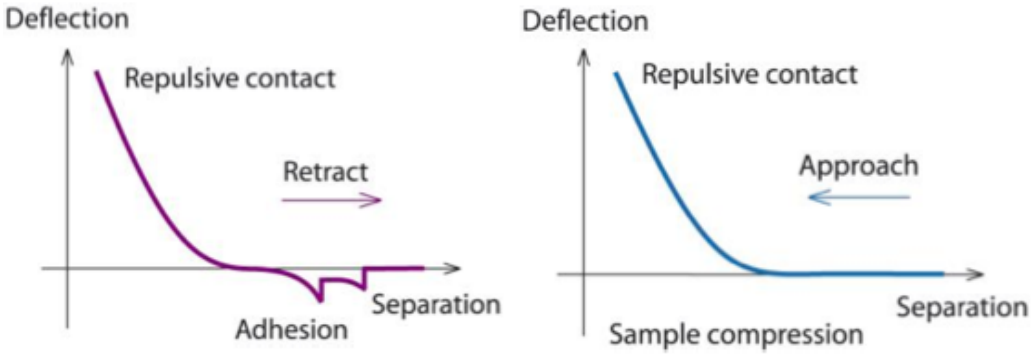

Figure 14. Hysteresis can happen when the tip retracts from the surface. The tip is anchored on the surface of the sample until there is enough force to break free the adhesion. The force curves

can be repeated at multiple locations to generate a map of tip-surface interaction. Data processing for analysis is done by measuring the movement of the force curve against the deflection which can also be referred to as distance vs force (Web).

In **Figure 14**, the event of hysteresis can happen between the extend and the retract portion of the force curve owning to the viscous behavior of the hydrogels. Most of the biological samples are neither homogeneous nor absolutely elastic which is in conflict with the Hertz model.

Figure 15. An interaction occurs when the cantilever in the air is approaching the surface followed by adhesion of the tip and the sample (Web).

4.5. Young's Modulus

Young's modulus is known as the modulus of elasticity. Young's modulus has been commonly used to describe the elasticity of an object after a tension or compression is applied, and the resistance of an object to being deformed. It can evaluate the amount of compression or tension that needs to be applied for an object to deform (Gibson et al., 1996).

The Young's Modulus, E is given by:

$$E = \frac{tensile\ stress}{tensile\ strain}$$

$$tensile\ stress = \frac{tensile\ force}{cross\text{ - }sectional\ area} = \frac{F}{A}$$

$$tensile\ strain = \frac{extension}{original\ \ length} = \frac{\Delta L}{L}$$

Substituting (2) and (3) into (1) gives:

$$E = \frac{F.L}{\Delta L.A}$$

The material can begin to deform when it reaches a certain stress or tension. A stiff material has a high Young's Modulus, and the deformation can be minimal, whereas a soft material has a low Young's Modulus. Young's Modulus is an important factor when designing a material especially in the field of tissue engineering to prevent possible rupture or breakage (Wang, 1984).

Chapter 5: Methods

5.1. PER Imaging Preparation and PER-2 Ab staining

5.1.1. DNA Antibody Conjugation

DNA-thiol reduction

Thaw DNA oligo (from -80degree freezer) at RT. Rinse amicon ultra centrifugal filter (50k, 500 ul) with 400ul 1x PBS, centrifugate: 5000 rcf, 6 min, at RT. Dissolve DTT (1st drawer) with 100ul 1x PBS/EDTA (pH8.0) to get 500mM concentration (there is a pellet of DTT in the bottom of the tube, do not get rid of the foil because it will generate a smell with dissolved; when adding 1x PBS/EDTA, use the tip to press the pellet to make sure it dissolves completely) vortex, spin down, react for 2hr at RT, wrap with aluminum foil to avoid light.

Antibody-crosslinker

Add ~60ul 2mg/ml antibodies to filter, rinse tips with PBS. 5000 rcf, 6 min, at RT. Thaw crosslinker SM(PEG)2 at RT (SM(PEG)2 is sensitive to water, do not open the lid). Add 400ul PBS to filter to remove sodium azide. Centrifuge: 5000 rcf, 6 min, at RT. Weigh crosslinker, add DMF (DMF is on the 2nd shelf, use a syringe to get it) to dissolve the crosslinker with a final concentration of 10mg/ml, vortex. Add 50ul crosslinker to each new tube, store at -80°C (stock, should be used within 10days). Reverse the filter and put into new tube, 1000 rcf, 3 min, at RT, to collect antibodies. Measure the concentration of antibodies (protein 280, IgG, blank: PBS) and volume 183ul DMF + 17ul crosslinker. Add 2.5ul of the diluted crosslinker into 100ul Ab solution. Vortex with low speed briefly. Add another 2.5ul of the crosslinker and vortex (200ug

Ab ~ 5ul crosslinker). Seal antibodies with parafilm, wrapped with aluminum foil at rotator at 4°C for 2 hr.

Purify DNA oligos with column (remove DTT)

Wash the NAP column with 10ml nuclease-free water in total (3mlx3+1ml, add water when the column stops dripping). Prepare 10 1.5ml eppendorf tubes in advance, and label them. Add 100ul DNA oligos (all, carefully but not too slowly). Add 400ul water (100ulx4, add to the wall slowly, change tips) and flow through, collect the liquid in the 1st tube. Add 500ul water directly. Immediately collect DNA oligos into 10 1.5ml eppendorf tubes (3 drops in the 2nd tube, 2 drops in next 3 tubes, 1 drop in rest tubes). Measure the concentration of DNA oligos (ssDNA) (from the 3rd one, measure the tubes until the concentration decreases). Mix up the highest two tubes. Measure concentration of the mixed one.

Purify antibodies (remove excessive crosslinker)

Prepare Zeba Spin Column (in the drawer of the fridge), centrifugate: 1500 rcf, 1min, RT. Wash the column with 350 ul PBS, 1500 rcf, 1 min, RT, for three times. Put the column into a new tube and label the dose side. Add half volume (~50ul) of the antibodies prepared into each column. 1500 rcf, 2 min, RT, dose face outside.

antibody-crosslinker + reduced DNA

Ab: 2mg/ml in 100ul => 1.33nmol

DNA: xng/ul in (52500/x) ul => 15nmol (actually the volume depends on the molecular mass)

Store in cold room on a rotator overnight, wrap in aluminum to avoid light.

5.1.2. Imager strand HPLC purification

The sample was resuspended in 47.5 ul H2O and sealed with the parafilm, and vortexed shortly. 2.5 ul of 2 M TEAA was added, vortexed, and transferred to HPLC tubes. The sample bottle was positioned and the fraction collector was reset. The specific sequence was set and the pump pressure was checked before collecting the samples in a 96 well plate.

5.1.3. Conjugating imager strands with fluorophores

Conjugation.

a). Prepare 3′ (or 5′) amino-modified DNA oligonucleotide in ultrapure water at 1 mM concentration, prepare NHS ester-modified fluorophore (e.g., cy3b, atto655, atto647n) in DMSO at 20 mg/ml, and prepare 1 M NaHCO3 buffer at pH 8.0.

b). Prepare conjugation reaction solution by adding 20 µl amino-modified DNA solution, 2 µl NaHCO3 buffer, and 4 µl fluorophore NHS-ester solution in order, and gently vortex to mix.

c). Incubate the conjugation solution on a shaker and protected from light for 2-4 hr (room temperature).

Column purification.

a). Pre-wash size-exclusion column (GE NAP-5) with 2 ml ultrapure water four times.

Bring total volume of conjugation solution to 100 µl and add to column, and add more ultrapure water (~3 ml) to finish collection. Collect every three droplets to a separate well on a microplate.

B). Determine peak position and width with fluorescence plate reader (optional), and combine and collect the wells with brightest signals (typically 3–4 wells close to the beginning).

C). Freeze the sample with liquid nitrogen, cover with aluminum foil, and lyophilize overnight.

5.1.4. Primer exchange reaction

Run Experiments:

Set up experiments on ice; set PCR machine at 37°C.

Combine hairpins with primers at 100 nM each

Prepare reactions on ice:

- Create dNTP dilution
- Create Clean G dilution
- Dilute 100 um probe pools to 10 um in 1xTE
- Create 10ul of hairpin dilution
- Create master mix (x10)
- Vortex and spin master mix
- Put 80uL of master mix into each tube on ice
- Move to 37°C and incubate for 15 min
- Quickly add 10ul of primers into reactions
- Run PCR
- Make Gel experiment

PCR machine protocol.

Pause at 37°C. Incubate at 37°C for 1.25 hr (15 min pre-incubation; then 1 hr normal). Heat inactivate at 80°C for 20 min. Heated lid: fix at 100C. Hold at 4°C.

Gel Experiment.

Use 2x 1% E-Gel EX (G402001). Dilute ladder and samples 1 in 10 in water. Heat shock ladder and sample at 95°C for 2 minutes, then load from the cold plate. Run the gel for 10 minutes. Scan the gel with Sybr Gold at 425 V.

5.1.5. PER-2 Ab Staining

Fix cells with 4% PFA at RT for 15 minutes. Wash once briefly with 1x PBS and quench with 50mM NH4CL for 7min wash once with 1x PBS permeabilize and block cells with 2% BSA + 0.1% Triton +1mg/ml sheared sperm DNA for at least 1h at RT dilute antibodies (1:50) in 125ul 2% BSA + 0.1% Triton + 1mg/ml sheared sperm DNA + 6% dextran sulfate; vortex well and pipette up and down to make sure the dextran sulfate is settled down to the bottom of the tube. Incubate antibodies at 4°C overnight. Wash twice briefly with 2% BSA + 0.1% Triton in 1x PBS and wash 3x5min with the same buffer. Wash 2x5min with 1x PBS. Fix with BS(PEG)9 for 45 minutes and quench with 1x TBS for 10 minutes. Wash with 1x PBS once. Block the cells with 2% BSA + 0.1% Triton + 0.02% (wt/v) SDS + 10% dextran sulfate + 20% formamide + 0.5mg/ml sheared sperm DNA for 1 hour. Dilute the elongated strands (1:10) in 125ul block buffer and incubate at RT overnight. Wash with 1x PBS + 20% formamide (2brief + 3x5min) wash with buffer C (1x PBS + 500 mM NaCl) twice briefly. Dilute imager strands (1:100 dilution from 100uM stock to 1uM; prefer not using 10 uM) in buffer C. Incubate cells with imager strands at RT for at least 30 min. Wash with buffer C 3x5min.

5.1.6. Fluorescence Microscopes

Zeiss TIRF/LSM 710 confocal was used to image Alexa 647 labeled BSC cells.

5.2. No-amplification, 2'Ab and HCR-amplification staining
15 um mouse brain sections.

With with 0.1% Triton + 0.02% sodium azide in PBS for 3x 5 minutes. Block with 5% donkey serum + 0.05mg/ml sperm DNA + 0.3% Triton in PBS for 1 hr at RT. Incubate primary antibodies in 5% donkey serum + 0.2mg/ml sperm DNA + 0.3% Triton + 0.2% sodium azide + 0.1% dextran sulfate at RT overnight. Wash with 2% BSA + 0.1% Triton in PBS for 3x 20 min at RT. Wash with 1x PBS for 2x 10 min at RT. Post-fix with BSA + 0.1% Triton in PBS for 3x 20 min at RT. Wash with 1x PBS for 2x 10 min at RT. Post-fix with BS(PEG)9 for 1 hr at RT and quench with 1x TBS for 15 min. For no amplification (No AMP), block with 1x PBS + 20% formamide for 1 hr at RT, then incubate in imager strands (1:100 to 1um final concentration in 1x PBS + 20% formamide) for overnight; for 2'Ab amplification (2'Ab AMP), block with 5% donkey serum + 0.1% Triton for 1 hr and add secondary antibodies diluted in 5% donkey serum + 0.1% Triton + 0.2% sodium azide for overnight; for HCR, block with amplification buffer and incubate in snap-cooled hairpins overnight at RT. (Protect from light) For No AMP, wash with 1x PBS for 3x 20 min; for 2'Ab AMP, wash with 2% BSA + 0.1% Triton for 3x 20 min; for HCR AMP, wash with 5x SCC + 0.1% Tween 20 for 3x 20 min.

5.3. Expansion Microscopy

5.3.1. Original ExM Gel

Monomer solution recipe:

Components	Stock Concentration	Amount (mL)	Final Concentration
Sodium acrylate	38	2.25	8.6
Acrylamide	50	0.5	2.5
N,N'-Methylenebisacrylamide	2	0.75	0.15
Sodium chloride	29.2	4	11.7
PBS	10X	1	1X
Water		1	
Total		9.5	

Table 1. Monomer solution recipe.

Monomer solution (**Table 1**) was mixed in aliquots and stored at -20°C. The monomer solution was always on ice to prevent premature gelation. Stained cells were incubated with the monomer solution + APS (ammonium persulphate) /TEMED (*N,N,N′,N′*-tetramethylethylenediamine) at 4°C for 30 min. The pregel solution was then sandwiched between two glass plates separated by coverslips. The sandwiched chambers then were transferred to a humidified 37°C warm room for 2 hr incubation.

5.3.2. Magnified Analysis of the Proteome Gel (MAP)

Cells were washed and embedded into the polymer by adding the monomer solution (20% AA, 7% SA, 0.1% BA, 0.5% TEMED, 0.5% APS in PBS). The MAP solution was left for polymerization in the warm room for overnight.

5.3.3. DMAA Gel

3.3 g of DMAA was added to 6.7 g of DI water. The solution was purged with Nitrogen gas for 45 min. 0.089 g of APS was added, followed by purging the solution with Nitrogen gas for another 15 min. 40 ul of TEMED was added and the pregel solution was introduced into a sandwiched chamber. The sample was left to polymerize for overnight at RT in the warm room.

5.3.4. Alginate/ Acrylamide Gel

Powders of alginate and acrylamide are dissolved in water equally (7%), resulting in water content fixed at 86 wt %. APS was added as a photo-initiator for polyacrylamide, and *N,N*-methylenebisacrylamide was added as a crosslinker for polyacrylamide. TEMED was aided as a crosslinking accelerator for polyacrylamide and calcium sulphate slurry as the ionic crosslinker for alginate after degasing the premixed solution in the vacuum chamber. The pregel solution was introduced into a sandwiched chamber. The gel was left to polymerize for overnight at RT in the warm room.

5.3.5. Gel Digestion and Expansion

Remove the coverslip and trim excess gel with a razor blade. The digestion solution (50 mM Tris, 1 mM EDTA, 0.5% Triton X-100, 0.8 M Guanidine HCL and 8 units/mL of Proteinase K) was added to the gel in excess volume. The gels were incubated in digestion buffer for overnight.

5.3.6. Bind Silane Coverslip treatment.

Working solution:

	A	B
1	Ethanol	8 mL
2	Glacial Acetic acid	200 uL
3	Bind-silane	10 uL
4	ddH2O	1.8 mL

Table 2. Working solution for the bind silane coverslip treatment.

The slides were cleaned with ddH2O and Ethanol, followed by air drying the slides. The work solution (**Table 2**) was pipetted onto the slides and distributed equally over the slide. The slides were left on the bench for 1-1.5 hr. The slides were rinsed with ddH2O and then rinsed with 100% ethanol. The slides were left on the bench to allow for air dry.

5.3.7. Re-embedding

The gels were transferred to a bind-silane treated slide, then the gels were placed in excess volume of de-ionized water until the size of the gel reached a plateau. The re-embedding solution (100 ul of 19:1 Acrylamide*: N,N*-Methylenebisacrylaide (40%), 5 ul of 10% TEMED, 5 ul of 10% APS and 890 ul of water. The gel was trimmed with a razor blade to a desired size.

5.4. Force Spectroscopy using AFM

JPK instruments NanoWizard 4a AFM was used to measure the mechanical properties of the three types of gels. The model of the cantilever used in the experiment was AC240Ts-R3 with a spring constant of 2 N/m and frequency of 70 kHz. The cantilever was clamped to the block with a cantilever spring, followed by setting up the laser detection system via laser alignment. The laser beam was adjusted to aim at the tip of the cantilever. The reflection beam was adjusted to fall onto the photodiode detector. Force spectroscopy was selected. The relative set point was set to 10 nN, the z length was set to 0.5 um with the extend speed set to 1 um/s. All the gels were emerged in liquid when the measurement was done.

5.5. Mechanical Tests were performed Using a Tensile Machine

TA.XT Plus was used as a texture analyzer to measure the physical and mechanical characteristics of the gels. The gel was glued to two clamps and the measurements were conducted in air at room temperature. The test speed was set to 0.25 mm/sec and the distance was set to 200 mm.

Chapter 6: Result, Outcomes and Future Directions

6.1. Development of PER Imaging Techniques Using BSC cells

First, the primer is bound onto the user-designed hairpin at the primer -binding site. Once hybridized, the strand displacing polymerase starts synthesizing the new sequence domain until it reaches a stop sequence. The strand displacing polymerase will fall off while the newly synthesized sequence starts competing with the user-designed hairpin in a random walk process that is referred to as branch migration. At this point, the newly synthesized strand can be completely replaced by the hairpin, resulting in the newly synthesized strand only binds to the original primer sequence. Eventually, the primer dissociates from the hairpin due to the short primer-binding site. The newly synthesized sequence will be released as a result of transcript dissociation for another subsequent round of reaction. The large Bst polymerase is incorporated into the primer-hairpin solution for characterization of primer exchange reaction. The denaturing gel is used to track the progression and the extension of different hairpin species that are presented. Long concatemers are produced in addition to the single hairpin system, and this concatemerization can be used as an alternative method for signal amplification by designing a specific sequence to a particular fluorescent dye to achieve direct visualization of the specimen (**Figure 16**).

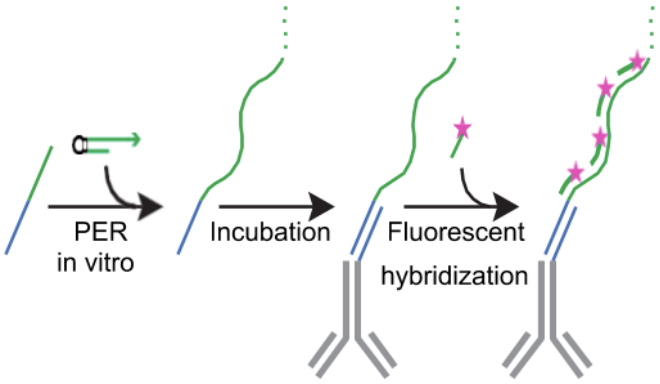

Figure 16. PER cascades can be used as a signal amplification method that grows the fluorescent concatemer when responding to a particular miRNA signal.

The BSC cells were fixed and stained with DNA-label antibodies (alpha tubulin), followed by incubating with the PER oligos, and direct visualization was achieved via fluorophore-conjugated imager strands. The PER imaging technique was compatible with the current conventional confocal microscopes, and the method overcame the limitation of producing the identical copies of the fixed sequences. We performed the fluorescent imaging using PER to examine the architecture of BSC cells. The BSC cells were immunostained for tubulin (green), and the images were acquired using mouse secondary antibody (2' Ab). The PER oligos were extended with a user prescribed hairpin (5' ACA TCAT CATGG GCC TTT TGG CCCAT) and the strand displacing polymerase, thus resulting in signal amplification. We had introduced PER imaging technique that improved the signal of the immunostained specimens. The use of PER signal amplification method was a highly preferable imaging model due to its wide range of applications. PER method could be applied to immunofluorescence or to fluorescent in situ hybridization via extending primary or secondary probes.

PER Imaging (20x)

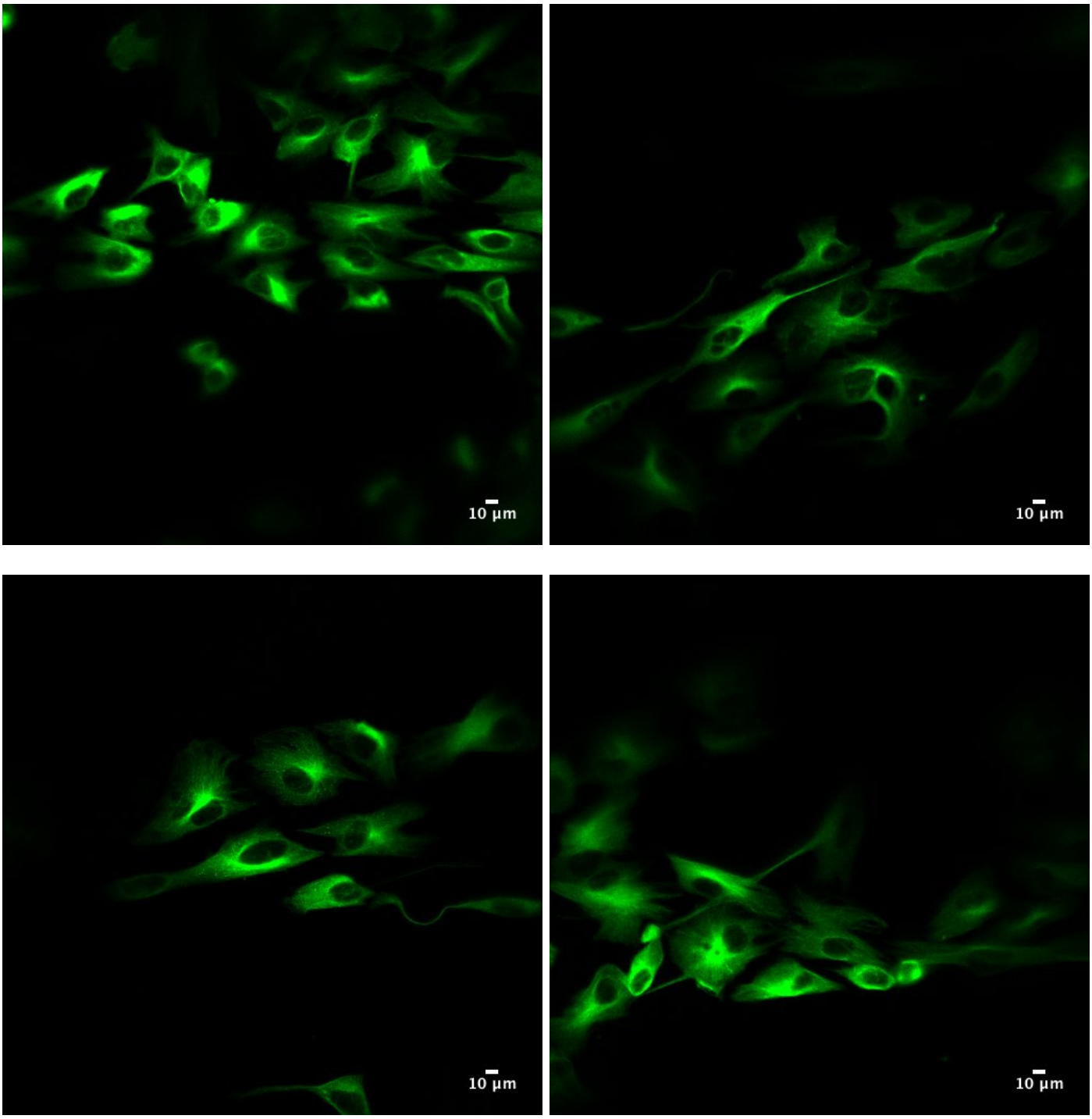

PER Imaging (40x)

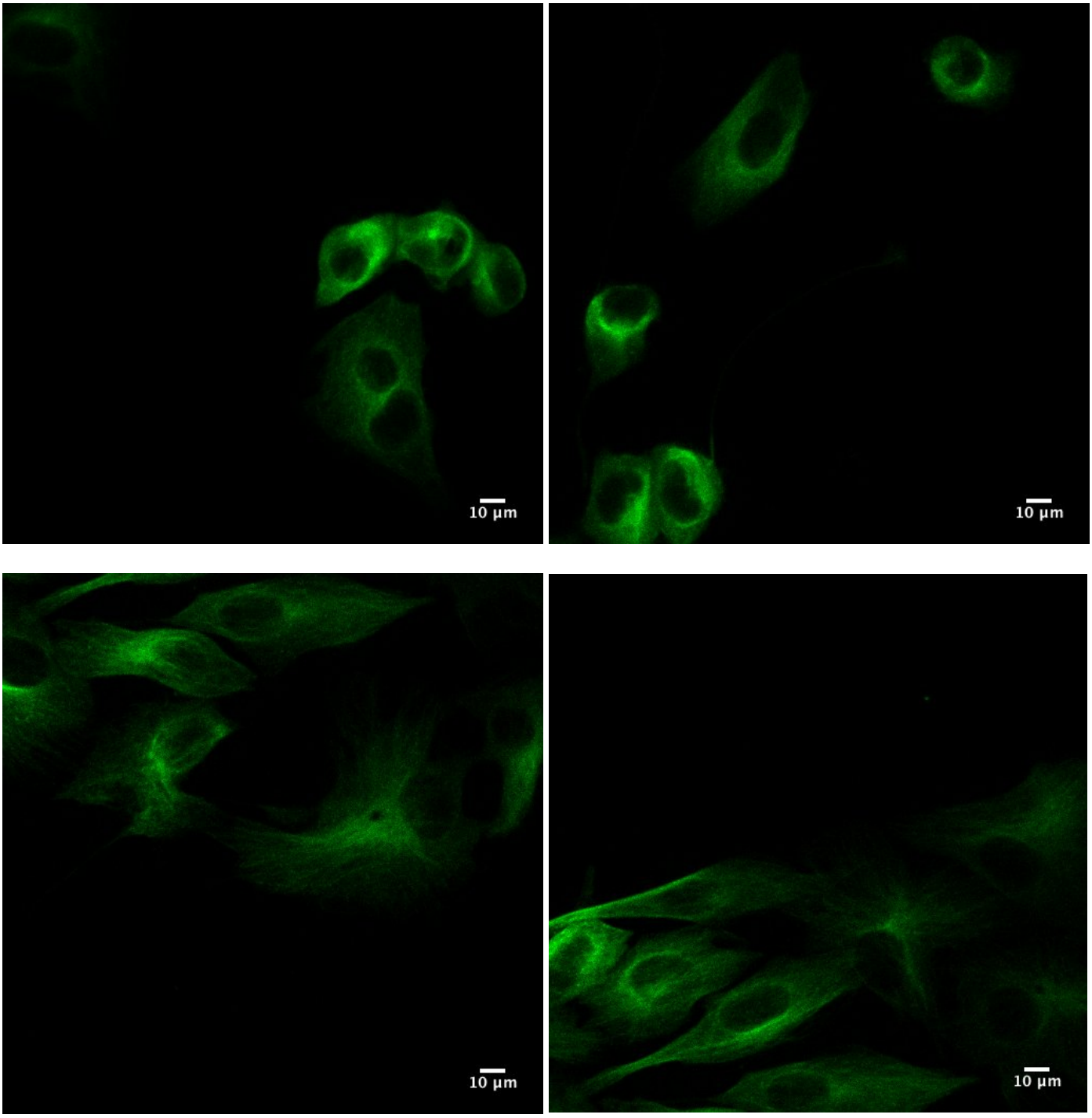

PER Imaging (63x)

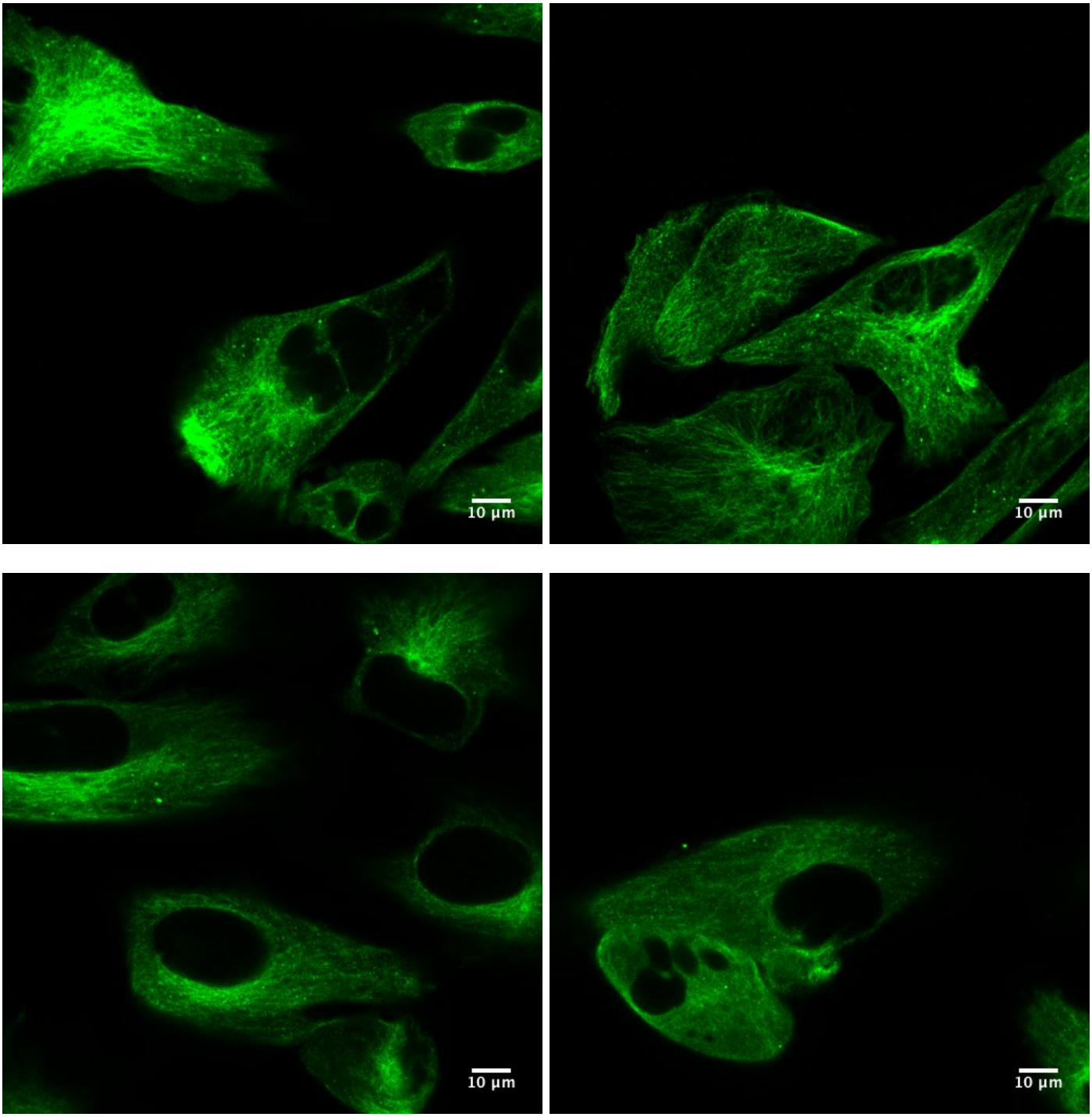

Figure 17. The long concatemerization created via PER cascades promotes signal amplification by binding the fluorescent dye to a specific sequence that undergoes oligo extension, and the specimen can be visualized via fluorophore conjugated imager strands. The images are acquired using Alexa 647-conjugated mouse secondary antibodies.

6.1.1 Conclusion

The results showed promising data with PER when used as a signal amplification method in imaging the neuron cells, suggesting that PER imaging technique could be an alternative platform for protein imaging via in vitro extended probes (**Figure 17**). We adapted the PER imaging technique that could function as fluorescent signal amplification method to achieve high resolution imaging while preventing the need to use harsh chemical treatments that might disrupt and damage the biological specimen. In summary, we demonstrated that PER cascades could be used for immunofluorescence, and this technique could be applied to investigating the distribution of microtubules and synaptic junctions in the brain. The detailed investigation of the cellular circuits in the brain provided connectivity information which could be useful to tackle many challenges that were still unresolved in neuroscience.

6.2. Comparison of No Amplification, 2'Ab and HCR Amplification Staining in BSC Cells

15 um mouse brain sections were blocked with formamide and incubated with GFAP-B5-Alexa 647. For No AMP, the BSC cells were blocked with donkey serum /Triton and stained with imager stands; for 2'Ab AMP, the BSC cells were stained with anti-rat Alexa-647 secondary antibody; for HCR AMP, the BSC cells were blocked with amplification buffer and stained with snap-cooled hairpins. The fluorescent images of No AMP were taken using 4% and 50% laser due to the low fluorescent signal whereas the fluorescent images of 2'Ab and HCR AMP showed that using 4% laser was sufficient enough to bring forth high quality fluorescent images.

The goal of this experiment was to show that the amplification method promoted fluorescent signal amplification by 10 fold compared to tissue specimen with no amplification, thus implementing this signal amplification technique would allow enhancement of the imaging quality. Achieving nanoscale resolution of a specimen that could reveal more molecular information in depth. However, due to the complexity of the neuron circuits, there was still limitation to deliver the image in 3-D resolution. Our newly discovered materials made possible to extend the object into 3-D architecture, hoping of achieving nanoscale imaging while obtaining the complete magnified information from the swellable polymer.

No Amplification

4% laser

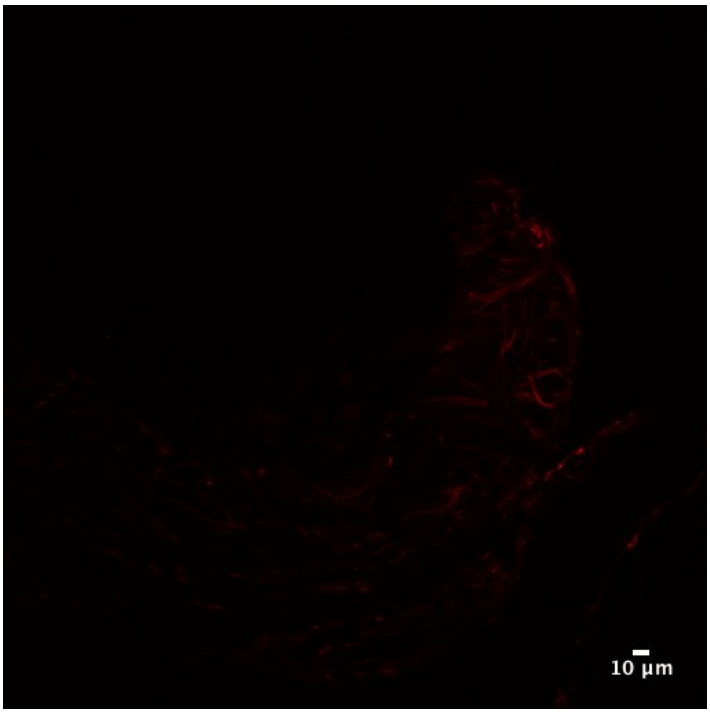

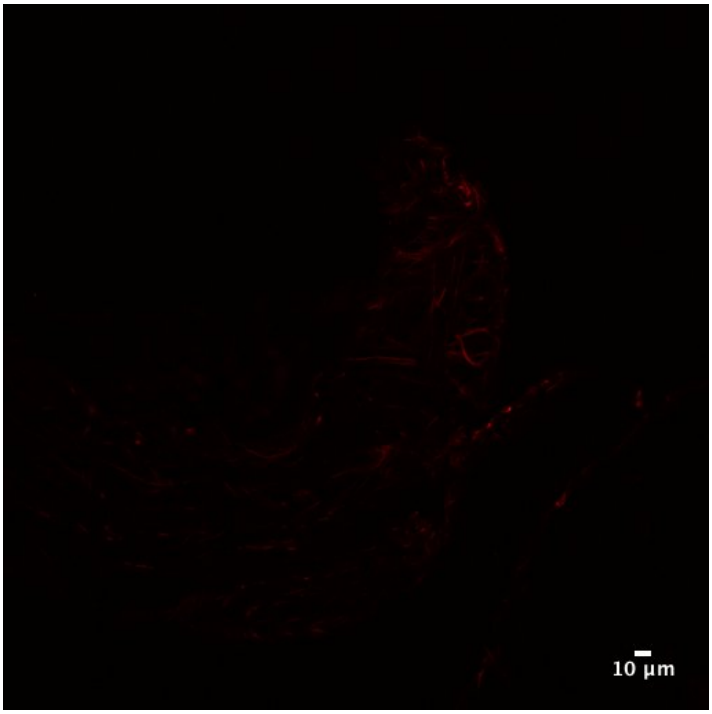

50% laser

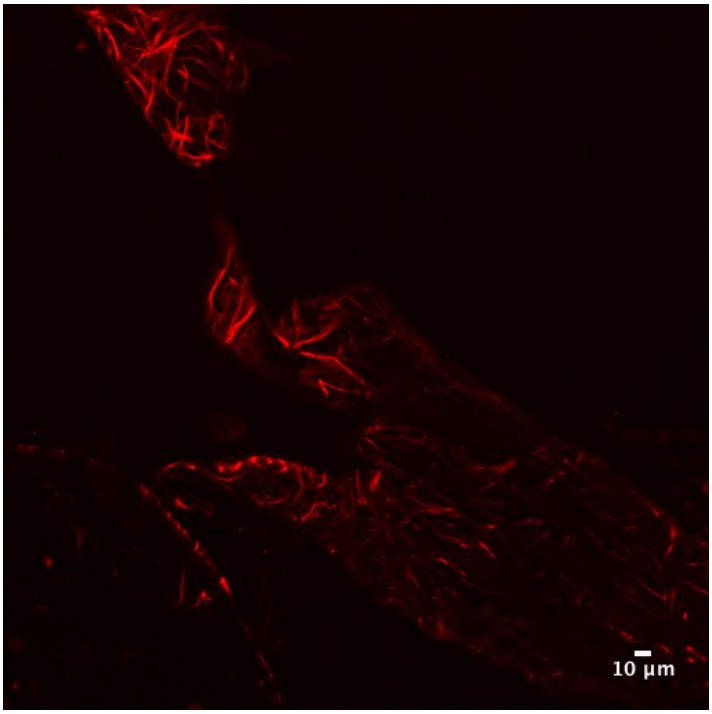

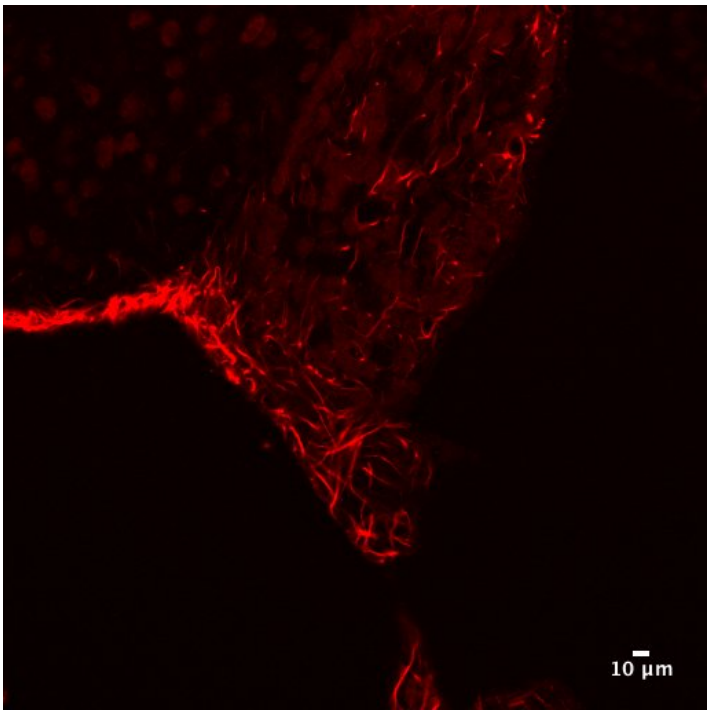

2'Ab

4% laser

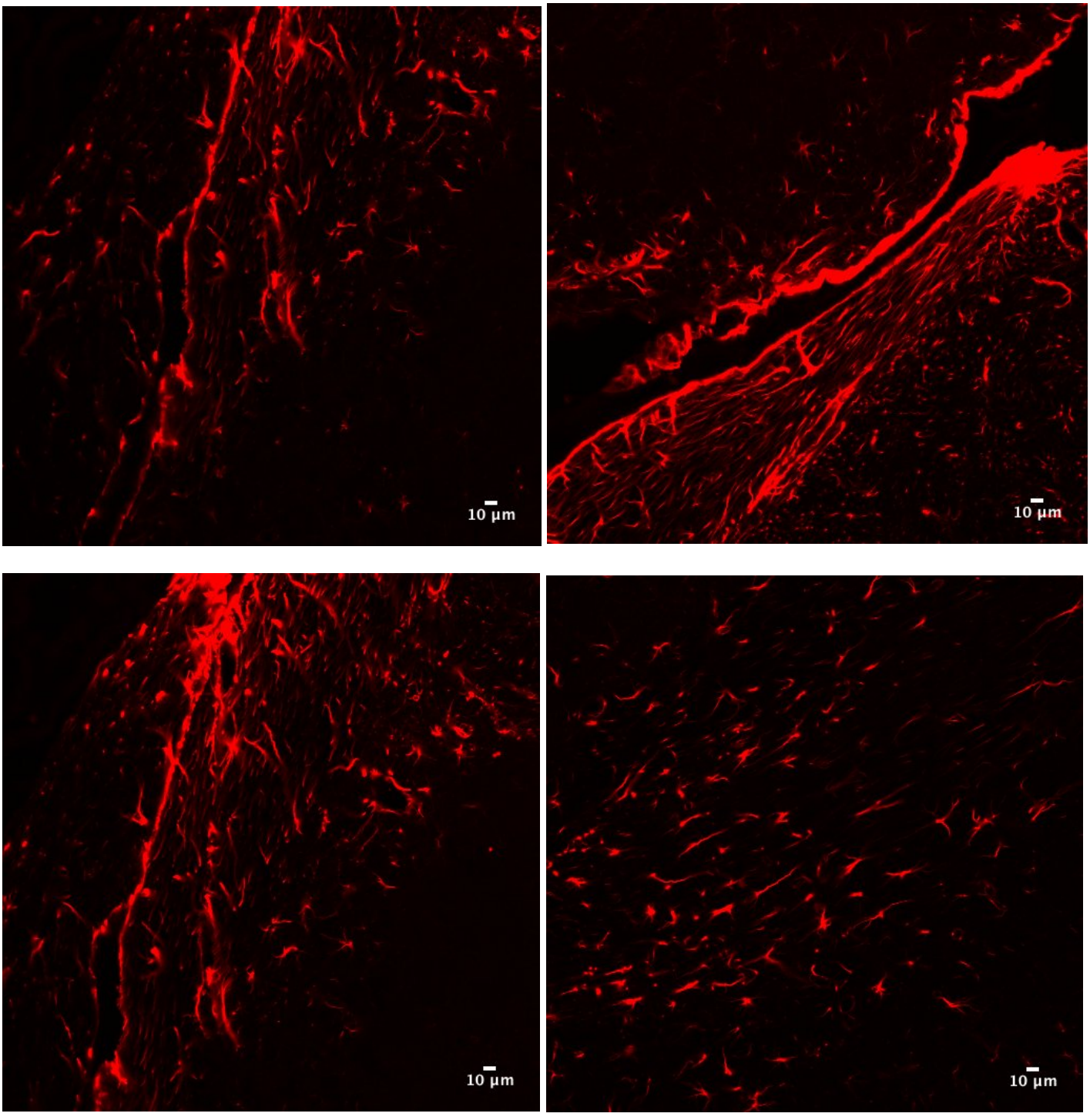

HCR

4% laser

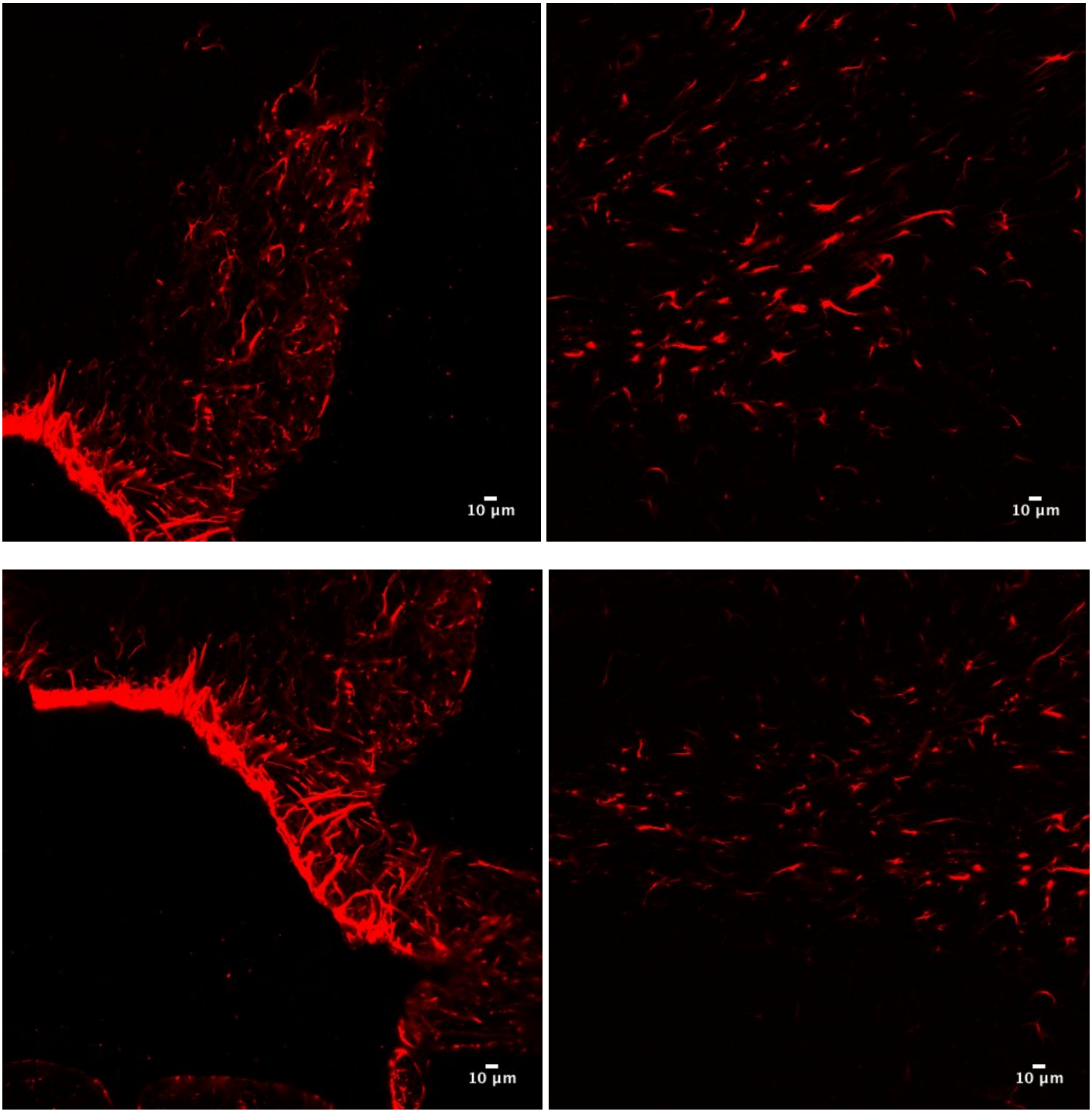

GFAP-B5-Alexa 647 (4% laser)

HCR Amplification *2'Ab Amplification* *No Amplification*

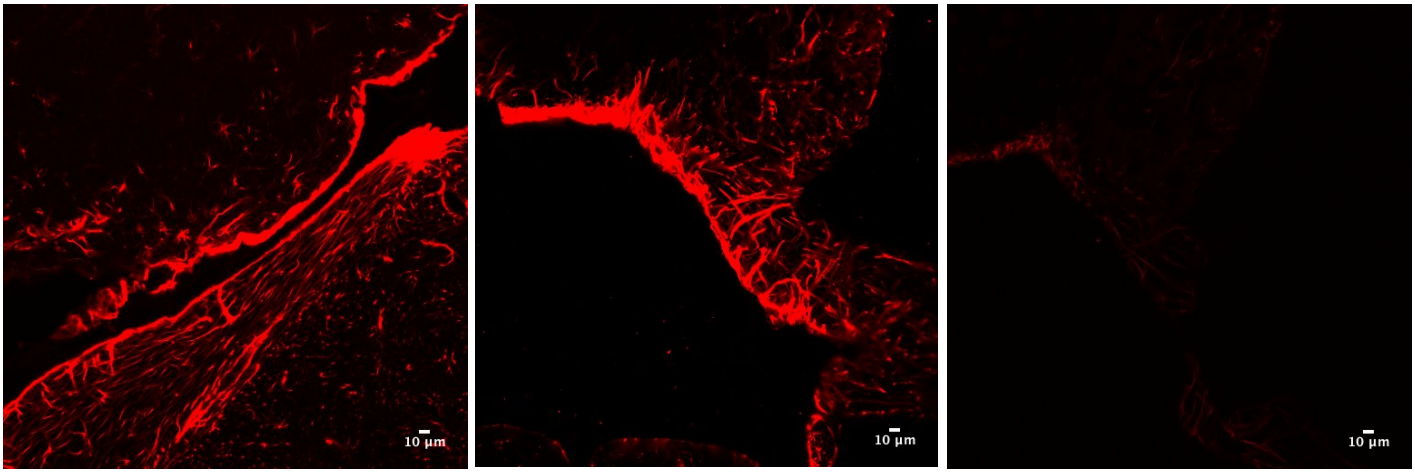

Figure 18. Comparison of the brain tissue stained with no amplification, 2'Ab amplification and HCR amplification. The images were acquired at the microscope setting 4% and 50% laser for no amplification, and 4% for 2'Ab amplification and HCR amplification. The tissues that were treated with signal amplification methods demonstrated 10x brighter fluorescent signal compared to untreated tissues.

6.2.1. Conclusion

The fluorescence intensity of the tissue specimen stained with either 2'Ab amplification or HCR amplification outperformed the tissue specimen with no amplification, demonstrating that the fluorescence signal amplification played a major role in improving the brightness of the immunostained specimens (**Figure 18**). PER imaging technique demonstrated similar performance compared to other highly multiplex imaging techniques.

Chapter 7: Development of a Superabsorbent Hydrogels That Are Highly Stretchable and Tough in Possessing Desired Mechanical Sturdiness as a Material for Expansion Microscopy

We measured the expansion factor of the original ExM gel, MAP gel, DMAA gel, DMAA/Acrylamide gel, and Alginate/Acrylamide gel as well as tested the mechanical properties via the AFM and the tensile tester of individual gels, hoping to develop superabsorbent hydrogels that could preserve the gels' toughness without rupture when the gel was being stretched. Our goals were to develop and synthesize hydrogels that were tough and highly stretchable to solve the common problems of expansion microscopy, including lack of mechanical supports, fragileness, low expansion factor, difficult in handling, and laborious procedures. The fragileness of the expanded hydrogels was the major drawback that people had experienced with expansion microscopy. The expanded gels often encountered ruptures or distortion when being handled or carried, resulting in tremendous efforts and time being consumed when conducting experiments.

7.1. Expanding Factor of MAP Gel, Original ExM Gel, DMAA Gel, DMAA/ Acrylamide Gel, Alginate/ Acrylamide Gel

MAP Gel

Average Expansion Factor: ~3.7 fold

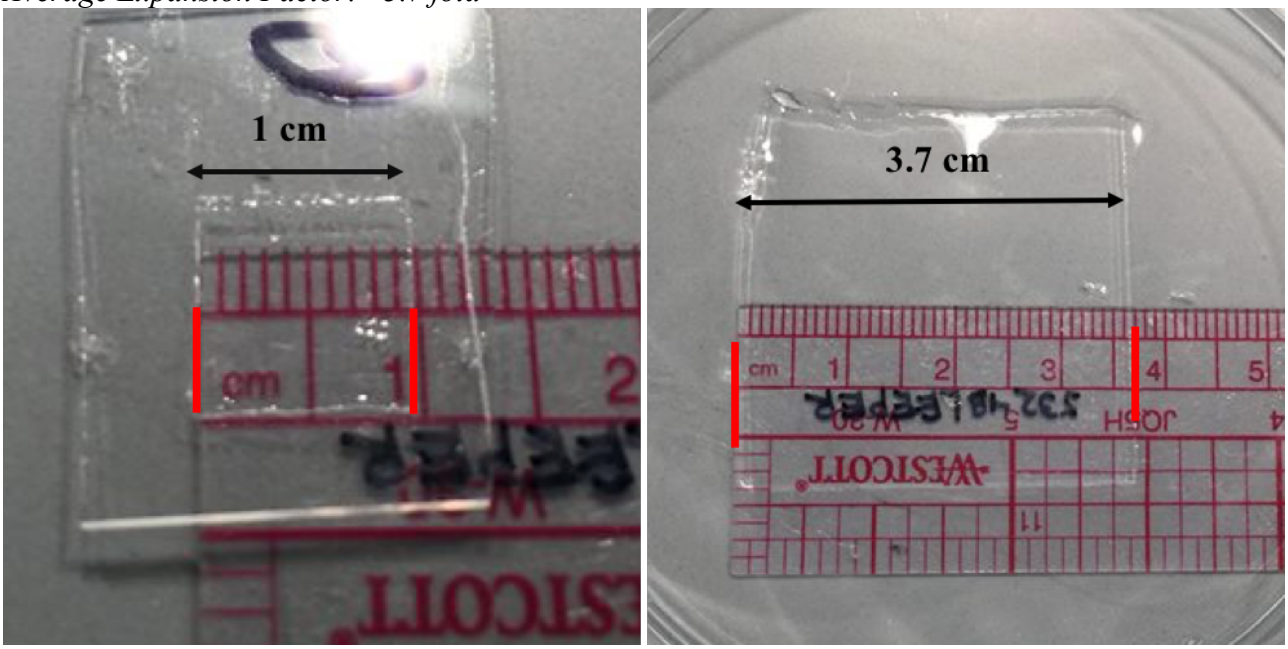

Original ExM Gel

Average Expansion Factor: ~4 fold

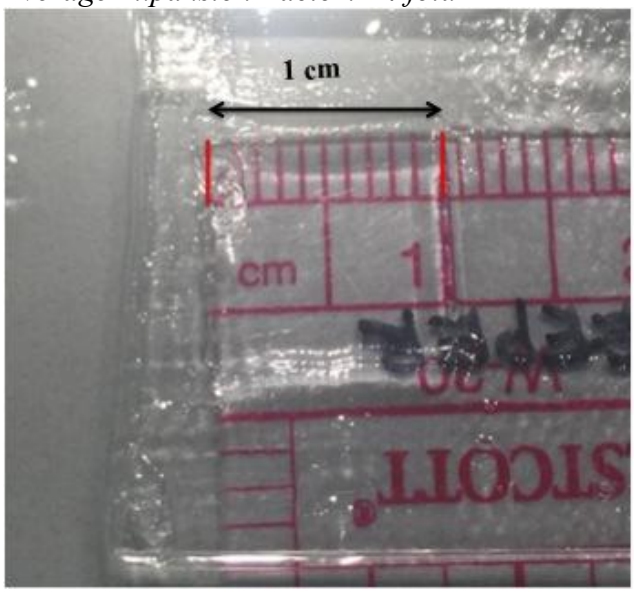

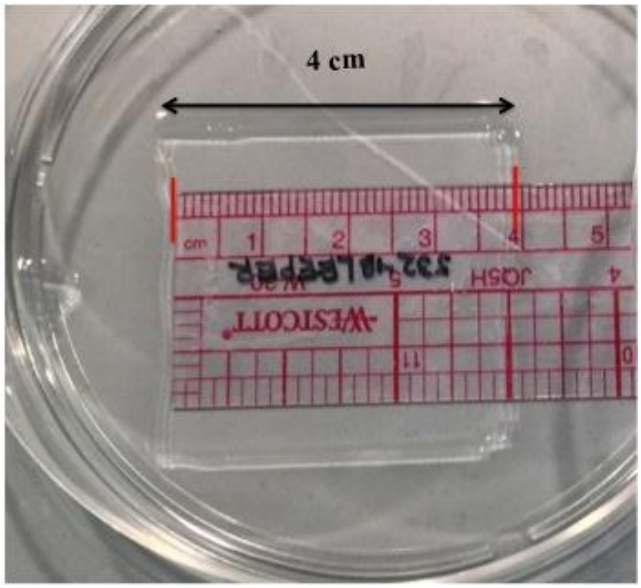

DMAA/Acrylamide Gel

Average Expansion Factor: ~5.5 fold

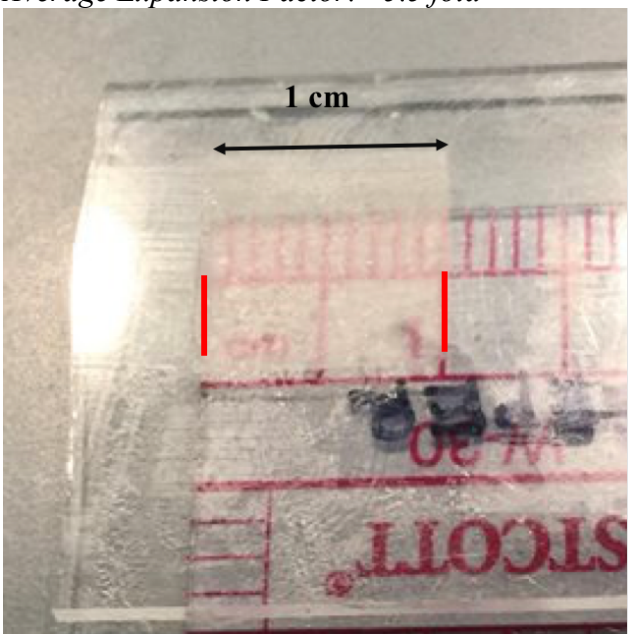

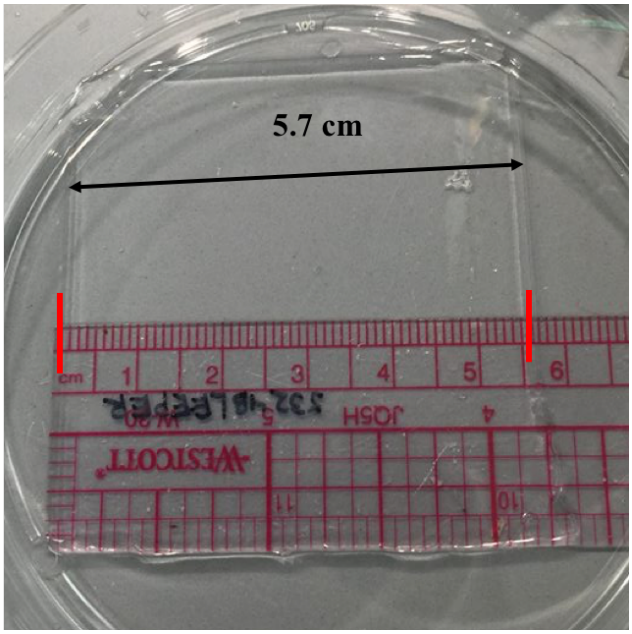

Alginate/Acrylamide Gel

Average Expansion Factor: ~7 fold

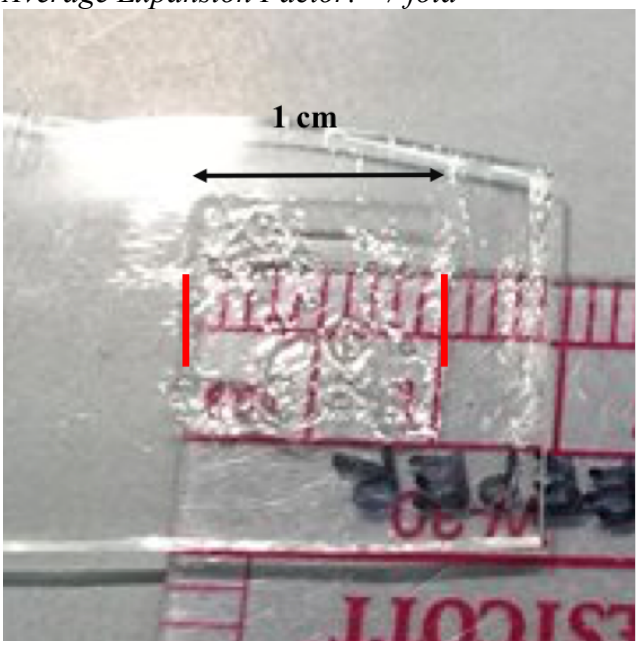

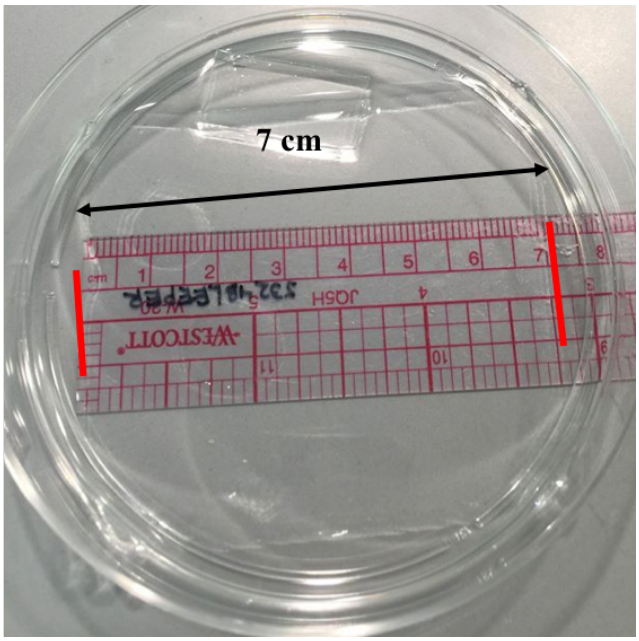

DMAA Gel

Average Expansion Factor: ~8 fold

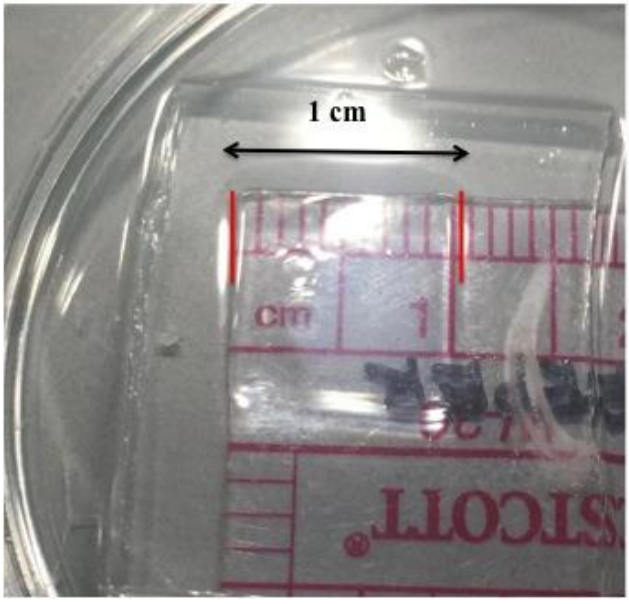

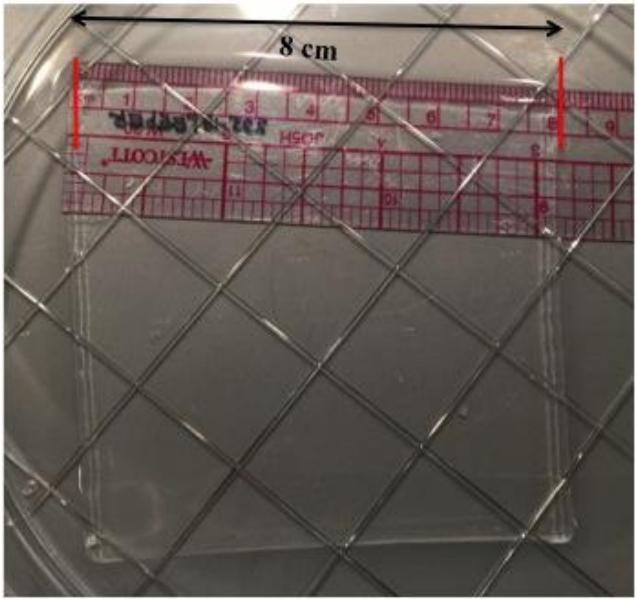

Figure 19. The lengths of the hydrogels that were composed of different chemicals were measured. DMAA gel was ranked the highest with ~8x linear expansion, followed by Alginate/Acrylamide ~7x linear expansion, DMAA/Acrylamide gel ~5.5x linear expansion, original ExM gel ~4x linear expansion and MAP gel ~3.7x linear expansion.

7.1.1. Conclusion

The DMAA gels produced roughly 8x linear expansion in which outperformed the rest of the ExM variants. Alginate/Acrylamide gels generated roughly 7x linear expansion which held the second highest expansion factor among other gels (**Figure 19**). DMAA/Acrylamide gel yielded roughly 5.5x linear expansion which still surpassed the current expansion methods developed by Boyden group and Chung group (~ 4x linear expansion and ~3.7x linear expansion).

7.2. Gel Expansion Factor Comparison Chart

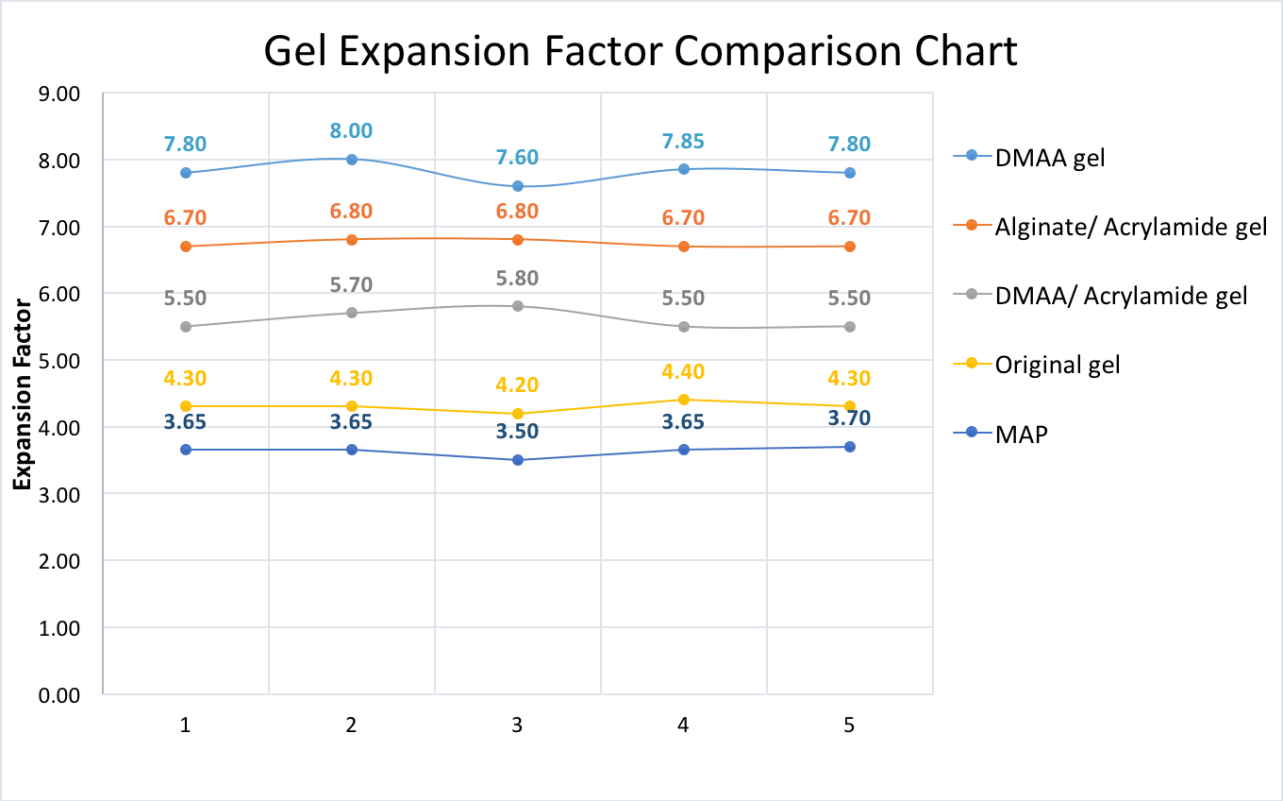

Figure 20. Among all methods for gel expansion, DMAA gels that held the capability of self crosslink turned out to yield the highest expansion factor (~8x fold), followed by Alginate/Acrylamide gels which were composed of ionically crosslinked alginate and covalently crosslinked acrylamide that produced ~7x linear expansion. DMAA/Acrylamide generated ~5.5x linear expansion which still exceeded the performances of the currently available ExM gels (original ExM gel by Boyden group and MAP gel by Chung group).

7.3. Expansion Factor of Different Ratios Between Acrylamide and DMAA

	Water (ul)	40% Acrylamide (ul)	40% DMAA (ul)	Expansion Factor
Condition 1	40	60	0	1.10
Condition 2	40	40	20	1.90
Condition 3	40	30	30	2.30
Condition 4	40	20	40	2.50
Condition 5	40	15	45	3.3
Condition 6	40	10	50	3.6
Condition 7	40	5	55	5.6
Condition 8	40	0	60	7.80

Table 3. The expansion factors of different ratios between acrylamide and DMAA.

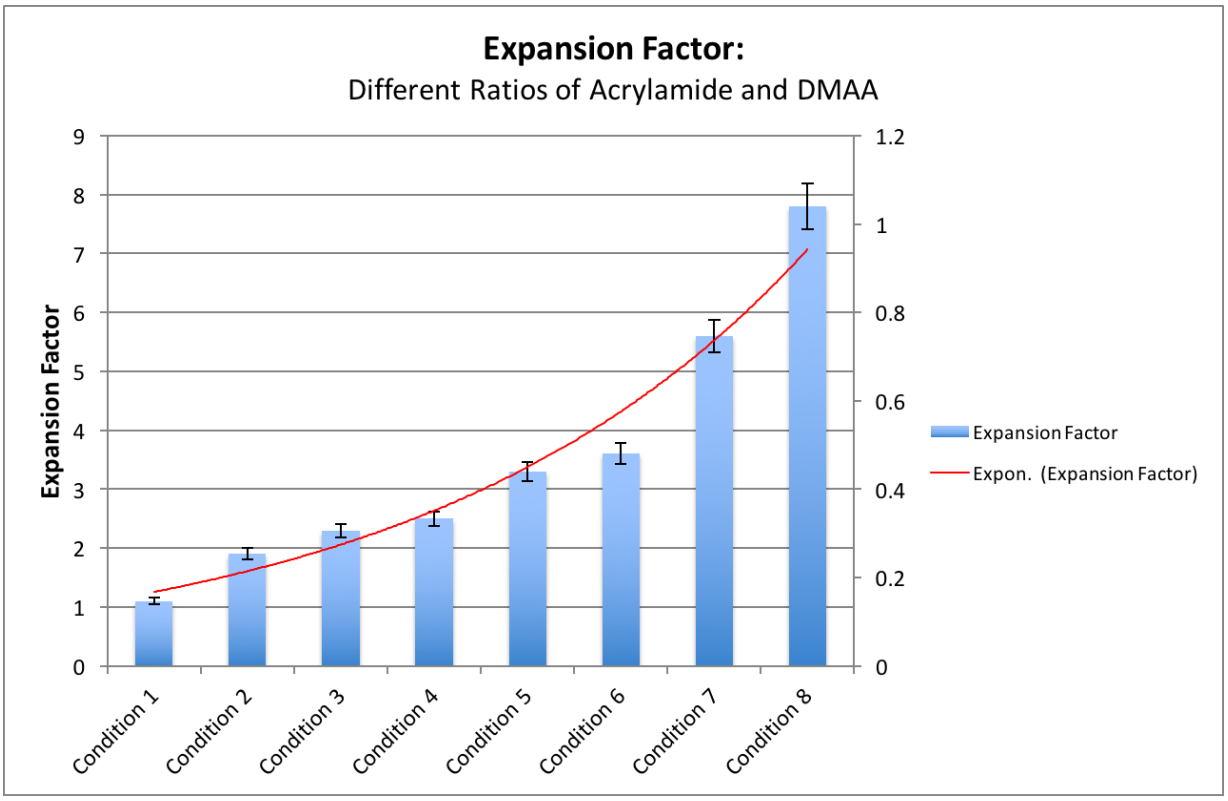

Figure 21. The bar graph shows an exponential increase as the ratio of acrylamide decreases.

7.3.1. Conclusion

From the charts above (**Figure 21**), we noticed that the expansion factor increased gradually when less acrylamide was added to the solution. The addition of acrylamide could inhibit the stretchability of the hydrogels. Supposedly, when the gel was stretched, the crosslinked polymer mesh would break and dissipated energy. Hence, adding covalently crosslinked acrylamide should attribute to the gel's toughness due to crack bridging ability by the network of covalently crosslinked polymers. However, it was concluded later in our research findings that DMAA gel alone yielded more toughness than the hybrid gels that were made from a mixture of crosslinks.

7.4. Mechanical Properties of MAP Gel, Original ExM Gel and DMAA Gel

MAP Gel (Young's Modulus)

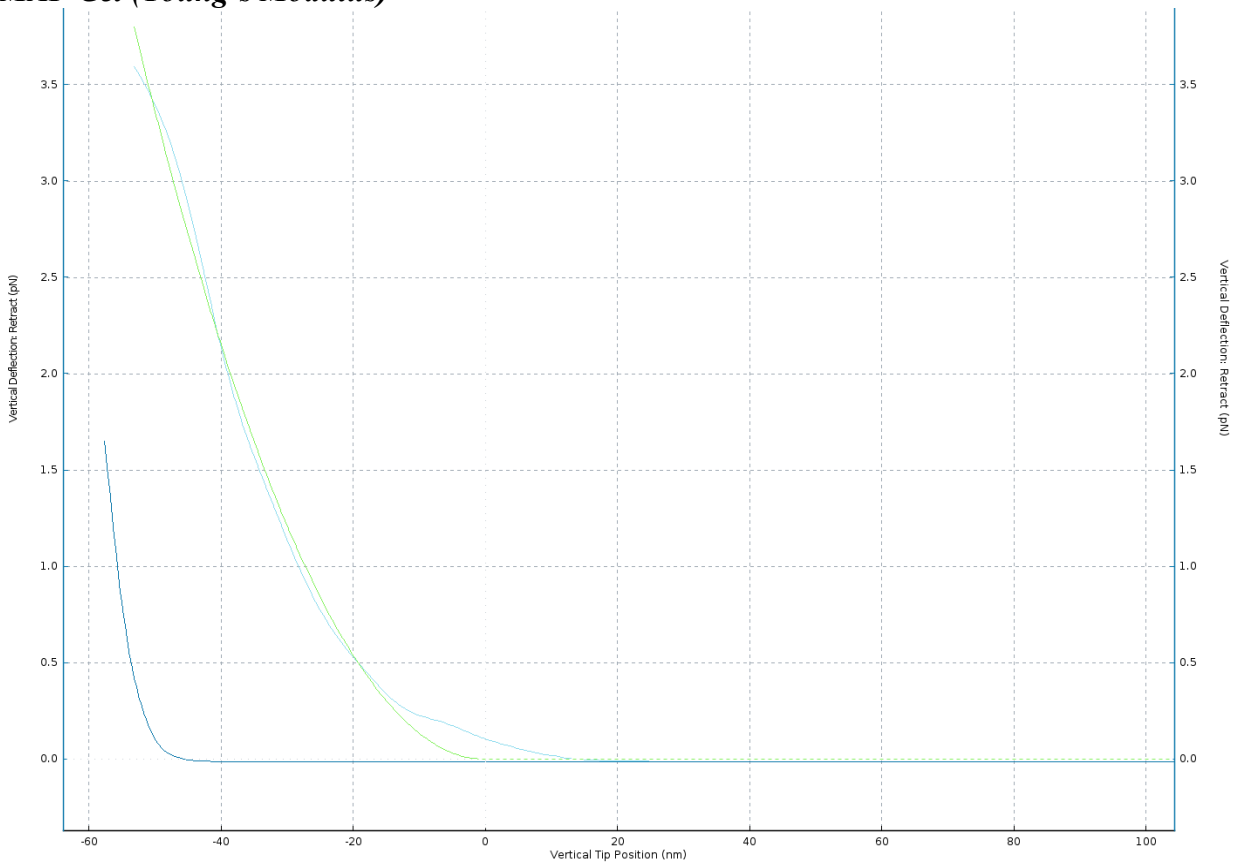

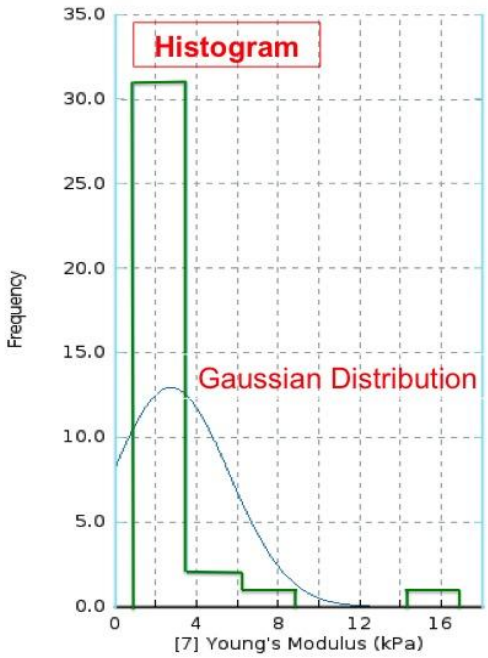

Young's Modulus	4.3 kPa
Contact Point	-80.45 nm
Baseline	3.035 x10^{-15} N

MAP Gel (Reference Force Height)

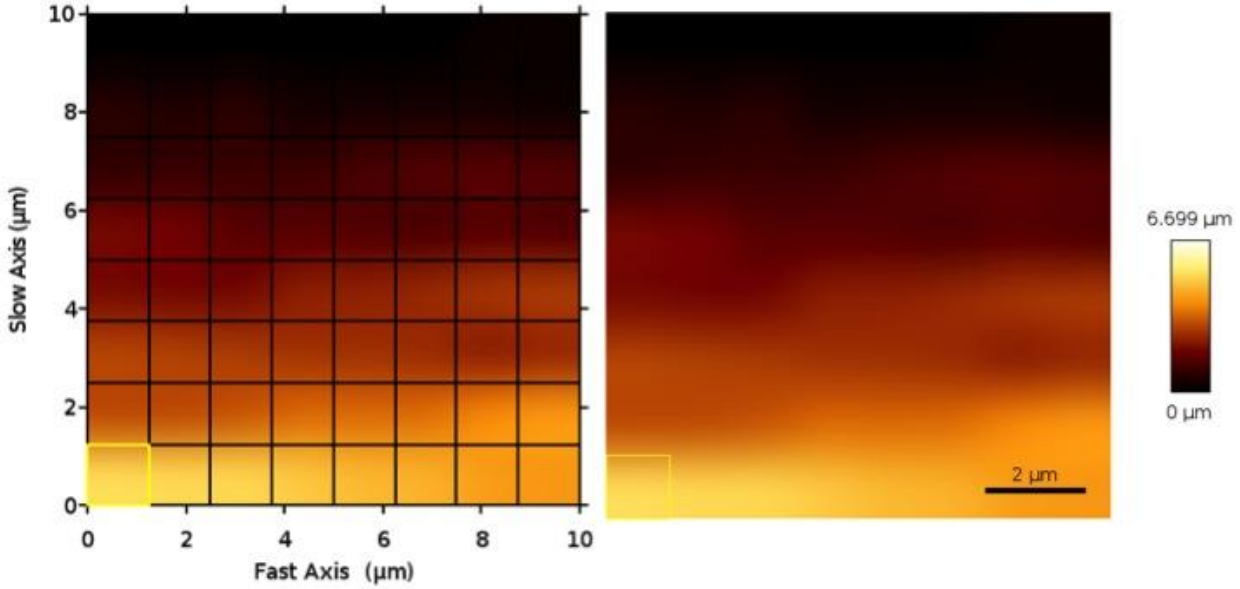

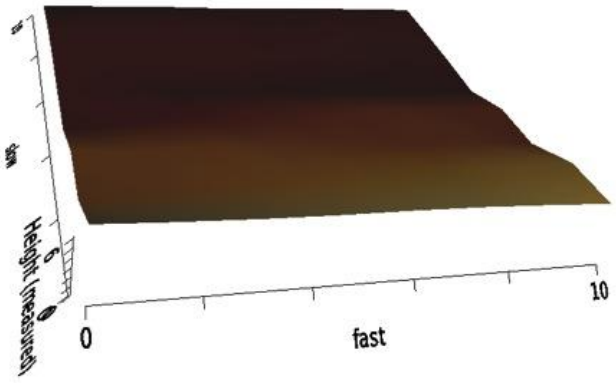

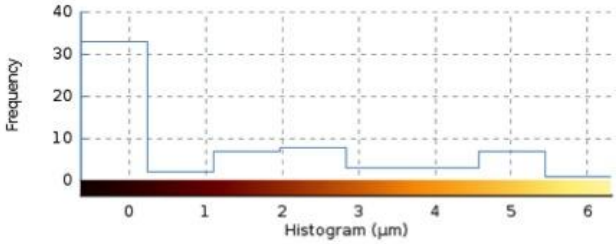

MAP Gel (Adhesion)

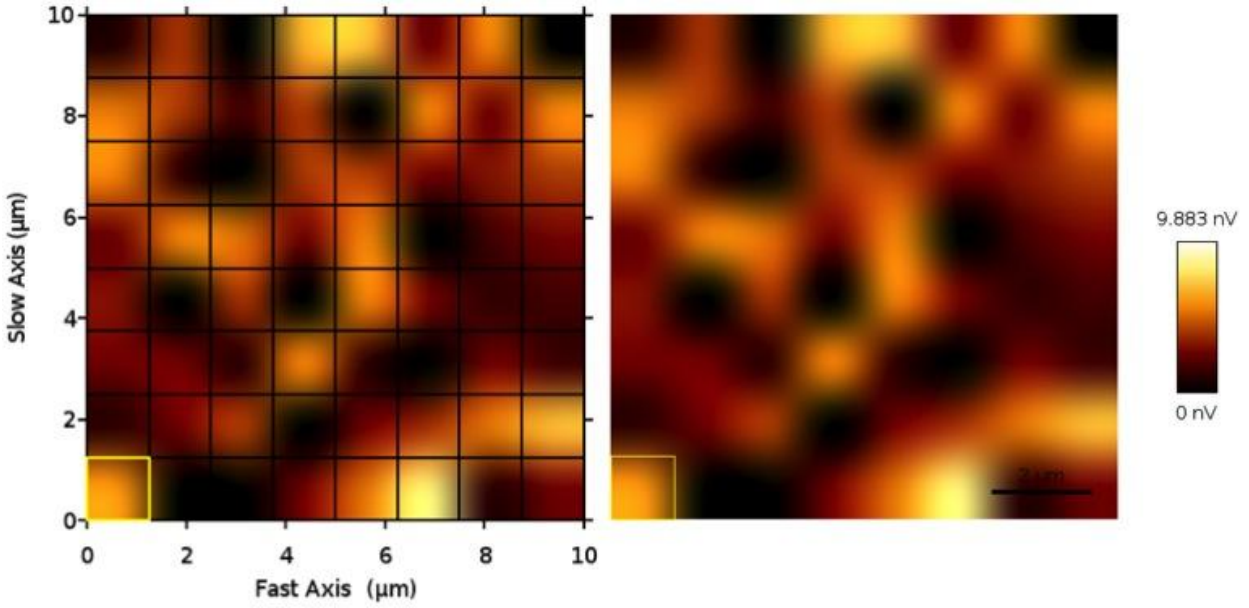

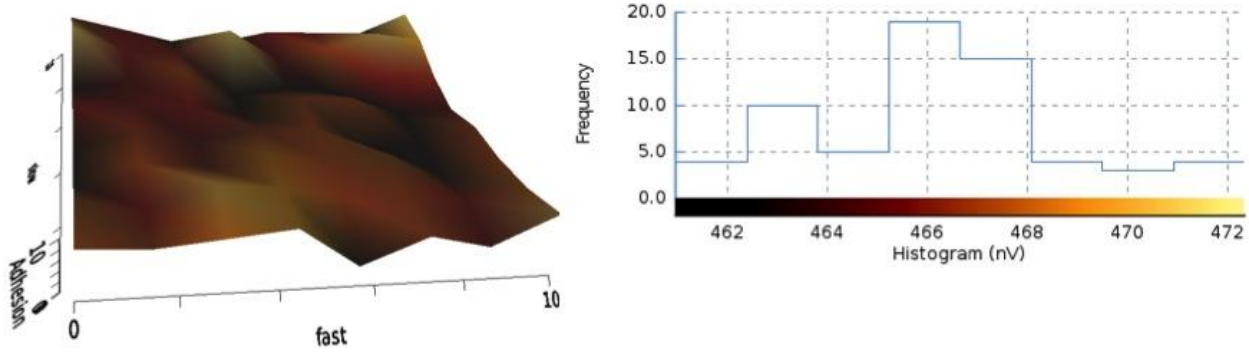

MAP Gel (Slope)

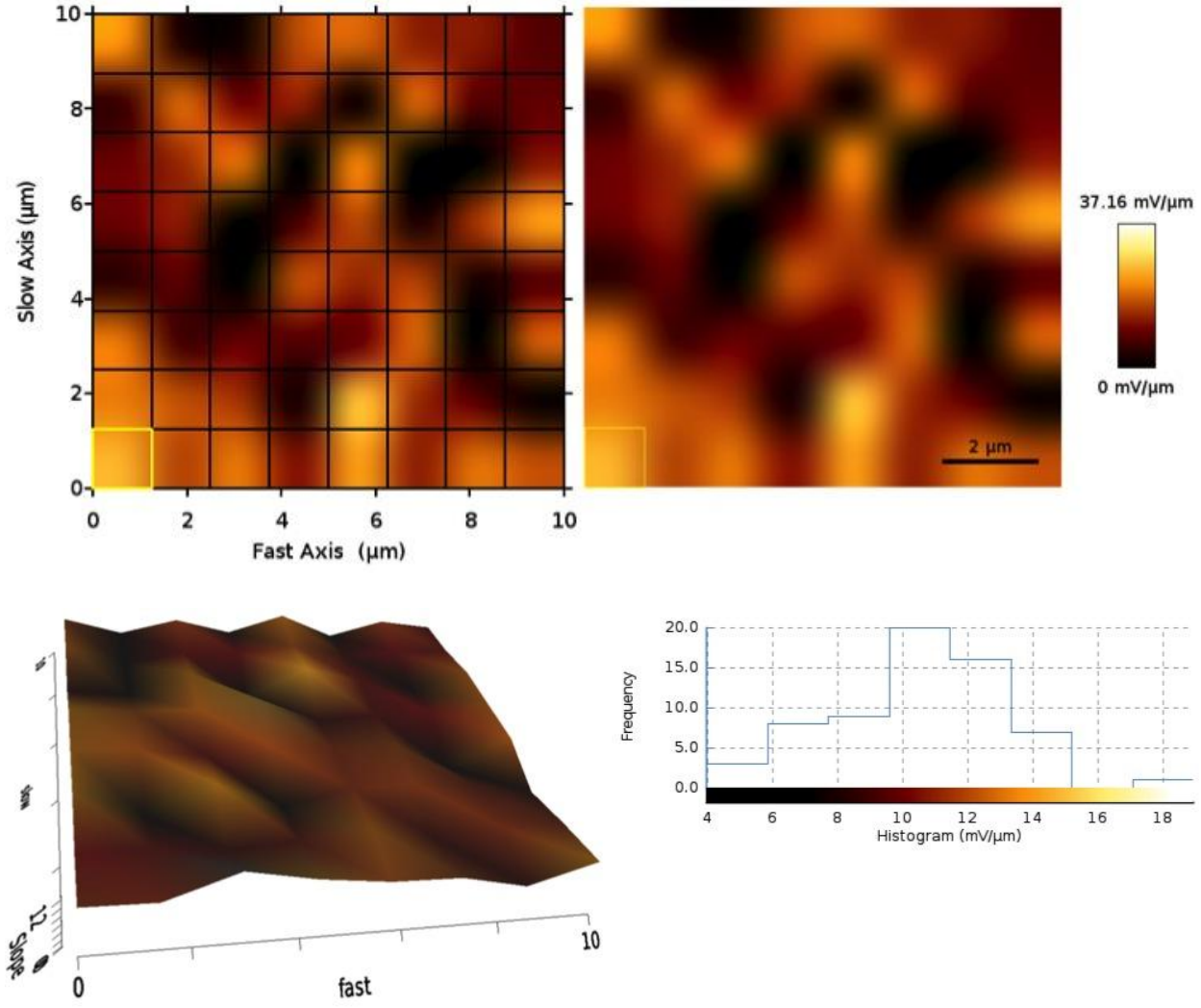

Figure 22. The force curve of the MAP gel in liquid. The average data of approach and retract trace were recorded. Elastic modulus could be obtained from the slope of the force curve which was 4.3kPa for the MAP gel (second softest gel among all the gel variants). Indentation, adhesion force and energy dissipation can be extracted from the raw data. The AFM image also showed 3D views and histograms of reference height, adhesion and slope of the MAP gels. Each square in the map represented one location of the gel.

Original ExM Gel (Young's Modulus)

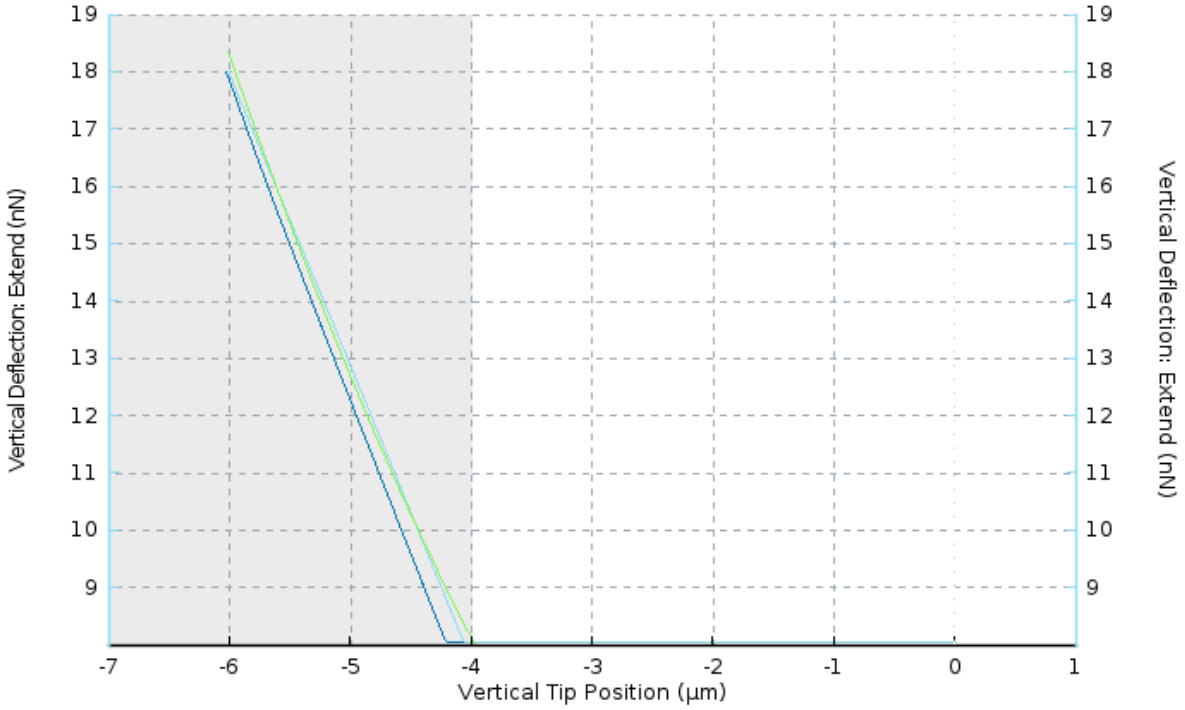

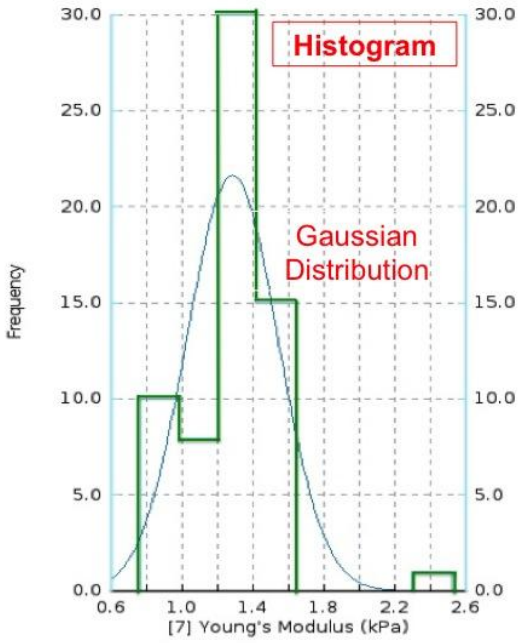

Young's Modulus	1.2 kPa
Contact Point	4.072 µm
Baseline	-8.071 nN

Original ExM Gel (Reference Force Height)

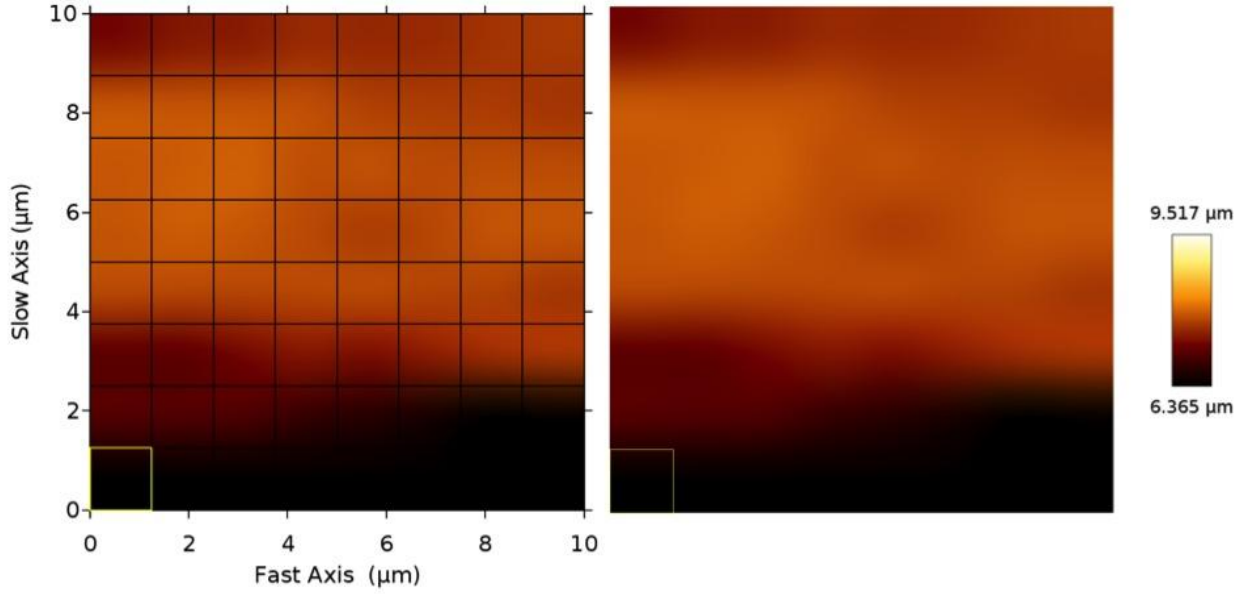

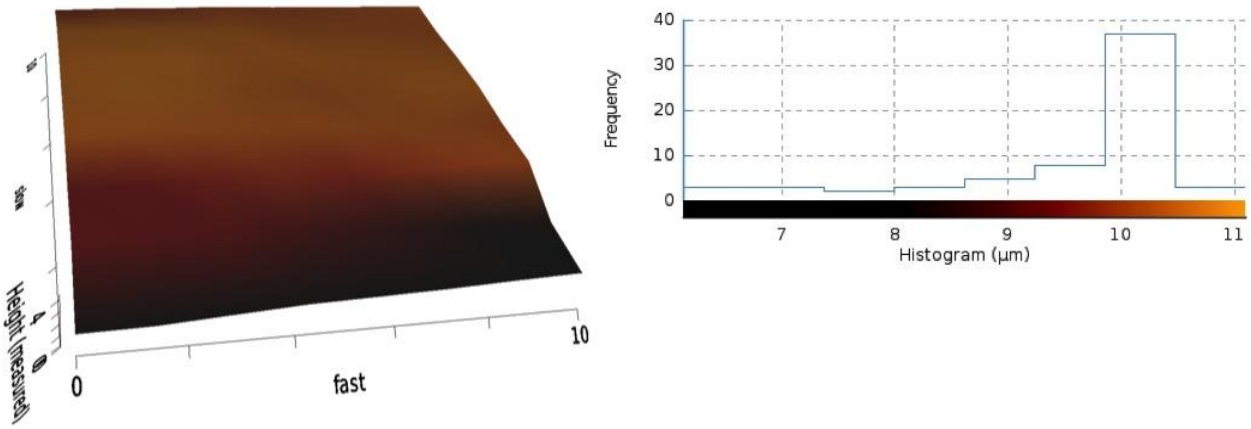

Original ExM Gel (Adhesion)

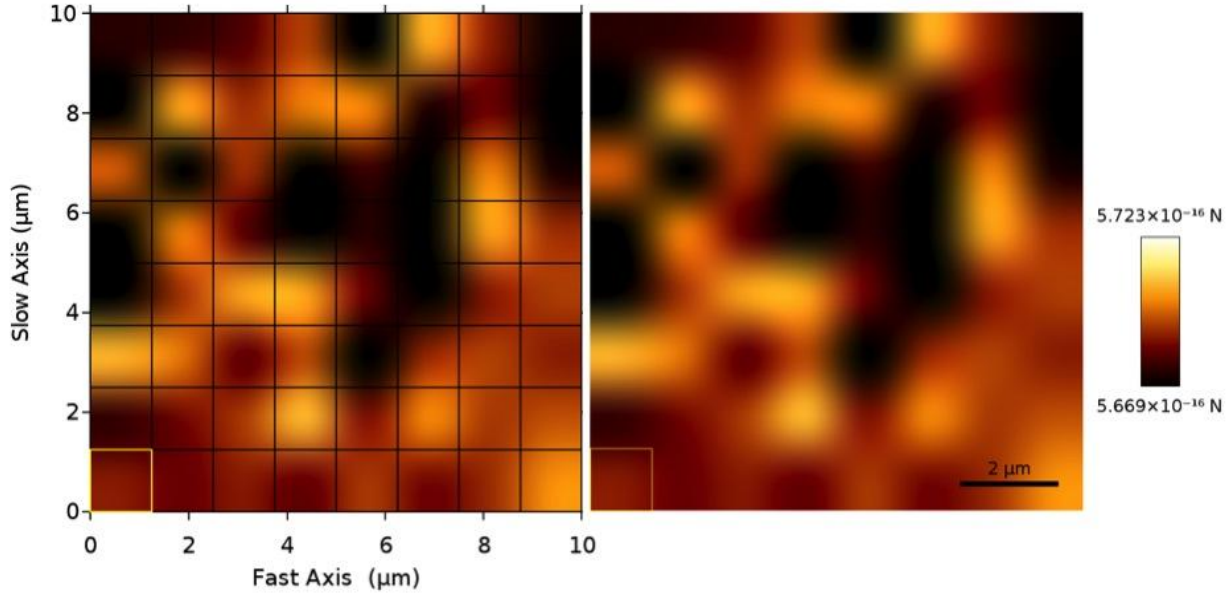

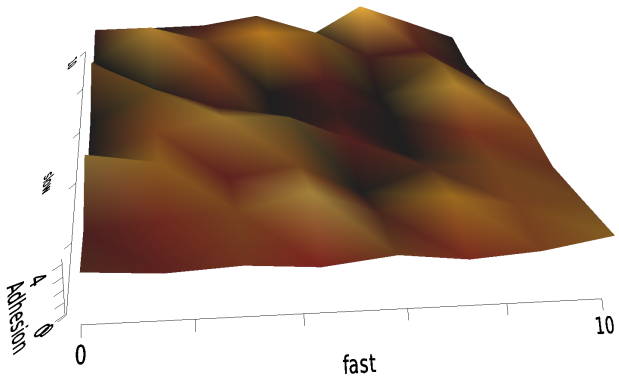

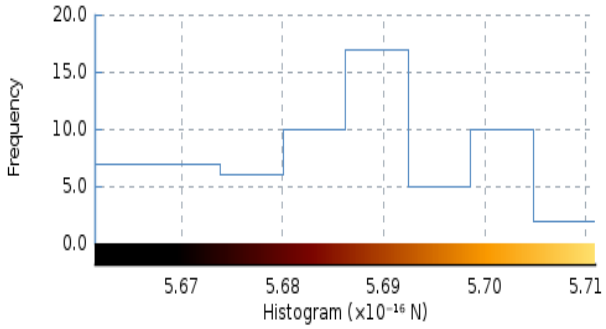

Original ExM Gel (Slope)

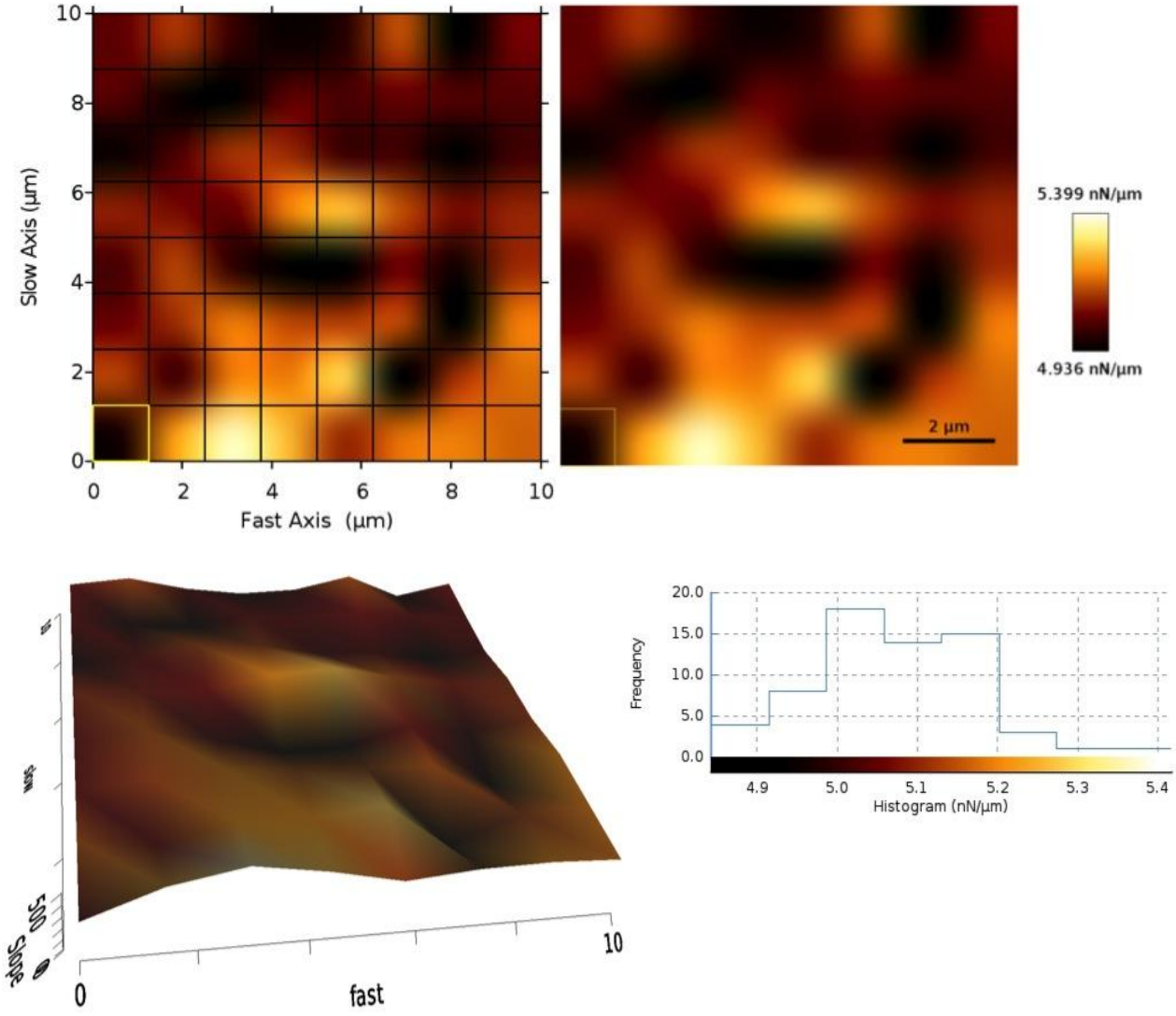

Figure 23. The force curve of the original ExM gel in liquid. Young's Modulus was calculated from the force-indentation curve. The original ExM gel exhibited an elastic modulus of 1.2 kPa which was the softest gel among all the gel variants. The AFM image provided 3D views and histograms of reference height, adhesion and slope of the original ExM gel which allowed us to better understand the topography of a particular gel.

DMAA Gel (Young's Modulus)

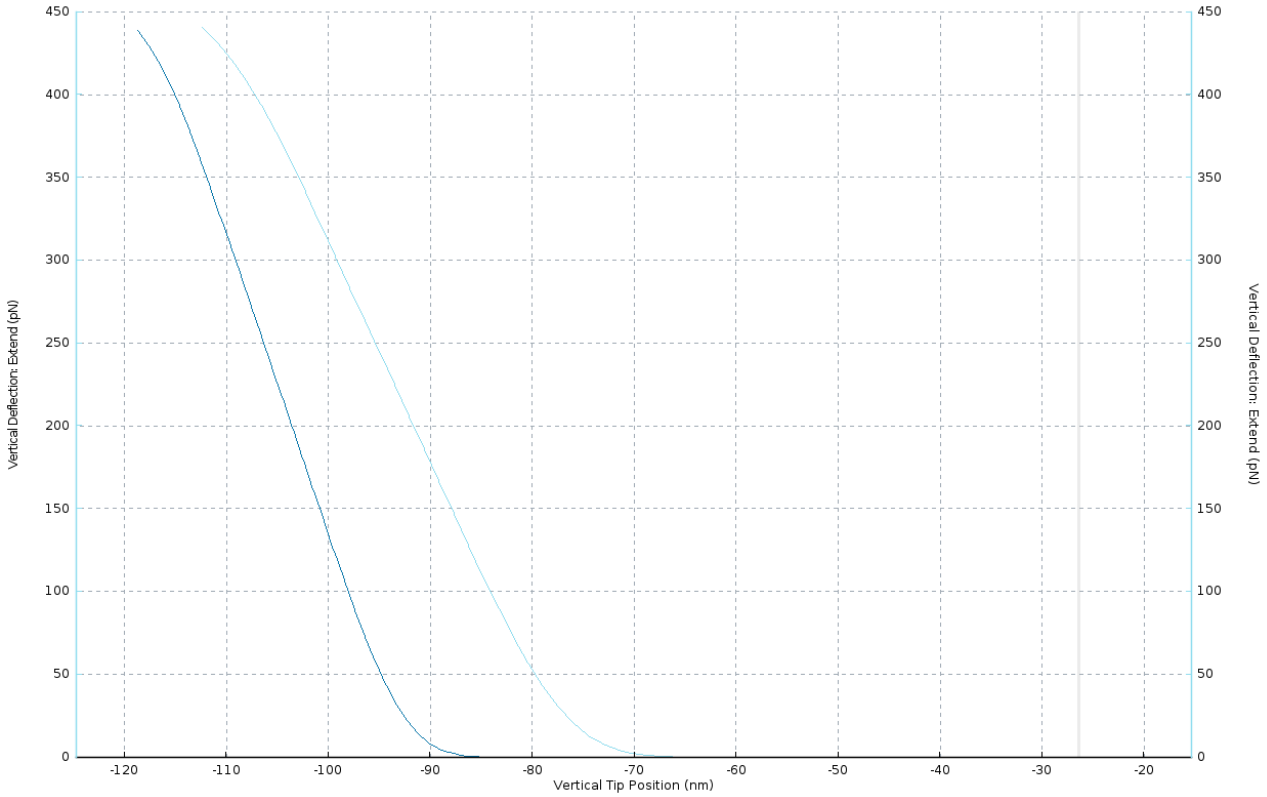

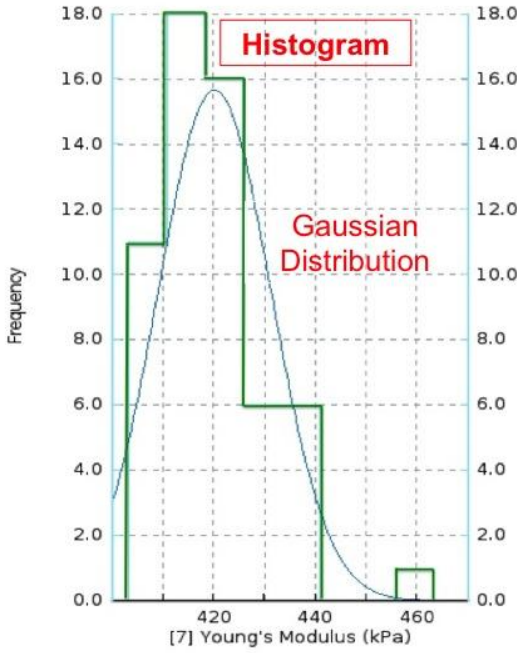

Young's Modulus	420.6 kPa
Contact Point	-59.51 nm
Baseline	-9.034 x 10^{-13} N

DMAA Gel (Reference Force Height)

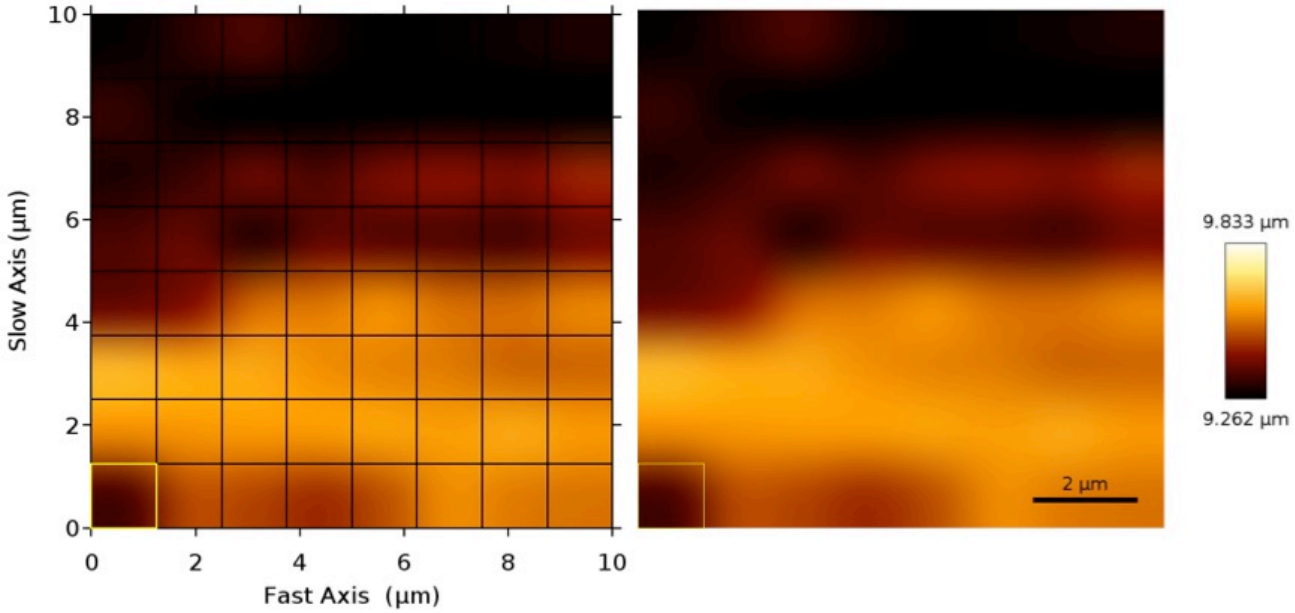

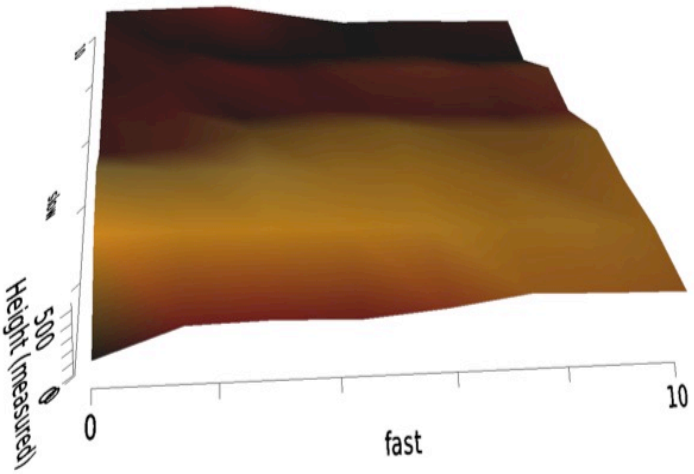

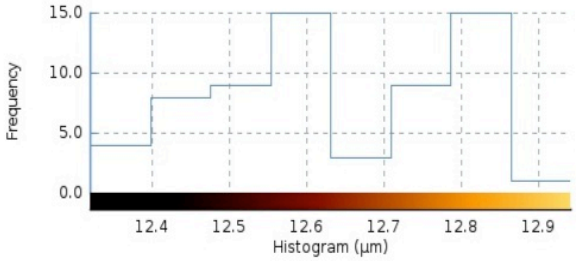

DMAA Gel (Adhesion)

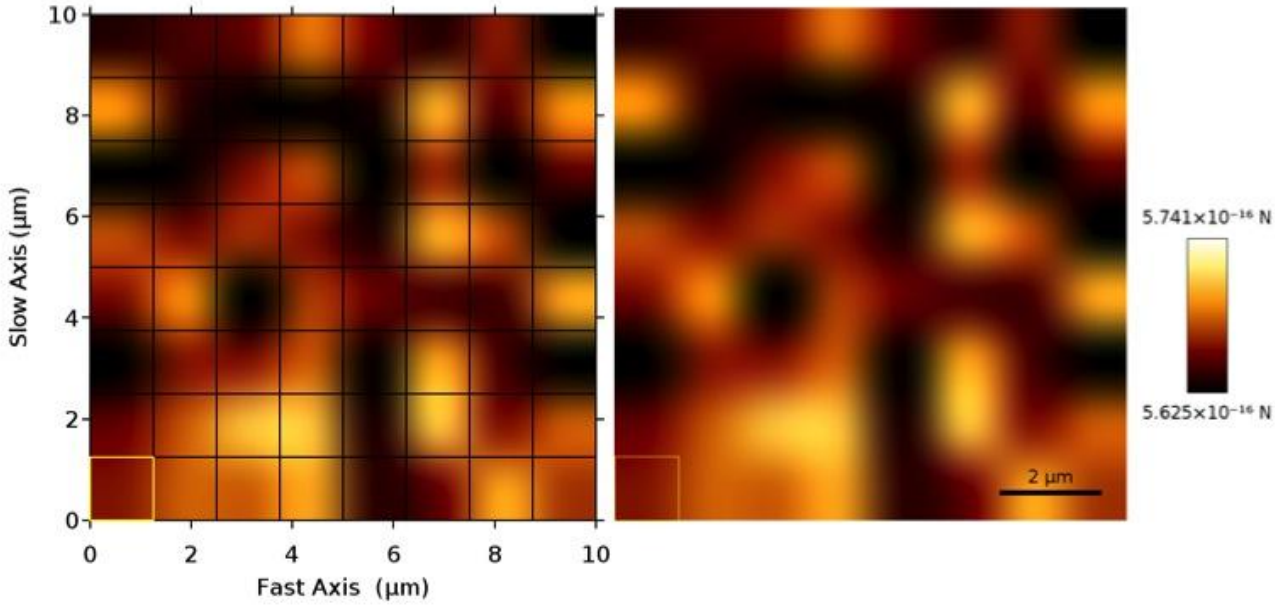

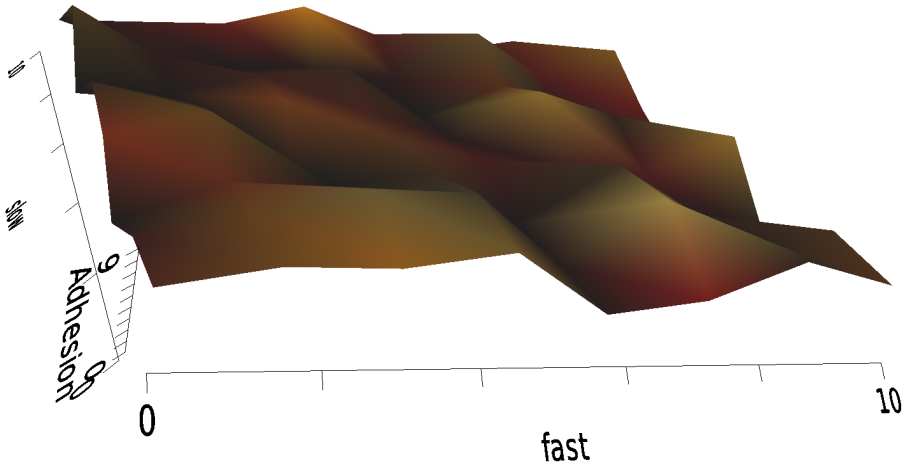

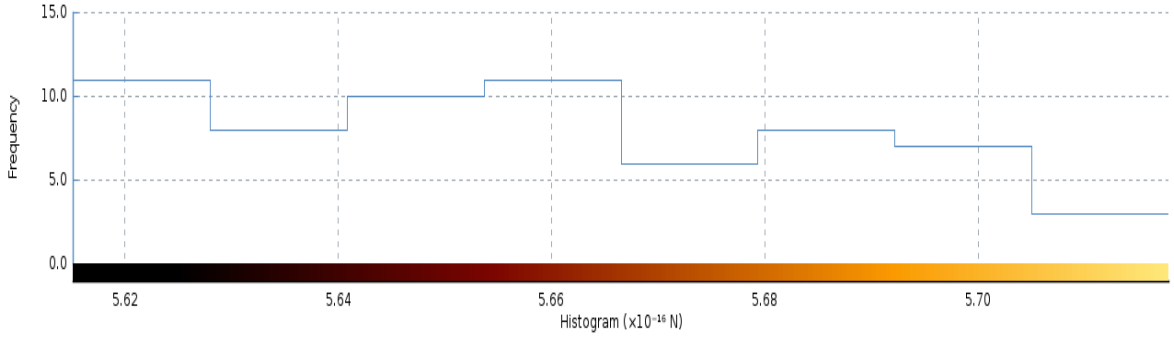

DMAA Gel (Slope)

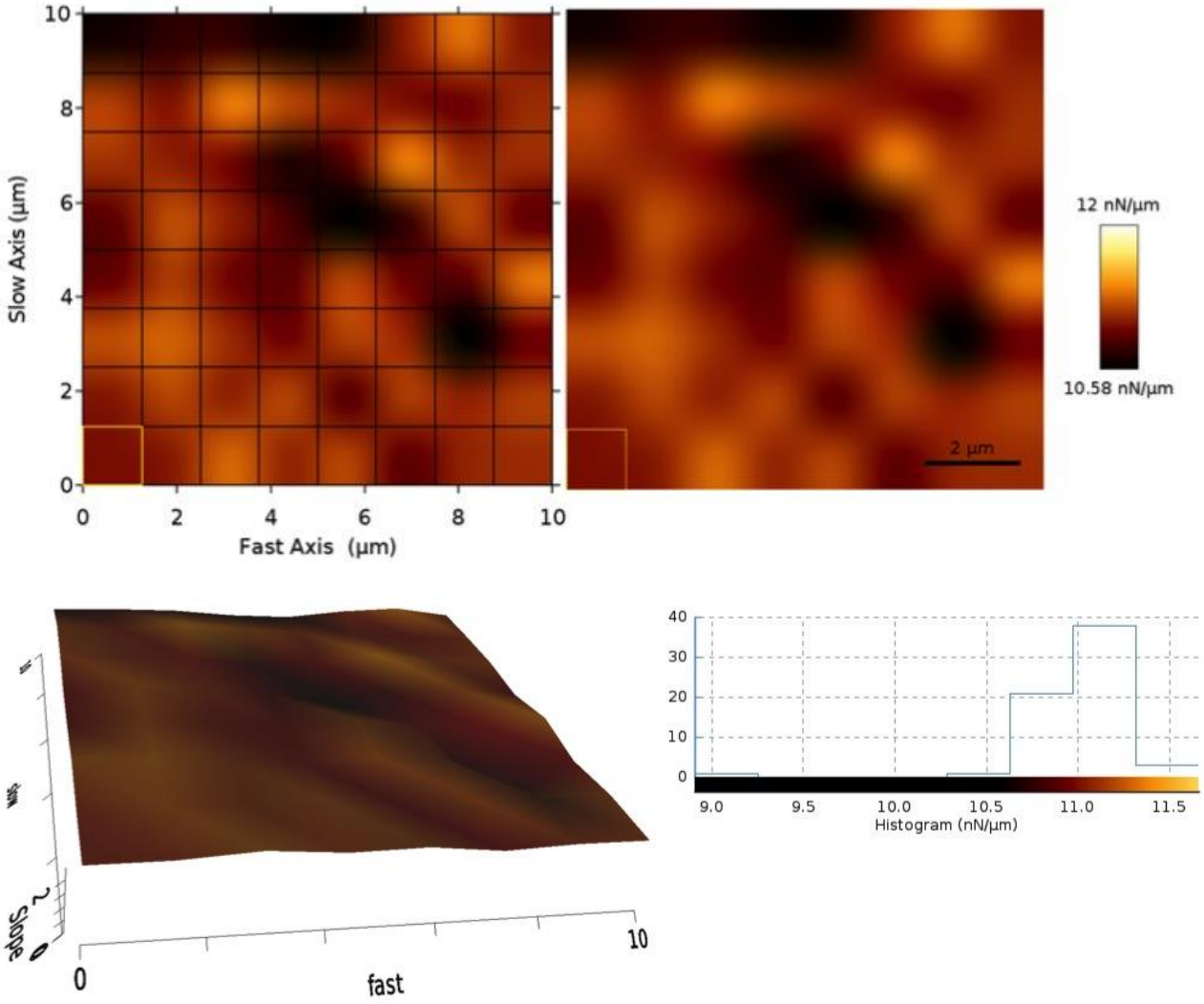

Figure 24. The force- curve derived from the AFM was used to analyze the quantitative values of Young's Modulus for the DMAA gel. The elastic modulus of the DMAA gel was 420.6 kPa, exhibiting the most excellent mechanical performance assumed by the AFM. Topographic images obtained using the force mapping mode provided in-depth information of the DMAA gel.

DMAA/ Acrylamide Gel (Young's Modulus)

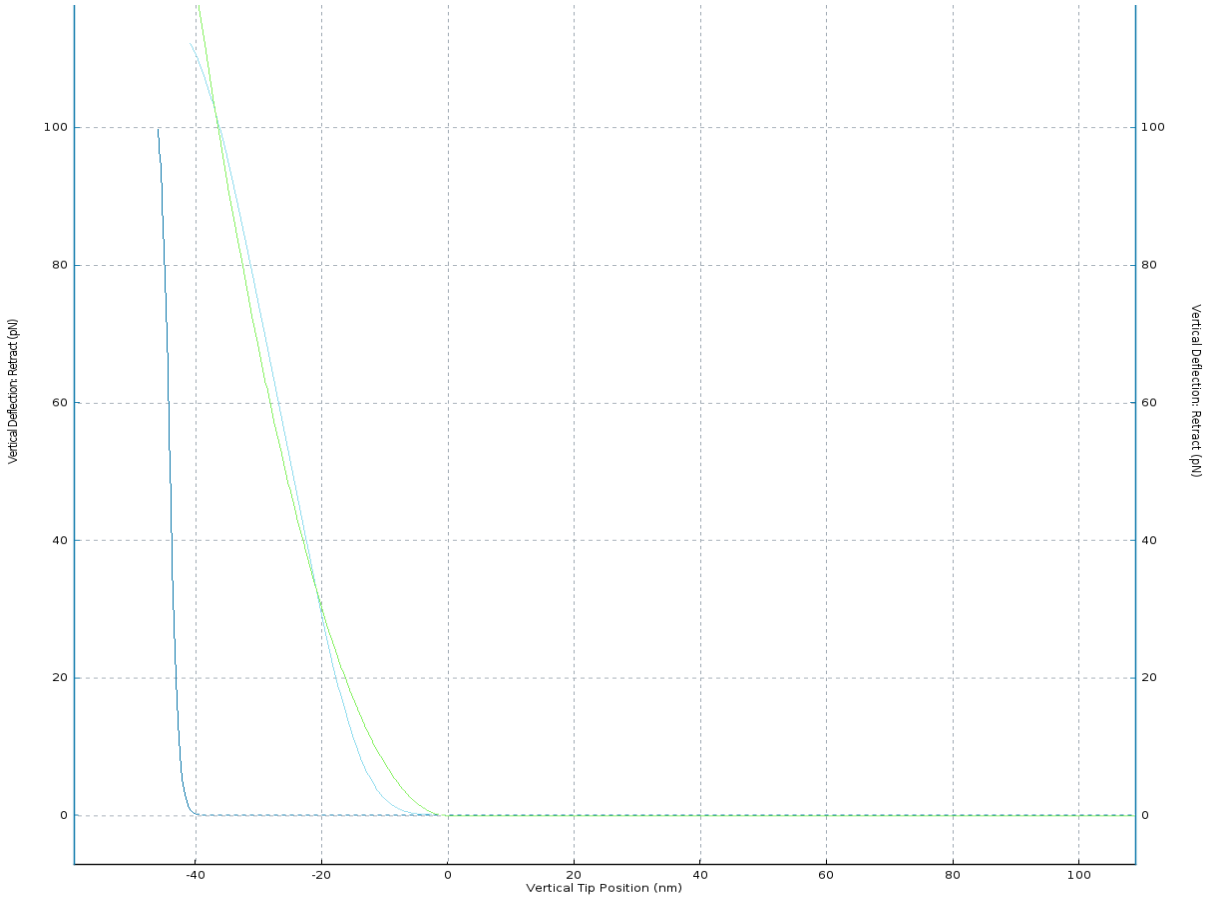

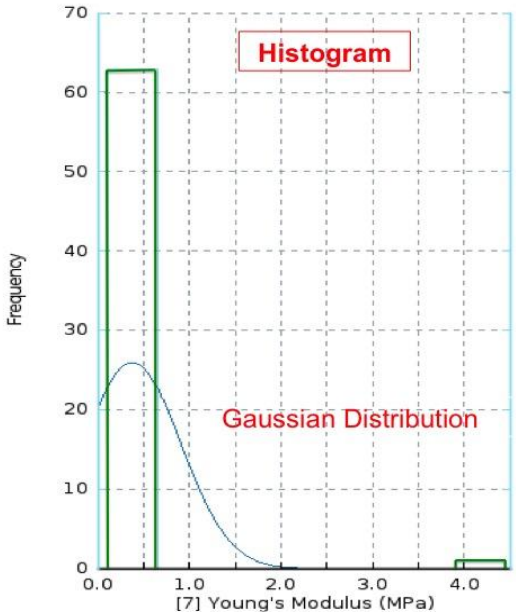

Young's Modulus	358.7 kPa
Contact Point	-79.15 nm
Baseline	-1.3×10^{-13} N

DMAA/ Acrylamide Gel (Reference Force Height)

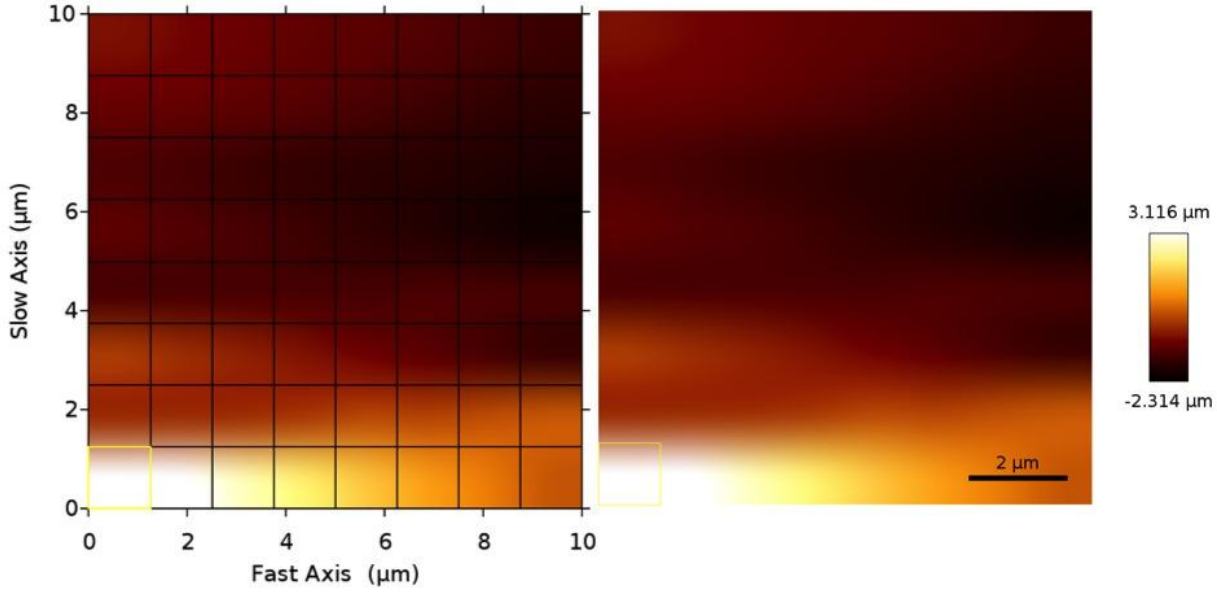

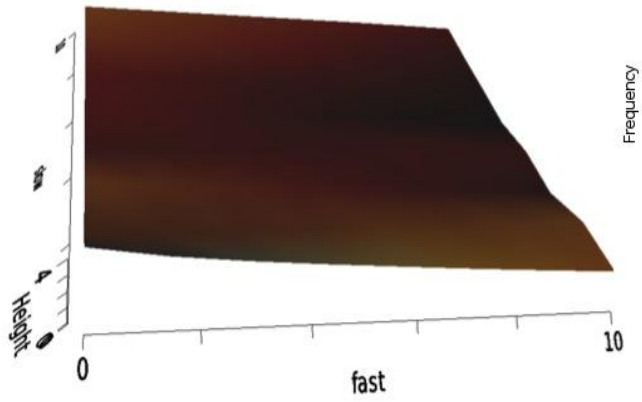

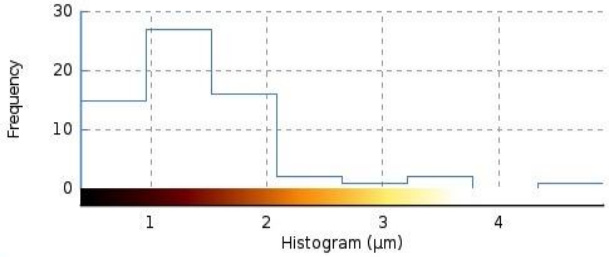

DMAA/ Acrylamide Gel (Adhesion)

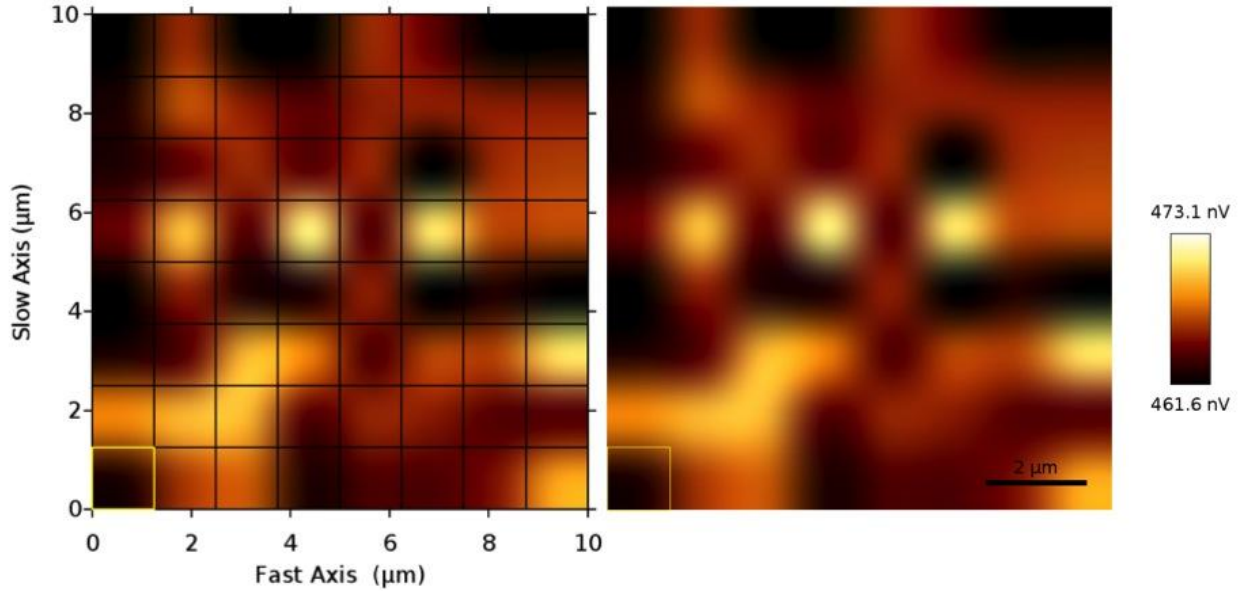

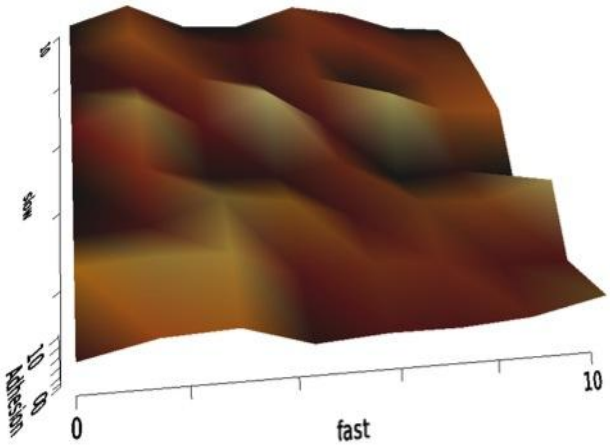

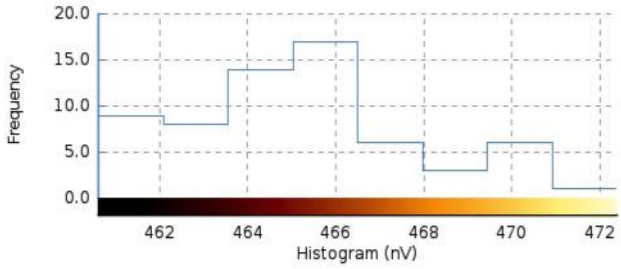

DMAA/ Acrylamide Gel (Slope)

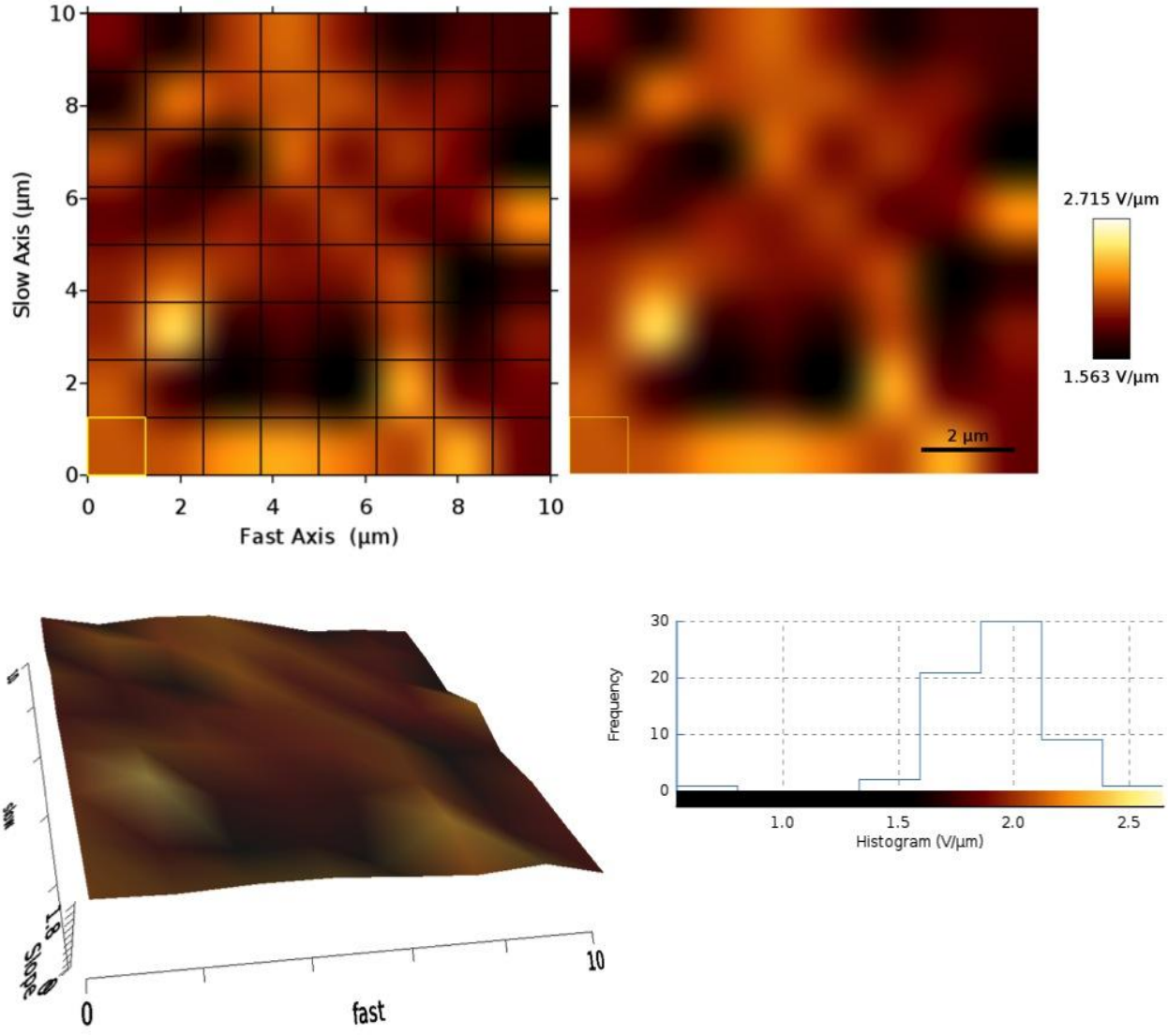

Figure 25. The force curve plotted the retraction of the AFM probe over the DMAA/Acrylamide gels demonstrating an event of hysteresis which could be the result of the viscous behavior of the DMAA/Acrylamide gels. DMAA/Acrylamide gels exhibited an elastic modulus of 358.7 kPa which was close to the elastic moduli of the DMAA gels (E=420.6 kPa). The mechanical properties of the hybrid gel exceeded those of the currently available ExM gels (original ExM gels and MAP gels, 1.2 kPa and 4.3 kPa).

Alginate / Acrylamide Gel (Young's Modulus)

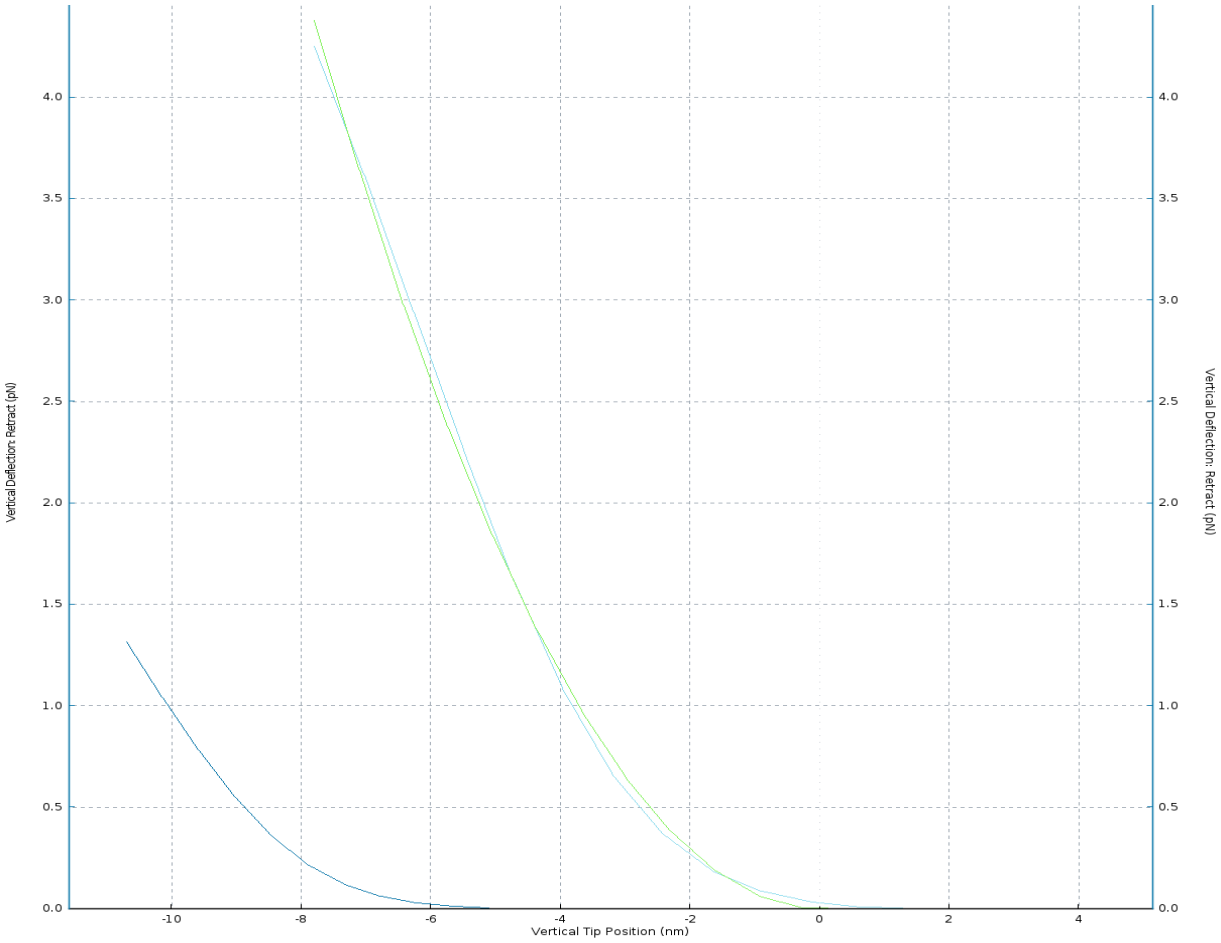

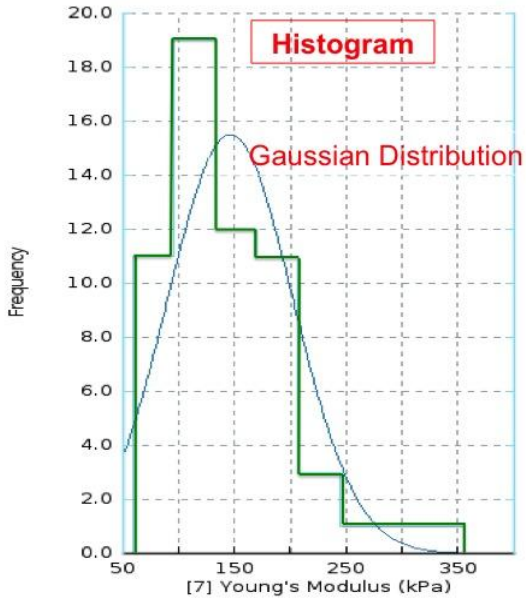

Young's Modulus	172.1 kPa
Contact Point	-101.8 nm
Baseline	8.878 x 10^{-18} N

Alginate / Acrylamide Gel (Reference Force Height)

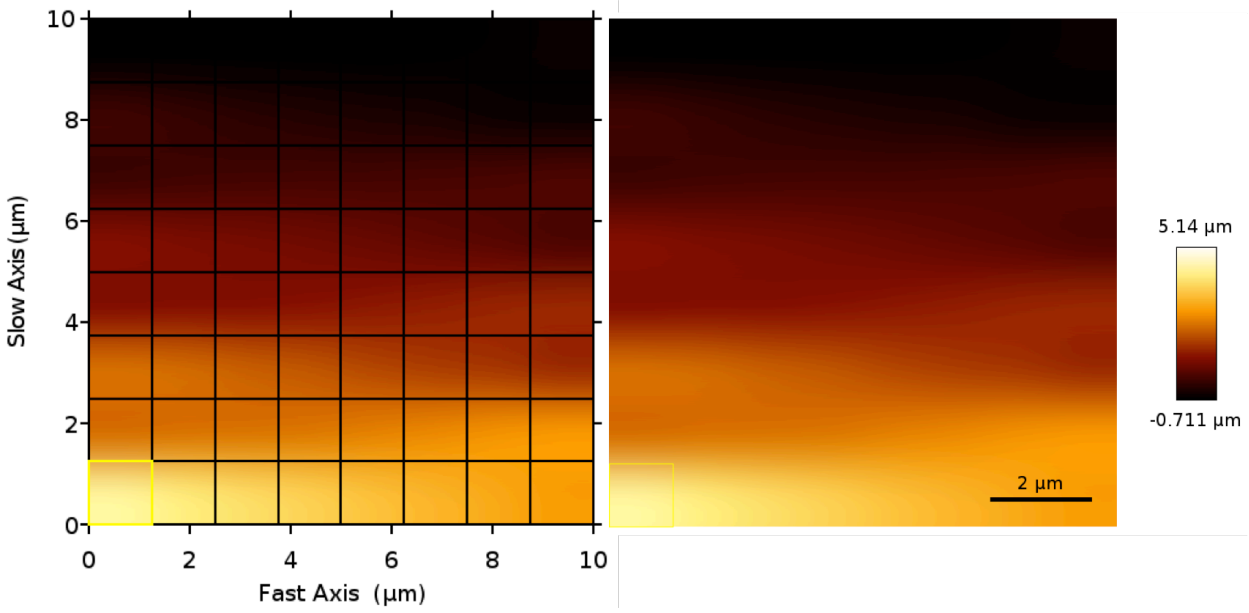

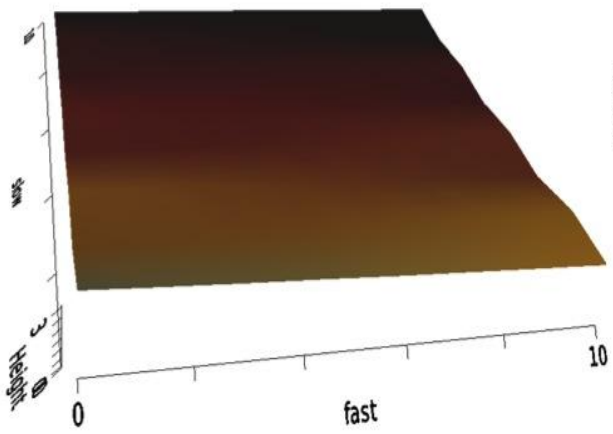

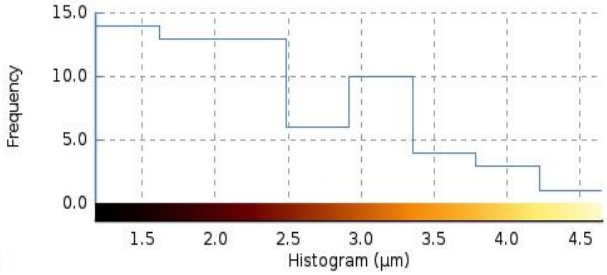

Alginate / Acrylamide Gel (Adhesion)

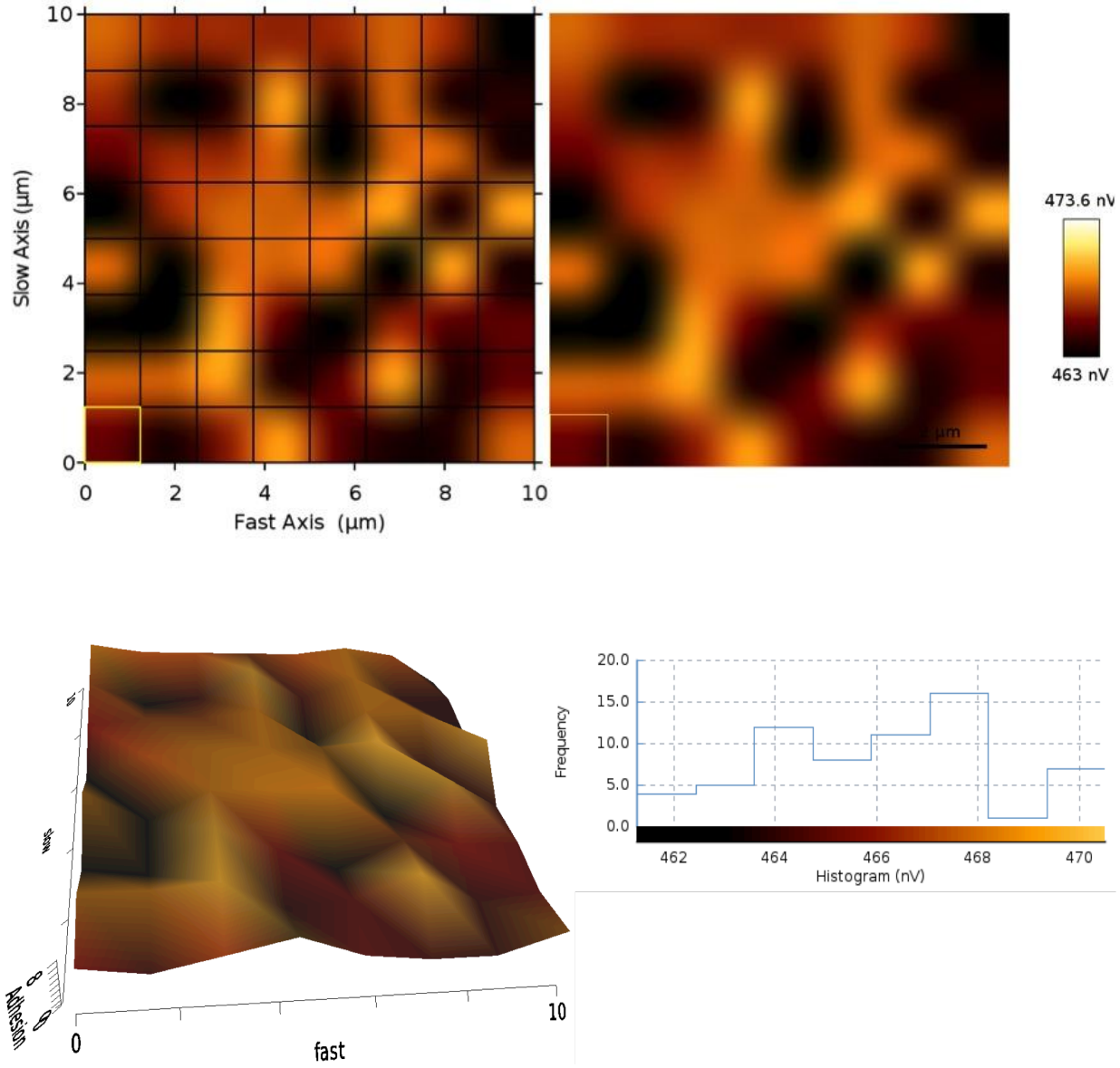

Alginate / Acrylamide Gel (Slope)

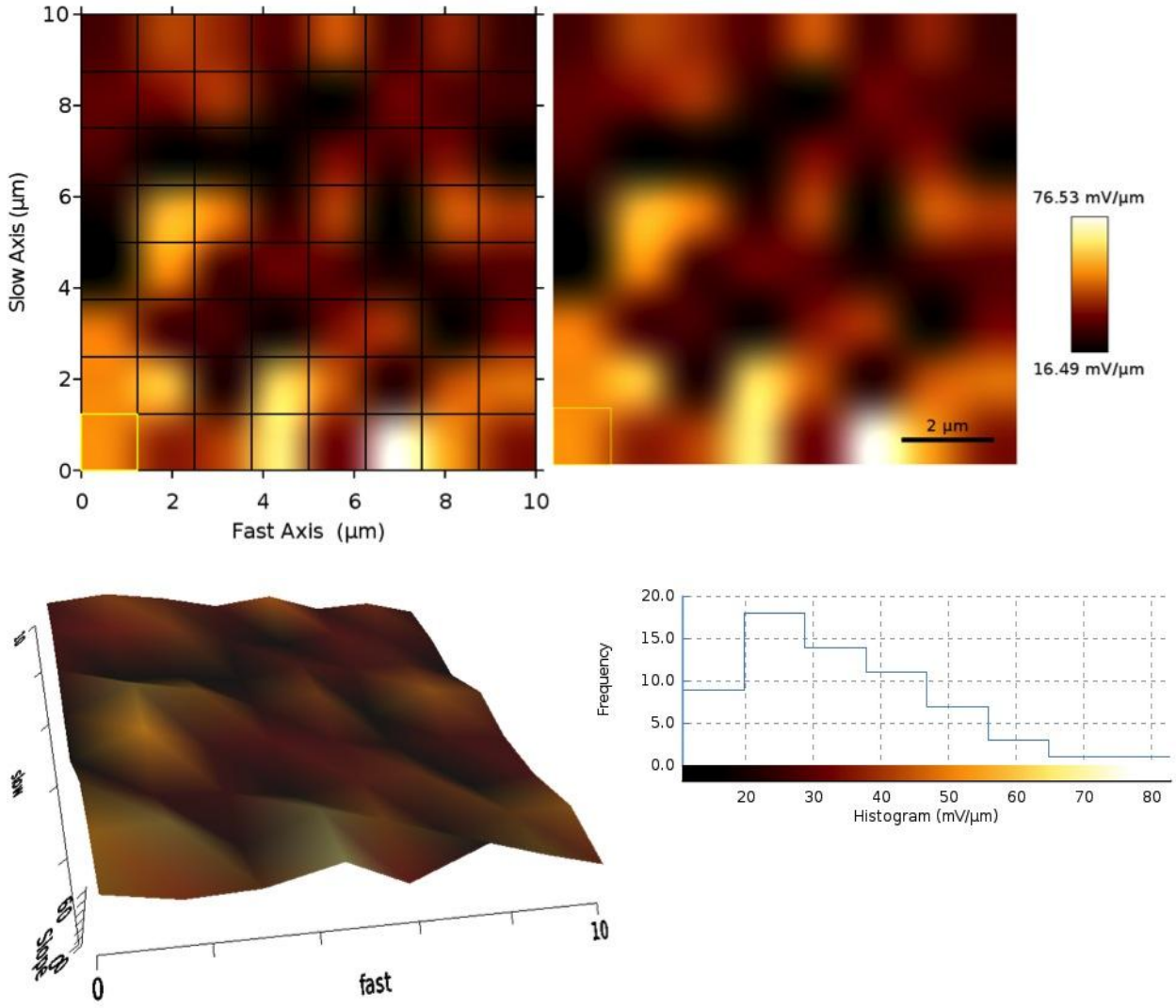

Figure 26. The force curve obtained from the AFM revealing the cantilever deflection and the indentation at a given force. The Hertz model was fitted to derive the Young's Modulus of the Alginate/Acrylamide gel which turned out to be 172.1 kPa. The Young's Modulus was known to describe the mechanical properties of samples, in this case, the Alginate/Acrylamide gels were superior to the currently available ExM gels (original ExM gels and MAP gels, 1.2 kPa and 4.3 kPa) assumed by AFM.

7.5. Tensile Tester

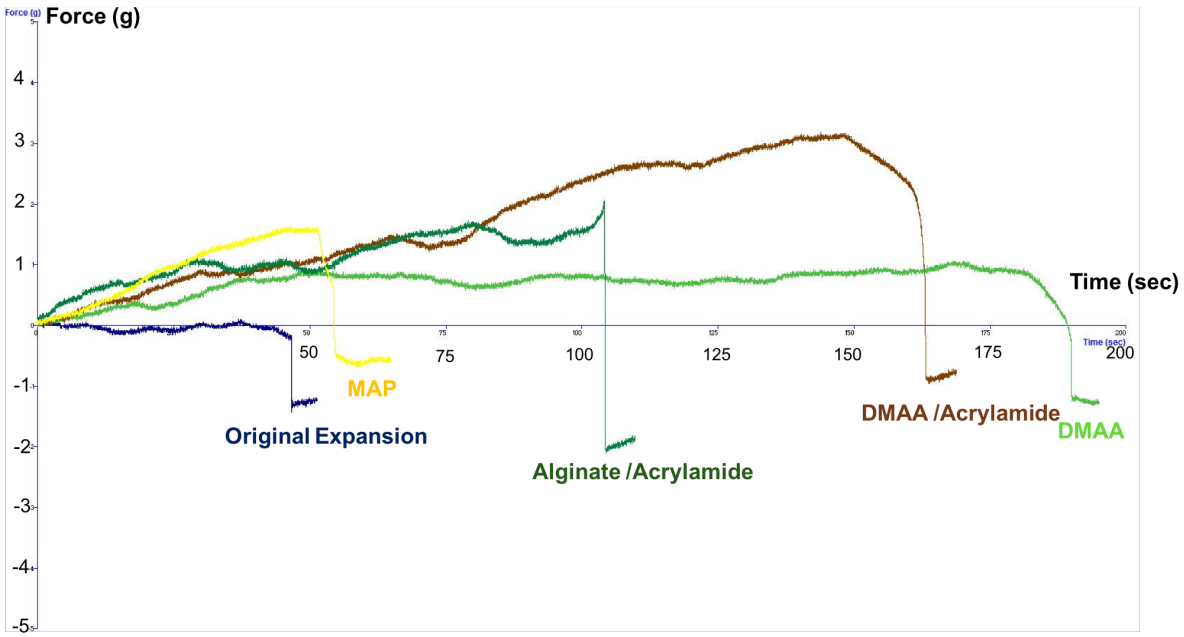

Figure 27. The gels were glued to two clamps with the same size 70 x 10 x 3 mm^3. The tensile tester was calibrated and performed in air. The test speed was set to 0.25 mm/sec. The gels were stretched to a point when there were ruptures appeared on the gel, resulting in dropping of the lines. DMAA demonstrated excellent elasticity among other gels, followed by DMAA/Acrylamide, Alginate/Acrylamide, MAP and original ExM gel. The result of the tensile graph matched the results of force spectroscopy via the AFM which fortified our hypothesis that DMAA was the ideal material for expansion microscopy and could exceed the performance of the currently available gel materials for expansion microscopy. Alginate/Acrylamide and DMAA/Acrylamide gels could be considered the alternative to DMAA gels due to their characteristics of hybrid crosslinks, resulting in relatively high toughness and expansion factor.

7.6. Gel Property Comparison

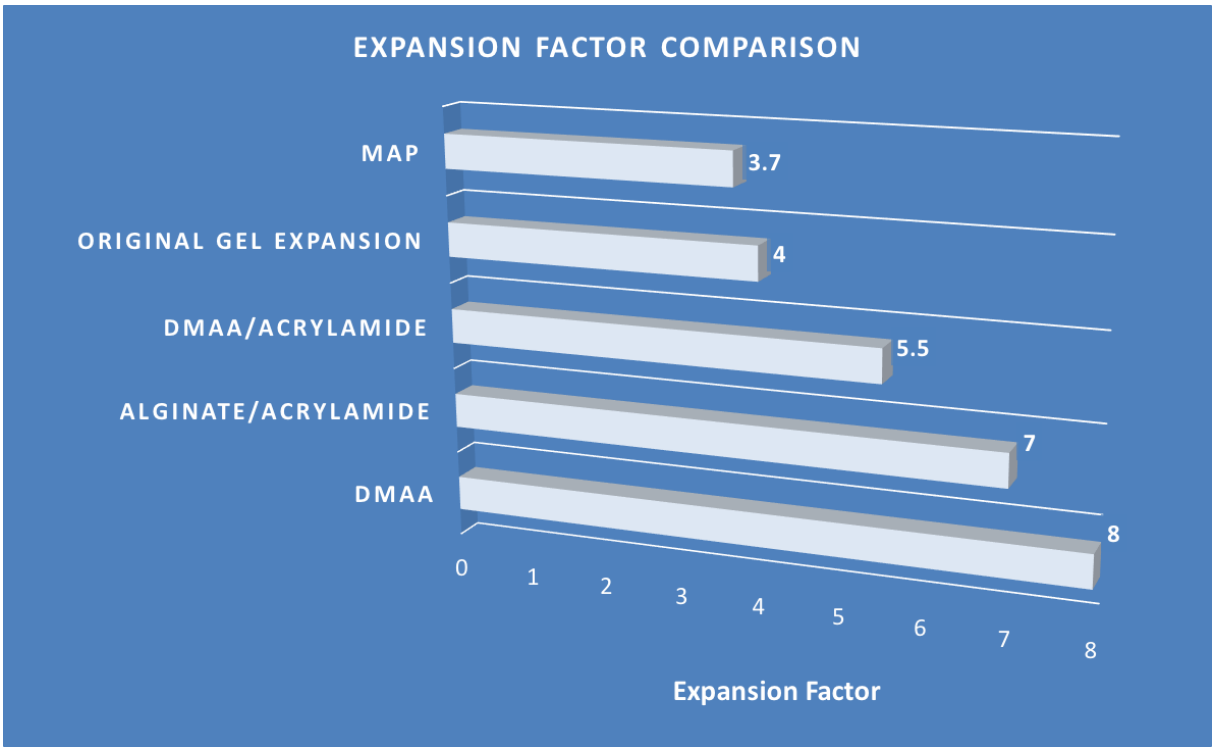

Figure 28. The comparison of different hydrogels in terms of their expansion factors.

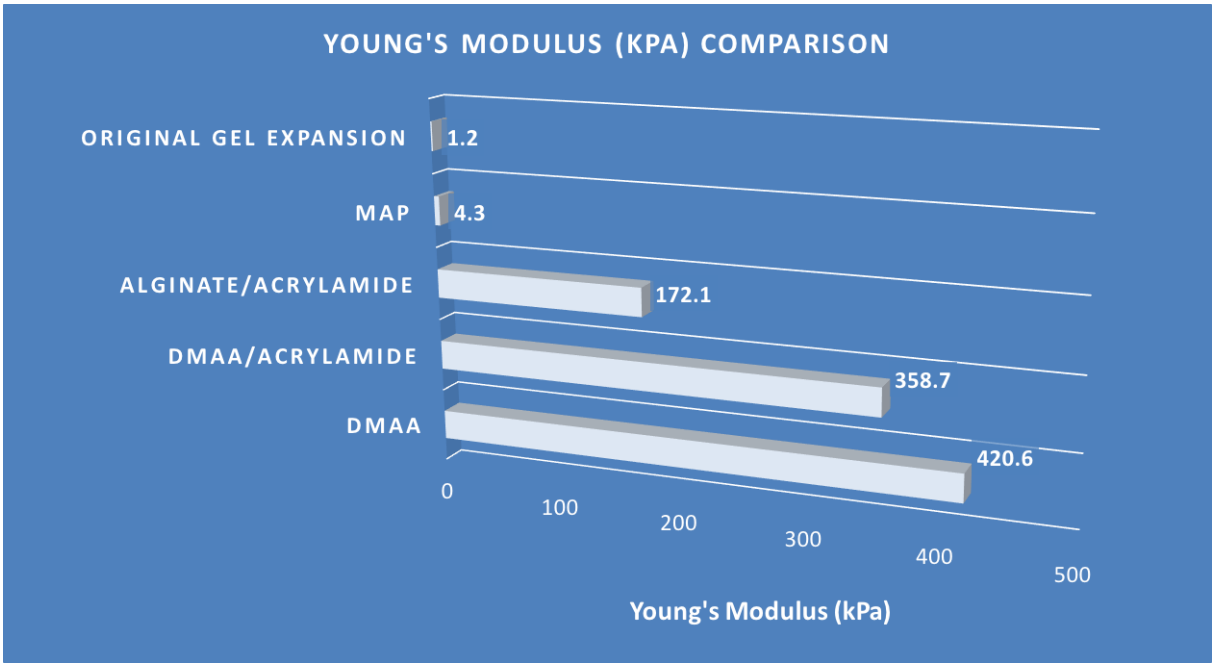

Figure 29. The comparison of Young's Modulus (kPa) derived from different hydrogels via AFM.

7.7. Conclusion

The Young's Modulus could be a normalized measure of the compressibility in which the higher the value the stiffer the sample. The Hertz model was used to analyze the AFM force-distance curves. The spectroscopy curves could be understood as the cantilever approaching the surface of an object, the initial force was too small to give a measurable deflection, resulting in the cantilever remained in the undisturbed state until the attractive force overcame the spring constant of the cantilever caused by the Van der Waals and capillary forces. At this point, the tip would be in contact with the surface of the object. As the sample separated from the base, the repulsive contact force increased, resulting in a deflection of the tip in which caused the cantilever to retract from the surface. The tip broke free when the force from the cantilever was sufficient enough to overcome the adhesion of the tip from the surface.

The elasticity of the sample could be determined by force applied to the sample via a tip, followed by deformation of the sample. At a given force, the stiffness of the sample corresponded to the indentation, hence the stiffer the sample the smaller the indentation (Vinckier et al., 1998). Among all the force distance curve taken on the hydrogels, it was difficult to define the point where the tip and the hydrogel came into contact due to the minimal deflection of the cantilever that caused the initial compression on the surface.

An event of hysteresis was observed from the force curves, indicating that the hydrogels were not perfectly elastic in which the Hertz model assumed. There was no obvious snap to

contact curve seen on the graphs owning to the viscous characteristic of the hydrogels (**Figure 22 ~ Figure 26**). The force mapping mode was applied to obtain the elasticity of the hydrogels. The extreme stretchable DMAA gels yielded 420.60 kPa which outperformed the hybrid gels (DMAA/Acrylamide gel and Alginate/Acrylamide) and acrylamide gels (original ExM gel and MAP gel). DMAA gels demonstrated excellent mechanical sturdiness while exhibited highest stretchability compared to other gel variants. DMAA/Acrylamide gels generated 358.7 kPa which still exhibited exceptional mechanical behavior and high expansion factor (~5.5 x linear expansion). Alginate/Acrylamide gels made of two mixing crosslinked polymers gave rise to relatively high stiffness (172.1 kPa) and high stretchability (~7x linear expansion) that could be further exploited in the application of expansion microscopy. MAP gels and original ExM gels were considered the softest in terms of their elastic modulus (4.3 kPa and 1.2 kPa) and they both exhibited low stretchability (~4 x linear expansion) (**Figure 27, Figure 28**).

DMAA gels could be stretched to more than 10 times its initial length while recovered from the damage when unloaded. The extremely stretchable DMAA gels outperformed other gels regarding the elasticity, stretchability, recovery and stiffness which could be the most ideal choice of material when applied to expansion microscopy. Alginate/Acrylamide gels could be an alternative choice next to the DMAA gels due to the toughness caused by the crack bridging ability of the covalent crosslinks, and the ionic crosslinks that could re-from when the polymer meshes ruptured and dissipated energy. Alginate/Acrylamide gels were less sticky during the handling procedures which aid in retaining the completeness of the biological specimen. These superabsorbent polymers combined relatively high toughness and high expansion factor along with easy handling and synthesis could resolve the limitations hindered by the current

expansion microscopy application such as fragileness, limited expansion factor, lack of mechanical support and distortion of the biological specimens.

7.8. Future Directions

Our future direction is to implement expansion microscopy technology using our ideal materials (DMAA or Alginate/Acrylamide gel) onto primer exchange reaction imaging method to achieve super-resolution imaging that is needed to answer many unsolved puzzles of neurosciences. Primer exchange reaction is a new technology that can be served as a signal amplification aiming to achieve high resolution imaging. ExM is an emerging technology that provides 3D scales of biological specimens by physically magnifying the tissue via swellable polymer meshes. PER is considered compatible with the conventional fluorescence microscopy while the ExM is compatible with majority of the imaging techniques, making them desired components for super-resolution imaging. We believe that combining the two technologies will address the need for nanoscale precision as well as the need for extended 3D specimens that may help us visualize synaptic contacts between neurons to tackle some of the most complex neuroscience problems.

References

Agarwal, K., Buchi, H., Caruthers, M., Gupta, N., Khorana, H., Kleppe, K., Kumar, A., Ohtsuka, E., Rajbhandary, U., Van De Sande, J., Sgaramella, V., Weber, H. and Yamada, T. (1970). Total Synthesis of the Gene for an Alanine Transfer Ribonucleic Acid from Yeast. *Nature*, 227(5253), pp.27-34.

Albanese, A. and Chung, K. (2016). Whole-brain imaging reaches new heights (and lengths). *eLife*, 5.

Alivisatos, A., Chun, M., Church, G., Greenspan, R., Roukes, M. and Yuste, R. (2012). The Brain Activity Map Project and the Challenge of Functional Connectomics. *Neuron*, 74(6), pp.970-974.

Betzig, E., Patterson, G., Sougrat, R., Lindwasser, O., Olenych, S., Bonifacino, J., Davidson, M., Lippincott-Schwartz, J. and Hess, H. (2006). Imaging Intracellular Fluorescent Proteins at Nanometer Resolution. *Science*, 313(5793), pp.1642-1645.

Betzig, E., Trautman, J., Harris, T., Weiner, J. and Kostelak, R. (1991). Breaking the Diffraction Barrier: Optical Microscopy on a Nanometric Scale. *Science*, 251(5000), pp.1468-1470.

Biolabs, N. (n.d.). *Isothermal Amplification | NEB*. [online] Neb.com. Available at: https://www.neb.com/applications/dna-amplification-pcr-and-qpcr/isothermal-amplification.

Calvert, P. (2009). Hydrogels for Soft Machines. *Advanced Materials*, 21(7), pp.743-756.

Chen, F., Tillberg, P. and Boyden, E. (2015). Expansion Microscopy. *Science*, 347(543), p.8.

Chen, F., Wassie, A., Cote, A., Sinha, A., Alon, S., Asano, S., Daugharthy, E., Chang, J., Marblestone, A., Church, G., Raj, A. and Boyden, E. (2016). Nanoscale imaging of RNA with expansion microscopy. *Nature Methods*, 13(8), pp.679-684.

Choi, H., Chang, J., Trinh, L., Padilla, J., Fraser, S. and Pierce, N. (2010). Programmable in situ amplification for multiplexed imaging of mRNA expression. *Nature Biotechnology*, 28(11), pp.1208-1212.

Chozinski, T., Halpern, A., Okawa, H., Kim, H., Tremel, G., Wong, R. and Vaughan, J. (2016). Expansion microscopy with conventional antibodies and fluorescent proteins. *Nature Methods*, 13(6), pp.485-488.

Chung, K. and Deisseroth, K. (2013). CLARITY for mapping the nervous system. *Nature Methods*, 10(6), pp.508-513.

Chung, K., Wallace, J., Kim, S., Kalyanasundaram, S., Andalman, A., Davidson, T., Mirzabekov, J., Zalocusky, K., Mattis, J., Denisin, A., Pak, S., Bernstein, H., Ramakrishnan, C., Grosenick, L., Gradinaru, V. and Deisseroth, K. (2013). Structural and molecular interrogation of intact biological systems. *Nature*, 497(7449), pp.332-337.

Cipriano, B., Banik, S., Sharma, R., Rumore, D., Hwang, W., Briber, R. and Raghavan, S. (2014). Superabsorbent Hydrogels That Are Robust and Highly Stretchable. *Macromolecules*, 47(13), pp.4445-4452.

Cleveland, J., Manne, S., Bocek, D. and Hansma, P. (1993). A nondestructive method for determining the spring constant of cantilevers for scanning force microscopy. *Review of Scientific Instruments*, 64(2), pp.403-405.

Dani, A., Huang, B., Bergan, J., Dulac, C. and Zhuang, X. (2010). Superresolution Imaging of Chemical Synapses in the Brain. *Neuron*, 68(5), pp.843-856.

Dirks, R. and Pierce, N. (2004). From The Cover: Triggered amplification by hybridization chain reaction. *Proceedings of the National Academy of Sciences*, 101(43), pp.15275-15278.

Douglas, S., Dietz, H., Liedl, T., Högberg, B., Graf, F. and Shih, W. (2009). Self-assembly of DNA into nanoscale three-dimensional shapes. *Nature*, 459(7245), pp.414-418.

Dunn, K., Dannenberg, F., Ouldridge, T., Kwiatkowska, M., Turberfield, A. and Bath, J. (2015). Guiding the folding pathway of DNA origami. *Nature*, 525(7567), pp.82-86.

Eaton, P. and West, P. (2010). *ATOMIC FORCE MICROSCOPY*. [S.l.]: OXFORD UNIV PRESS.

Feng, G., Mellor, R., Bernstein, M., Keller-Peck, C., Nguyen, Q., Wallace, M., Nerbonne, J., Lichtman, J. and Sanes, J. (2000). Imaging Neuronal Subsets in Transgenic Mice Expressing Multiple Spectral Variants of GFP. *Neuron*, 28(1), pp.41-51.

Gao, R., Asano, S. and Boyden, E. (2017). Q&A: Expansion microscopy. *BMC Biology*, 15(1).

Gerdes, M., Sevinsky, C., Sood, A., Adak, S., Bello, M., Bordwell, A., Can, A., Corwin, A., Dinn, S., Filkins, R., Hollman, D., Kamath, V., Kaanumalle, S., Kenny, K., Larsen, M., Lazare, M., Li, Q., Lowes, C., McCulloch, C., McDonough, E., Montalto, M., Pang, Z., Rittscher, J., Santamaria-Pang, A., Sarachan, B., Seel, M., Seppo, A., Shaikh, K., Sui, Y. and Zhang, J. (2013). Highly multiplexed single-cell analysis of formalin-fixed, paraffin-embedded cancer tissue. *Proceedings of the National Academy of Sciences*, 110(29), pp.11982-11987.

Gibson, C., Watson, G. and Myhra, S. (1996). Determination of the spring constants of probes for force microscopy/spectroscopy. *Nanotechnology*, 7(3), pp.259-262.

Glass, G., Papin, J. and Mandell, J. (2009). Simple: A Sequential Immunoperoxidase Labeling and Erasing Method. *Journal of Histochemistry & Cytochemistry*, 57(10), pp.899-905.

Gong, J., Katsuyama, Y., Kurokawa, T. and Osada, Y. (2003). Double-Network Hydrogels with Extremely High Mechanical Strength. *Advanced Materials*, 15(14), pp.1155-1158.

Gustafsson, M. (2005). Nonlinear structured-illumination microscopy: Wide-field fluorescence imaging with theoretically unlimited resolution. *Proceedings of the National Academy of Sciences*, 102(37), pp.13081-13086.

Hell, S. and Wichmann, J. (1994). Breaking the diffraction resolution limit by stimulated emission: stimulated-emission-depletion fluorescence microscopy. *Optics Letters*, 19(11), p.780.

Henderson, K., Zhou, T., Otim, K. and Shull, K. (2010). Ionically Cross-Linked Triblock Copolymer Hydrogels with High Strength. *Macromolecules*, 43(14), pp.6193-6201.

Huang, B., Bates, M. and Zhuang, X. (2009). Super-Resolution Fluorescence Microscopy. *Annual Review of Biochemistry*, 78, pp.993-1016.

Ke, Y., Ong, L., Shih, W. and Yin, P. (2012). Three-Dimensional Structures Self-Assembled from DNA Bricks. *Science*, 338(6111), pp.1177-1183.

Kherlopian, A., Song, T., Duan, Q., Neimark, M., Po, M., Gohagan, J. and Laine, A. (2008). A review of imaging techniques for systems biology. *BMC Systems Biology*, 2(1), p.74.

Kishi, J., Schaus, T., Gopalkrishnan, N., Xuan, F. and Yin, P. (2017). Programmable autonomous synthesis of single-stranded DNA. *Nature Chemistry*, 10(2), pp.155-164.

Kosuri, S. and Church, G. (2014). Large-scale de novo DNA synthesis: technologies and applications. *Nature Methods*, 11(5), pp.499-507.

Ku, T., Swaney, J., Park, J., Albanese, A., Murray, E., Cho, J., Park, Y., Mangena, V., Chen, J. and Chung, K. (2016). Multiplexed and scalable super-resolution imaging of three-dimensional protein localization in size-adjustable tissues. *Nature Biotechnology*, 34(9), pp.973-981.

Lake, G. (1995). Fatigue and Fracture of Elastomers. *Rubber Chemistry and Technology*, 68(3), pp.435-460.

Lee, K. and Mooney, D. (2001). Hydrogels for tissue engineering. *Chemical Reviews*, 101, pp.1869-1879.

Leung, B. and Chou, K. (2011). Review of Super-Resolution Fluorescence Microscopy for Biology. *Applied Spectroscopy*, 65(9), pp.967-980.

Lin, J., Fallahi-Sichani, M. and Sorger, P. (2015). Highly multiplexed imaging of single cells using a high-throughput cyclic immunofluorescence method. *Nature Communications*, 6(1).

Liu, Z., Lee, H., Xiong, Y., Sun, C. and Zhang, X. (2007). Far-Field Optical Hyperlens Magnifying Sub-Diffraction-Limited Objects. *Science*, 315(5819), pp.1686-1686.

Lizardi, P., Huang, X., Zhu, Z., Bray-Ward, P., Thomas, D. and Ward, D. (1998). Mutation detection and single-molecule counting using isothermal rolling-circle amplification. *Nature Genetics*, 19(3), pp.225-232.

Matus, A., Walters, B. and Mughal, S. (1975). Immunohistochemical demonstration of tubulin associated with microtubules and synaptic junctions in mammalian brain. *Journal of Neurocytology*, 4(6), pp.733-744.

Michelson, A. and Todd, A. (1955). Nucleotides part XXXII. Synthesis of a dithymidine dinucleotide containing a 3′: 5′-internucleotidic linkage. *J. Chem. Soc.*, 0(0), pp.2632-2638.

Mohammed, A., Šulc, P., Zenk, J. and Schulman, R. (2016). Self-assembling DNA nanotubes to connect molecular landmarks. *Nature Nanotechnology*, 12(4), pp.312-316.

Rehfeldt, F. Engler, A., Eckhardt, A., Ahmed, F. and Discher, D. (2007). Cell responses to the mechanochemical microenvironment—Implications for regenerative medicine and drug delivery. *Advanced Drug Delivery Reviews*, 59(13), pp.1329-1339.

Richardson, D. and Lichtman, J. (2015). Clarifying Tissue Clearing. *Cell*, 162(2), pp.246-257.

Rust, M., Bates, M. and Zhuang, X. (2006). Sub-diffraction-limit imaging by stochastic optical reconstruction microscopy (STORM). *Nature Methods*, 3(10), pp.793-796.

Wang, J. (1984). Young's modulus of porous materials. *Journal of Materials Science*, 19(3), pp.809-814.

Willig, K., Kellner, R., Medda, R., Hein, B., Jakobs, S. and Hell, S. (2006). Nanoscale resolution in GFP-based microscopy. *Nature Methods*, 3(9), pp.721-723.

MORITA, S. (2016). *NONCONTACT ATOMIC FORCE MICROSCOPY*. [Place of publication not identified]: SPRINGER INTERNATIONAL PU.

Nanophys.kth.se. (n.d.). *NanoWizard AFM Handbook*. [online] Available at: http://www.nanophys.kth.se/nanophys/facilities/nfl/afm/jpk/manuf-manuals/handbook-2.2a.pdf.

Oh, S., Harris, J., Ng, L., Winslow, B., Cain, N., Mihalas, S., Wang, Q., Lau, C., Kuan, L., Henry, A., Mortrud, M., Ouellette, B., Nguyen, T., Sorensen, S., Slaughterbeck, C., Wakeman, W., Li, Y., Feng, D., Ho, A., Nicholas, E., Hirokawa, K., Bohn, P., Joines, K., Peng, H., Hawrylycz, M., Phillips, J., Hohmann, J., Wohnoutka, P., Gerfen, C., Koch, C., Bernard, A., Dang, C., Jones, A. and Zeng, H. (2014). A mesoscale connectome of the mouse brain. *Nature*, 508, pp.207–214.

Peak, C., Wilker, J. and Schmidt, G. (2013). A review on tough and sticky hydrogels. *Colloid and Polymer Science*, 291(9), pp.2031-2047.

Schaus, T., Woo, S., Xuan, F., Chen, X. and Yin, P. (2017). A DNA nanoscope via auto-cycling proximity recording. *Nature Communications*, 8(1).

Schermelleh, L., Carlton, P., Haase, S., Shao, L., Winoto, L., Kner, P., Burke, B., Cardoso, M., Agard, D., Gustafsson, M., Leonhardt, H. and Sedat, J. (2008). Subdiffraction Multicolor Imaging of the Nuclear Periphery with 3D Structured Illumination Microscopy. *Science*, 320(5881), pp.1332-1336.

Schubert, W., Bonnekoh, B., Pommer, A., Philipsen, L., Böckelmann, R., Malykh, Y., Gollnick, H., Friedenberger, M., Bode, M. and Dress, A. (2006). Analyzing proteome topology and function by automated multidimensional fluorescence microscopy. *Nature Biotechnology*, 24(10), pp.1270-1278.

Singh-Gasson, S., Green, R., Yue, Y., Nelson, C., Blattner, F., Sussman, M. and Cerrina, F. (1999). Maskless fabrication of light-directed oligonucleotide microarrays using a digital micromirror array. *Nature Biotechnology*, 17(10), pp.974-978.

Sun, J., Zhao, X., Illeperuma, W., Chaudhuri, O., Oh, K., Mooney, D., Vlassak, J. and Suo, Z. (2012). Highly stretchable and tough hydrogels. *Nature*, 489(7414), pp.133-136.

Tillberg, P., Chen, F., Piatkevich, K., Zhao, Y., Yu, C., English, B., Gao, L., Martorell, A., Suk, H., Yoshida, F., DeGennaro, E., Roossien, D., Gong, G., Seneviratne, U., Tannenbaum, S., Desimone, R., Cai, D. and Boyden, E. (2016). Protein-retention expansion microscopy of cells and tissues labeled using standard fluorescent proteins and antibodies. *Nature Biotechnology*, 34(9), pp.987-992.

Tomer, R., Ye, L., Hsueh, B. and Deisseroth, K. (2014). Advanced CLARITY for rapid and high-resolution imaging of intact tissues. *Nature Protocols*, 9(7), pp.1682-1697.

Vinckier, A. and Semenza, G. (1998). Measuring elasticity of biological materials by atomic force microscopy. *FEBS Letters*, 430(1-2), pp.12-16.

Wang, Y., Woehrstein, J., Donoghue, N., Dai, M., Avendaño, M., Schackmann, R., Zoeller, J., Wang, S., Tillberg, P., Park, D., Lapan, S., Boyden, E., Brugge, J., Kaeser, P., Church, G., Agasti, S., Jungmann, R. and Yin, P. (2017). Rapid Sequential in Situ Multiplexing with DNA Exchange Imaging in Neuronal Cells and Tissues. *Nano Letters*, 17(10), pp.6131-6139.

Wei, B., Dai, M. and Yin, P. (2012). Complex shapes self-assembled from single-stranded DNA tiles. *Nature*, 485(7400), pp.623-626.

Weston, P. and Avrameas, S. (1971). Proteins coupled to polyacrylamide beads using glutaraldehyde. *Biochemical and Biophysical Research Communications*, 45(6), pp.1574-1580.

Willig, K., Rizzoli, S., Westphal, V., Jahn, R. and Hell, S. (2006). STED microscopy reveals that synaptotagmin remains clustered after synaptic vesicle exocytosis. *Nature*, 440(7086), pp.935-939.

Winfree, E., Liu, F., Wenzler, L. and Seeman, N. (1998). Design and self-assembly of two-dimensional DNA crystals. *Nature*, 394(6693), pp.539-544.

Yildiz, A. (2003). Myosin V Walks Hand-Over-Hand: Single Fluorophore Imaging with 1.5-nm Localization. *Science*, 300(5628), pp.2061-2065.